THE EFFECT OF CORAL DEGRADATION ON THE WAVE TRANSFORMATION AND RUNUP NEAR WHITEHOUSE BEACH, JAMAICA

MARJOLEIN VAN DEN BROEK

Universiteit Utrecht

The effect of coral degradation on the wave transformation and runup near Whitehouse beach, Jamaica

by

M.A (Marjolein) van den Broek
student : 6632963
Final version

in partial fulfillment of the requirements for a degree of

Master of Science
Earth, surface and Water

at Utrecht University,
department Geo-sciences, May 21, 2021

Supervisor:
dr.ir. Jaap Nienhuis
prof. dr. Gerben Ruessink

Abstract

Sea level rise and global warming form an ever-growing thread to the health of the corals reefs and the safety of the coastal areas. Coral reefs form diverse ecosystems that protect coastal area all around the world against wave runup, flooding and erosion by dissipating wave energy at some distance from the shoreline. This is also true for the fringing reef at Whitehouse bay in Jamaica.

In the last view decades, Jamaica experienced a 85% loss in coral reefs due to a series of natural and man-made disasters. Degraded reefs from bleaching events or physical damage can lead to a reduction in structural complexity and results in a lower bottom friction and roughness. Coral reefs can form complex 3-dimensional structures, with a high variety in width, height and vegetation density. A large part of wave transformation across reefs is controlled by the structural complexity of coral reefs.

This master thesis will investigate the effect of reef structures and a loss of reef structures on the wave propagation across coral reefs. First, an observational study on the structural complexity of the corals and sea-grass in Whitehouse Bay was preformed.

I used structure for motion to quantify the structural complexity of the corals and sea-grass in the study area. Structure for motion creates 3-dimensional image and digital elevation models (DEM) of the reef out of 2-dimensional images by estimating the motion of these images. The results from the structure for motion survey were then used to determine the structural complexity of corals in the study area. The results show an average coral height of 0.78 [m] and an average sea-grass height of 0.4 [m].

The next part of this study uses the structural complexity of corals to modelling the wave propagation across the fringing reef in Whitehouse bay, Jamaica. Recent studies show the importance of low frequency or infragravity waves, with frequencies lower than 0.04 Hz, in reef hydrodynamics. Xbeach Surfbeat was used to model the effect of coral degradation on the propagation of waves across the coral reef and to determine the contribution of low frequency waves to the wave height and runup near the beach.

The results showed an increase in low frequency runup between 11% and 55409%, an increase in low frequency wave height between 403% and 1409% and an increase in setup between 76% and 328%, when comparing the current situation to a state where the corals are completely degraded. The results also show that the amount of coral degradation influences the location of the fictional dissipation. In the current state, the frictional dissipation is largest offshore the reef crest. Whereas the frictional dissipation is largest further onshore when the corals are eroded.

Acknowledgement

Before you lies the results of 10 months of work which marks the end of my life as a student. This thesis is in partial fulfilment for a Master of Science degree at the University of Utrecht, for the master Earth, Surface and Water.

I would like to thank all the people who helped me achieve this milestone. A special thanks to my supervisors Jaap Nienhuis and Gerben Ruessink for their support, feedback and for sparking my interest in coastal wave processes, and for all their help regarding the Xbeach model. I would also like to thank Chris Daly, for providing much of the data that I used and for answering many of my questions.

A big thanks to my parents and friends for providing some much needed distraction at times. I hope you all enjoy reading my thesis report.

Marjolein van den Broek

Contents

1 Introduction **1**
1.1 Motivation . . . 1

2 Background **3**
2.1 Coral reefs . . . 3
2.1.1 Morphology . . . 3
2.1.2 Structural zones . . . 3
2.1.3 Forming of coral reef . . . 5
2.1.4 Degradation of coral reef in Jamaica . . . 6
2.2 Reef Hydrodynamics . . . 8
2.2.1 Wave generation . . . 8
2.2.2 Wave transformation and propagation on reefs . . . 11
2.2.3 Wave dissipation . . . 16

3 Objectives and thesis outline **21**
3.1 Research objective . . . 21
3.2 Research questions . . . 21
3.3 Thesis outline . . . 21

4 Field site **23**

5 Reef Structure **25**
5.1 Structure for motion . . . 25
5.1.1 Data collection reef . . . 25
5.1.2 Creating digital elevation model (DEM) . . . 26
5.1.3 Determining vegetation parameter . . . 28

6 Calibration of drag coefficient **29**

7 Numerical simulation **33**
7.1 Methodology . . . 33
7.1.1 Data collection . . . 33
7.1.2 Xbeach . . . 34
7.1.3 Model formulation . . . 34
7.2 Model setup . . . 35
7.2.1 Bathymetry . . . 35
7.2.2 Computational grid . . . 36
7.2.3 parameter settings . . . 36
7.3 Input selection . . . 36
7.3.1 Boundary conditions . . . 36
7.3.2 Scenarios . . . 37
7.4 Output selection . . . 38
7.5 Post-Processing . . . 39

8 Results **41**
8.1 IG wave height . . . 41
8.2 Wave energy . . . 43
8.3 IG runup . . . 44

9 Discussion **49**

10 Conclusion & Recommendations **53**
10.1 Conclusion 53
10.2 Recommendations 54

11 Bibliography **57**

I Appendix **64**

12 Appendix A 'parm.file' **64**

13 Appendix B Results DEM **67**

14 Appendix C Sensitivity analysis **74**

15 Appendix D Wave propagation **78**
15.1 IG wave height 78
15.2 Dissipation due to waves breaking and vegetation 81
15.3 IG runup timeseries 86

List of Figures

1 Evolution of coral reefs from a volcanic island into a Atoll reef according to Darwin (Webb, 2020) . . . 3
2 Different reef zone in cross shore section (Bruckner, 2011) . . . 4
3 Reproduction of coral. The black arrows show the reproduction of broadcast spawning, the blue arrows show the reproduction of Brooder corals and the red arrows show the A-sexual reproduction of corals. Adapted from (Bruckner, 2011) . . . 6
4 (a) healthy corals, (b) bleached corals, (c) death corals [The Ocean Code, 2019] . . . 6
5 Energy spectrum for different types of waves (Munk, 1951) . . . 8
6 (a) The merging of two wave trains of slightly different wave lengths, but the same amplitude. (b). The two wave trains form wave groups and induce a long bound wave. Modified from Open University (Houthuys et al., 1994) 9
7 Generation of a bound long wave by a moving breakpoint (Pearson, 2016) . 10
8 The total runup against a beach is shown left and the different components, setup, IG swash and incident swash are shown right (Pearson, 2016) . . . 13
9 Effect of depth of submergion on the flow over a canopy adapted from (Roelvink, 2019) . . . 18
10 (a) shows the Whitehouse resort, (b) shows picture of the debris on the beach and [google earth] (c) shows a closeup of the sediment on the beach [google earth] . . . 23
11 Location of the where the wave data shown in figure 11 is collected (Chawla et al., 2013) . . . 23
12 Wave height, Peak period and Wave direction from data point show in figure 11. Data collected from (Chawla et al., 2013) . . . 23
13 (a) Boad with a single beam echo sounder attached to a pole (b) Drone with a camera attached. A drone like this was used to create underwater images of the reef. (c) Ground control point at the location where the images were taken by a diver (Daly and Nienhuis, 2018) . . . 26
14 Locations of the SfM surveys [google earth] . . . 26
15 Method used to process reef images into a DEM, using Agisoft Metashape . 27
16 Steps used in photo processing to get bv an N from images. (a) shows the original images, (b) shows the smooth images and (c) is used to calculate the stems (Daly and Nienhuis, 2018) . . . 28
17 Location of coral and sea-grass on transects 2 . . . 29
18 Location and names of the pressure sensors [google earth] . . . 30
19 Observed vs measured data from part 1 of the calibration for different coral drag coefficients . . . 31
20 root-mean-square error [-], bias [-] and Scatter index [-] for part 1 of the calibration . . . 31
21 Observed vs measured data from part 2 of the calibration for different coral drag coefficients . . . 31
22 root-mean-square error [-], bias [-] and Scatter index [-] for part 2 of the calibration . . . 32
23 Study area. The red dots indicate the location of the pressure sensors and the blue squares represent the location of the structure for motion surveys. The red lines show the locations of transect 1, 2, 3 and 4 (Daly and Nienhuis, 2018) . . . 33
24 Bed profile of transect 1,2,3 and 4. The transects are perpendicular to the coast line and X is positive towards the shore. . . . 36

25 Location of coral and sea-grass along the 4 different transects 38
26 Average low frequency (IG) wave height [m] for scenario S, S2, S3 and S4. Transect 1 41
27 Average low frequency (IG) wave height [m] for scenario S, S2, S3 and S4. Transect 2 42
28 Average low frequency (IG) wave height [m] for scenario S, S2, S3 and S4. Transect 3 42
29 Average low frequency (IG) wave height [m] for scenario S, S2, S3 and S4. Transect 4 42
30 Average wave energy [Nm/m^2] for scenario S1, S2, S3 and S4. Transect 1 . 43
31 Average wave energy [Nm/m^2] for scenario S1, S2, S3 and S4. Transect 2 . 43
32 Average wave energy [Nm/m^2] for scenario S1, S2, S3 and S4. Transect 3 . 44
33 Average wave energy [Nm/m^2] for scenario S1, S2, S3 and S4. Transect 4 . 44
34 Average IG runup and $R_{2\%}$ for scenario S, S2, S3 and S4. Transect 1 45
35 Average IG runup and $R_{2\%}$ for scenario S, S2, S3 and S4. Transect 2 46
36 Average IG runup and $R_{2\%}$ for scenario S, S2, S3 and S4. Transect 3 46
37 Average IG runup and $R_{2\%}$ for scenario S, S2, S3 and S4. Transect 4 47
38 Acropora hyacinthus coral 49
39 parm.file Xbeach part 1 64
40 parm.file Xbeach part 2 65
41 parm.file Xbeach part 3 65
42 parm.file Xbeach part 4 66
43 Reef structure on location SfM_4 67
44 Reef structure on location SfM_5 68
45 Reef structure on location SfM_6 69
46 Reef structure on location SfM_7 70
47 Reef structure on location SfM_8 71
48 (a) DEM results from the structure for motion survey processed in Agisoft Metashape, for location SfM_4. (b) Adjusted DEM (c) slope 72
49 (a) DEM results from the structure for motion survey processed in Agisoft Metashape, for location SfM_5. (b) Adjusted DEM (c) slope 72
50 (a) DEM results from the structure for motion survey processed in Agisoft Metashape, for location SfM_6. (b) Adjusted DEM (c) slope 72
51 (a) DEM results from the structure for motion survey processed in Agisoft Metashape, for location SfM_7. (b) Adjusted DEM (c) slope 73
52 (a) DEM results from the structure for motion survey processed in Agisoft Metashape, for location SfM_8. (b) Adjusted DEM (c) slope 73
53 water level (z_0) [m], water depth (h) [m], tidal level (tide) [m], wave height (H_{m0}) [m] and peak period (T_p) [s] data from offshore pressure sensor $OSSI_{WH01}$ 74
54 The red centre line denotes the median value (50th percentile) The blue box marks the 25th to 75th percentiles, while black whiskers mark the 5th and 95th percentiles. 76
55 Influence of the vegetation height, stem thickness, drag coefficient and vegetation density respectively on the runup 77
56 Influence of the Stem thickness, stem thickness, drag coefficient and vegetation density respectively on the runup 77
57 Influence of the drag coefficient, stem thickness, drag coefficient and vegetation density respectively on the runup 77
58 Influence of the vegetation density , stem thickness, drag coefficient and vegetation density respectively on the runup 77

59 Propagation of the low frequency wave height [m] for scenario S, S2, S3 and S4. Transect 1 78
60 Propagation of the low frequency wave height [m] for scenario S, S2, S3 and S4. Transect 2 79
61 Propagation of the low frequency wave height [m] for scenario S, S2, S3 and S4. Transect 3 79
62 Propagation of the low frequency wave height [m] for scenario S, S2, S3 and S4. Transect 4 80
63 Dissipation due to waves breaking [W/m^2] for scenario S, S2, S3 and S4. Transect 1 81
64 Dissipation due to vegetation [W/m^2] for scenario S, S2, S3 and S4. Transect 1 82
65 Dissipation due to waves breaking [W/m^2] for scenario S, S2, S3 and S4. Transect 2 82
66 Dissipation due to vegetation [W/m^2] for scenario S, S2, S3 and S4. Transect 2 83
67 Dissipation due to waves breaking [W/m^2] for scenario S, S2, S3 and S4. Transect 3 83
68 Dissipation due to vegetation [W/m^2] for scenario S, S2, S3 and S4. Transect 3 84
69 Dissipation due to waves breaking [W/m^2] for scenario S, S2, S3 and S4. Transect 4 84
70 Dissipation due to vegetation [W/m^2] for scenario S, S2, S3 and S4. Transect 4 85
71 IG runup for scenario S, S2, S3 and S4. Transect 1 86
72 IG runup for scenario S, S2, S3 and S4. Transect 2 87
73 IG runup for scenario S, S2, S3 and S4. Transect 3 87
74 IG runup for scenario S, S2, S3 and S4. Transect 4 88

List of Tables

1 Accuracy of the SfM results . . . 28
2 Vegetation parameter results from the DEMs and photo processing . . . 28
3 Input parameters for coral and sea-grass: vegetation height ($ah[m]$), stem thickness ($bv[m]$), vegetation density ($N[corals/m^2]$), Drag coefficient ($Cd[-]$) 29
4 Offshore wave height and peak period for different simulations . . . 37
5 Vegetation input, vegetation height (ah) [m], stem thickness (bv) [m], . . . 38
6 X-locations of the point output and the runup gauge for each of the four transects. The locations are positive onshore . . . 39
7 Maximum increase in IG wave height for each transect . . . 41
8 Maximum increase in total wave energy for each transect . . . 43
9 Maximum increase in IG runup for each transect . . . 44
10 Maximum increase in IG $R2\%$ for each transect . . . 45
11 Maximum increase in setup for each transect . . . 45
12 Accuracy of the SfM results . . . 67
13 Standard input parameters for the sensitivity analysis . . . 75
14 Results of the sensitivity analysis for water level [m]. The table shows the water level when each of the four vegetation parameters are increased. It also shows the water level decrease in %, where - means there is an increase. This decrease is compared to the previous simulation . . . 75
15 Results of the sensitivity analysis for wave height [m]. The table shows the wave height when each of the four vegetation parameters are increased. It also shows the wave height decrease in %, where - means there is an increase. This decrease is compared to the previous simulation . . . 75
16 Results of the sensitivity analysis for dissipation due to vegetation [W/m^2]. The table shows the dissipation due to vegetation when each of the four vegetation parameters are increased. It also shows the dissipation due to vegetation decrease in %, where - means there is an increase. This decrease is compared to the previous simulation . . . 76
17 Results of the sensitivity analysis for runup [m]. The table shows the runup when each of the four vegetation parameters are increased. It also shows the runup decrease in %, where - means there is an increase. This decrease is compared to the previous simulation . . . 76

Nomenclature

a_v	vegetation height
b_v	stem thickness
C_D	bulk drag coefficient
D_f	dissipation due to bed friction
D_v	dissipation due to vegetation
H_{rms}	root-mean-square wave height
N	vegetation density
η	setup
ω	radial frequency of the low-frequency waves
ρ	water density
τ_b	mean bottom stress
C_d	drag coefficient
c_g	wave group velocity
d	time-averaged still water depth
D_w	dissipation due to waves breaking
D_{br}	wave-breaking dissipation
E	wave energy density
E_r	kinetic energy of the wave roller
g	gravitational acceleration
h	water depth
h_x	bed slope
H_{rms}	root-mean-square wave height
P	Pressure
Q_b	fraction of waves breaking
$R_{2\%}$	runup
R_{xx}	radiations stress
S_IG	infra-gravity swash
S_inc	sea-well swash
S_{xx}	crossshore component of the wave radiation stress tensor
$T_{(N,n)}$	the resonant (or natural) period
u	stream-wise velocity
x	cross-shore coordinate

1 Introduction

1.1 Motivation

Coral reefs near the coast of Jamaica are degrading at an alarming rate due to climate change and human activities. Between 1980 and 1990 Jamaica had faced a series of natural and man-made disasters, which resulted in an 85% loss in the country's coral reefs. The ones vibrant coral reefs that provided an ecosystem for many fish species have turned form wave-resistant structures into degraded coral communities with little biodiversity (Goreau and Hilbertz, 2012).

Reefs are important because they protect low-altitude coastal areas against wave runup, flooding and erosion, by dissipating wave energy at some distance from the shoreline (Quataert, 2015).

Waves propagation across reefs differs significantly from waves propagation across sandy coasts due to the complex and steep bathymetry of reefs and high roughness (Sous et al., 2019). Determining how incoming wave energy is transferred over reefs towards the beach depends on the reef topography, roughness, incoming wave features and water level (Symonds et al., 1995).

Wave breaking is the dominant wave energy dissipation on sandy coast, whereas frictional dissipation is dominant on reef lines coast.

Recent studies show the importance of low frequency or infragravity waves in reef hydrodynamics (Van Dongeren et al., 2013) (Pomeroy et al., 2012). (Van Dongeren et al., 2012) showed that short waves with a frequency between 0.04 and 0.2 Hz dominate on the fore-reef and near the reef crest, while inside the lagoon the infragravity waves with frequencies between 0.005 and 0.04 [Hz] become increasingly dominant, accounting up to 50% of the combined bottom stresses (Zijlema, 2012). (Young, 1989) found that even with the dissipation of short waves, significant infragravity energy remains across the reef.

The complex bathymetry and hydrodynamics of reef lined-coast make risk assessments difficult and expensive (Quataert, 2015). Better insight into the effect of coral reef degradation on the hydrodynamic processes can help stakeholders such as governments, engineering companies and citizens to make informed decisions, to reduce the risk of coastal hazards and protect the coast area in Jamaica against the dangers of sea-level rise and flooding.

2 Background

2.1 Coral reefs

2.1.1 Morphology

Coral reefs originate from coral larvae that attach themselves to a piece of land and start to grow. The skeletons of the coral reefs are essentially built of limestone and have a growth rate of a few millimetres per year (NOAA, 2020). Based on their geo-morphological characteristics, coral reefs can be divided into three distinct groups: fringing reefs, barrier reefs, and atolls (Smithers, 2011)

Fringing reefs are the youngest and most common type of reefs that grow directly along the coast, surrounding the island. This is also the type of reef that is found in Jamaica. Fringing reefs are characterized by steep slopes at the reef crest that transition into a shallow reef flat (Koehl and Hadfield, 2004) and are sometime separated from the island by shallow and narrow lagoons. Over time, the space between the reef and the coastline increases due to sea-level rise, erosion, and land subsidence. As the reef continues to grow, the fringing reef develops into a barrier reef (Smithers, 2011).

Barrier reefs are usually older structures located parallel to the shoreline, with a large lagoon separating the reef from the coast (NOAA, 2020). The lagoon of a barrier reef can be several kilometres wide and up to 70 metres deep. Smaller barrier reefs are often circular, surrounding an island or landmass. Larger barrier reefs can form complex linear features comprising chains and reef patches elongated into ribbon reefs (Bertin et al., 2018). If the island continues to subside and is no longer visible above the sea level, we get the last successive state of reef evolution, the atoll (Woodroffe and Biribo, 2011).

An atoll is a ring-shaped coral reef that surrounds a body of water (lagoon). The atoll protects the habitat inside the lagoon from the open sea. However, the low coral elevation makes the habitat inside the lagoon susceptible to changes in hydrodynamic forces and sea-level rise (Storlazzi et al., 2018). This means that the coral growth must keep up with the relative sea-level rise for an atoll to persist (Erickson and Kusky, 2009).

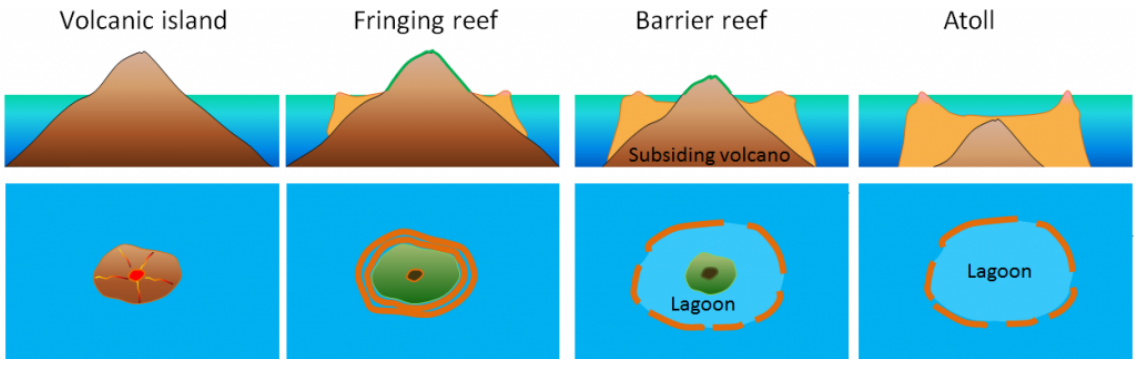

Figure 1: Evolution of coral reefs from a volcanic island into a Atoll reef according to Darwin (Webb, 2020)

2.1.2 Structural zones

Different structural zones can be recognized in the coral ecosystem. The reef flat (lagoon and back reef), reef crest and fore reef. These zones are based on the location within the reef and characteristics such as wave action, water depth, light intensity, temperature and water chemistry (Bruckner, 2011). Each zone has their own effect on the wave transformation and the zones are physically and ecologically interconnected. The zones vary depending on the type of reef (Moyle and Cech, 2004).

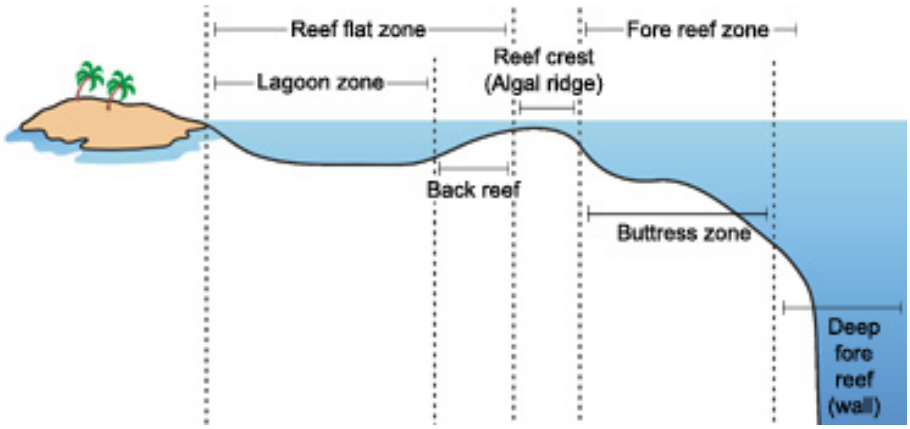

Figure 2: Different reef zone in cross shore section (Bruckner, 2011)

Reef flat

On fringing reefs, the reef flat is along the coastline. The width of the reef flat can range from a few metres to a few kilometres and depths range from a few centimetres to a few metres (Block, 2008). The low water depths cause fluctuations in temperature, salinity and exposure to air during low tide and makes this a tough place for coral to live. In order to survive in this area, the corals must adapt to the harsh environment. This causes the variety of corals in this area to be lower compared to other areas in the reef. Despite the tough environmental conditions, corals in this area are protected from wave breaking action by the reef crest (NOAA, 2020).

For barrier reefs, the reef flat is divided in a lagoon and back reef. The lagoon is similar to the reef flat but with larger water depths ranging from a view metres to 60 metres (King and Schwartz, 2019). The back reef is the area that slopes into the lagoon. Like the lagoon, this area is sheltered from the wave action by the reef crest (Moyle and Cech, 2004).

Reef crest

The reef flat extent out to the highest part of the reef, called the reef crest. This is the area that receives the most impact from wave energy due to breaking of incoming waves. The reef crest is close to the water surface and can even reach above the surface during low tide. The coral in this area receive large amounts of sunlight because of the high altitude of the reef crest (Block, 2008). A limited amount of organisms can live in this area due to the harsh conditions. The corals that live in this area are usually dominated by stoutly branching coral that are made of calcium carbon. The coral grow closely together to strengthen the structure (NOAA, 2020).

Fore reef

On the ocean side, the reef crest turns into the fore reef. The fore reef extends from the low-tide point into the deep water and is characterized by a steep slope that can sometimes form a vertical wall called a drop-off (NOAA, 2020). A great coral diversity is found at depths of 5 to 20 metres due to the high light exposure and low wave action in this area. Spurs (shore-normal ridges of coral) and groove (shore-normal patches sediment) formations occur in the upper part of the fore reef from the low-tide mark to about 20 metres deep. This system of spurs and grooves are primarily present in wave-dominated areas and help to both drain debris and sediment away from the reef into the deep water, and migrate the force of incoming waves back into the open sea(Munk and Sargent, 1954).

2.1.3 Forming of coral reef

The reproduction of corals can be a-sexual or sexual. A-sexual reproduction appears when coral fragments break from adult coral branches, settle somewhere else and grows further. This is often the result of external disturbances, such as fisheries or storms (Network, 2010).

Sexual reproduction is the most common form of coral reproduction. An important aspect of sexual reproduction is coral recruitment, which refers to the settlement of larvae. There is a difference in the recruitment of broadcast spawning corals and brooder corals. The former goes as follows:

1. To start with, mature corals produce gametes (eggs and sperm) through meiosis. The produced gametes are released into the water by the mature coral when the environmental conditions are right.
2. After this, the gametes will float towards the water surface where external fertilization takes place.
3. The fertilized egg, called a zygote, starts to drift in the current.
4. Next, the zygote undergoes cell division (mitosis). During this process the zygote divides into two cells, then four and so on, until an embryo forms.
5. The embryo keeps on developing and become a larva called a planula. The body of the planula is microscopic and is covered by small thread-like appendages called cilia. The cilia help the planula move through the water but are not strong enough to move against the current.
6. After some time the planula settles on the sea bed and the organism start to develop from a juvenile to either a sexual or an a-sexual adult coral (Leal et al., 2016).

The recruitment of brooder corals is a little different. Brooder corals maintain the egg while obtaining sperm from the water and fertilization takes place within the brooder coral. The brooder planula is then released to the water column. After the planula is released, it undergoes the same process as the broadcast spawning coral (step 5 & 6) (Leal et al., 2016). Figure 3 shows the recruitment of both broadcast spawning and brooder corals, and a-sexual coral reproduction.

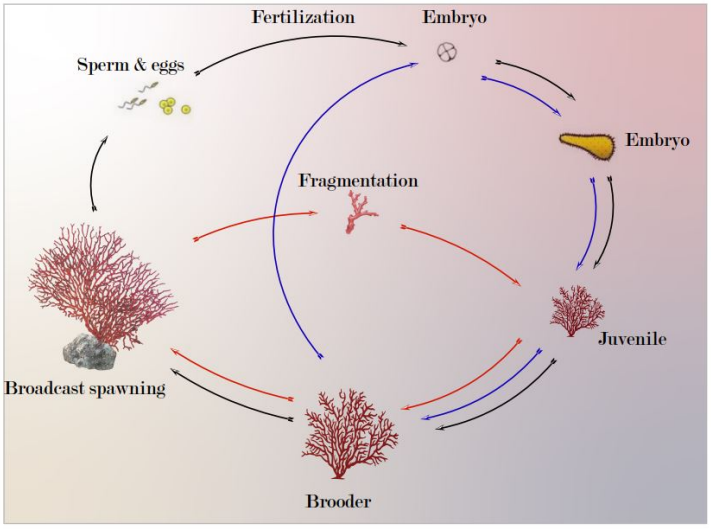

Figure 3: Reproduction of coral. The black arrows show the reproduction of broadcast spawning, the blue arrows show the reproduction of Brooder corals and the red arrows show the A-sexual reproduction of corals. Adapted from (Bruckner, 2011)

2.1.4 Degradation of coral reef in Jamaica

Coral reefs in Jamaica are degrading at an alarming rate (Nyström et al., 2000). Over population, fisheries, climate change and natural disasters cause a 50% decline in coral communities since 1970 (Aldred, 2014). (Plass-Johnson et al., 2015) showed that by 2005, up to 95% of the corals were bleached in different locations in Jamaica.

Coral bleaching appears when single-celled algae called symbiotic zooxanthellae are released from their coral organism due to stress caused by an increase in sea-water temperature or pollution. This makes climate change the driving factor of coral bleaching (Phinney et al., 2006). Coral bleaching leaves the corals with a white cast. However, bleached corals are not necessarily dead. Corals can recover and regain their vibrant colors when water temperatures decrease. However, when the temperatures keep increasing, the coral die completely as shown in figure 4.

Figure 4: (a) healthy corals, (b) bleached corals, (c) death corals [The Ocean Code, 2019]

When corals get bleached or die, their structural complexity can change. The structural complexity of corals can be defined as the physical 3-dimensional structure of coral branches or coral reefs (Jones et al., 1994). Corals with a high structural complexity are

found to dissipate larger amounts of wave energy compared to corals with low structural complexity, thus better protecting reef lines coast from wave impact (Nelson, 1994).

Corals that die do not automatically lose structural complexity. If dead corals are left undisturbed in areas with low wave- and human impact, the corals structures will remain intact. Structural complexity is only lost when erosion, due to environmental or human impact, occurs (Graham and Nash, 2013).

Human impact can form an even bigger threat than climate change. The coral reefs in Jamaica used to be the home of 135 different species of fish (Klomp et al., 2003). Fish are important for the maintenance of the reef, because they keep the algae level in check. With fishing being the primary source of income for around 69% of the inhabitants of Jamaica, over fishing is a huge problem in Jamaica. It caused a reduction in biomass of 80% between 1980 and 2000 (Klomp et al., 2003).

2.2 Reef Hydrodynamics

2.2.1 Wave generation

In order to predict the wave transformation over a reef area, it is important to know how waves are generated. Ocean waves are commonly generated by wind induced friction between the air and surface water. This friction causes a disturbance of the sea surface that results in oscillatory waves, also known as short free surface waves (Lowe et al., 2005).

Waves can be classified into different groups based on their frequency, period, and generation method, as shown in figure 5. The three most commonly used wave groups are: sea-swell waves, infragrafity waves (IG waves), and very low frequency waves (McDonald et al., 2006). The very low frequency waves are outside the scope of this project and will therefor not be elaborated.

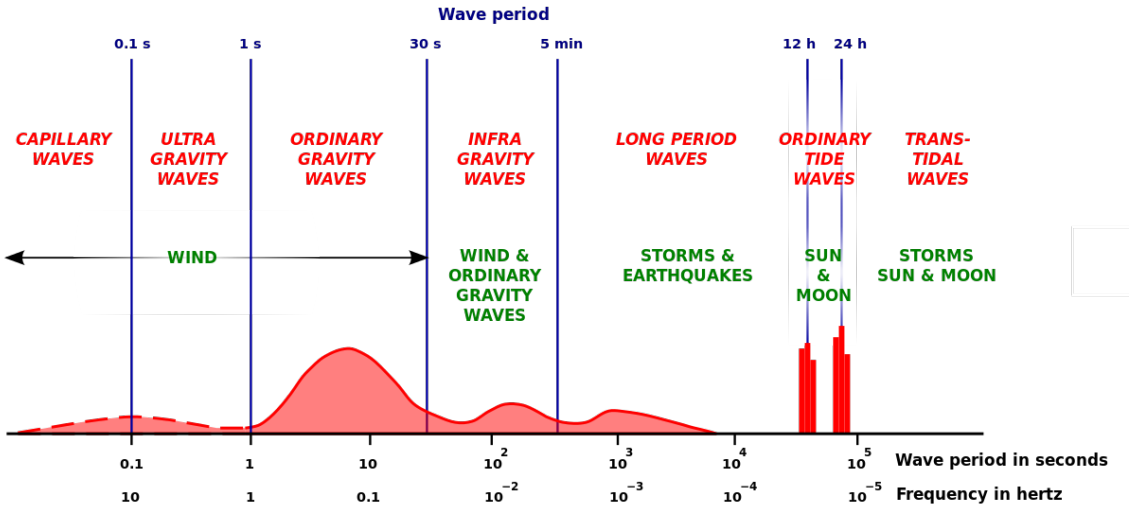

Figure 5: Energy spectrum for different types of waves (Munk, 1951)

Sea-swell waves

Sea-swell waves are also known as short waves and typically have high frequencies between 0.04 and 1 Hz (Nepf and Vivoni, 2000). Waves that are generated out of wind fields by low-altitude storms and far away from the shore are known as swell waves. During propagation towards the shore, swell waves behave monochromatic and transform from relative short and steep waves with wave a steepness of (L/H=20 [-]) and wave a period of (T=5 to 10 [s]) to relative long and flat waves (L/H=100 [-], T=10 to 30 [s]) (McDonald et al., 2006).

Sea waves are generated by local winds and tropical cyclones (Nepf and Vivoni, 2000), and can be described as sinusoidal waves with different directions, amplitudes, frequencies and phases (Munk et al., 1963).

Infragravity waves

IG waves are surface gravity waves with a frequency lower than wind-generated 'short waves'. IG waves typically have frequencies between 0.004 and 0.04 Hz, thus not corresponding with the part of the wave spectrum that is directly generated by wind forcing (Nepf and Vivoni, 2000). The wavelength of IG waves are longer than short waves, ranging from a few hundred metres to kilometres, whereas short waves typically have wavelengths ranging from a few metres to hundreds of metres (Nepf and Vivoni, 2000). When coupled

with high offshore water levels, IG waves can lead to over-swash at the beach. This can make areas more vulnerable to flooding (Cheriton et al., 2016).

IG waves can either appear as 'free' or 'bound' (Nepf, 2012). The two primary mechanisms that influence the generation of IG waves on a reef are the propagation of bound IG waves and the generation of IG waves by break point forcing (Pomeroy et al., 2012).

Bound IG waves

The generation of bound IG waves is linked to the phase-coupling (grouping) and non-linear interaction between short waves with similar frequencies. When two short wave trains with similar wavelengths and frequencies are in phase, the amplitudes are added. Similarly, when they are out of phase, the amplitudes damp each other out. This results in a radiation stress gradient that generates a third, irregular wave group structure. When the generated wave group structure is 180 degrees out of phase with the short wave group, a so-called bound IG wave is generated as shown in figure 6 (Herbers et al., 1995a). Bound IG waves can be generated in the open ocean where they are only a few centimetres in height and are stronger in high energy swell conditions (Herbers et al., 1995a) (Van Dongeren et al., 2003).

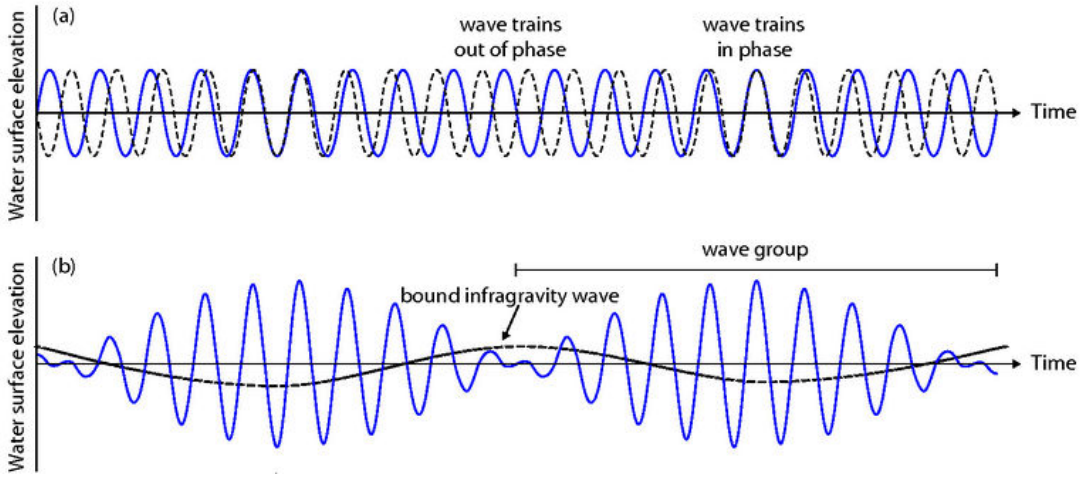

Figure 6: (a) The merging of two wave trains of slightly different wave lengths, but the same amplitude. (b). The two wave trains form wave groups and induce a long bound wave. Modified from Open University (Houthuys et al., 1994)

Moving break-point

The second IG wave generation mechanism is moving break-point location (the location where short waves break). The wave height of incident sea-swell wave change when they group together. As a result, the break-point location changes as well. (Symonds et al., 1982) proposed that freely propagating IG waves are generated as dynamic setup/down oscillations due to the fluctuating break-point of different sized wave groups.

The steepness and groupiness of incident wave groups determines the efficiency of the break-point mechanism (Evans and Jones, 2002) (Baldock, 2012). The groupiness of incident waves causes a variation in break-point location on a time scale of the wave group.

The break-point location also depends on the wave height relative to the water depth. Lower waves tent to break in shallow water closer to the shore, whereas higher waves tent to break in deeper water further offshore.

The maximum and minimum cross-shore location of the break-point determines the surf zone width and thus the setup. Waves breaking cause a momentum loss, that is compensated by a shore-wards water level increase (wave setup). Hence, the horizontal movement of break-point location causes fluctuation in the wave setup with frequencies similar to the incident wave groups (Symonds et al., 1982).

The mechanism of break-point forcing generates two IG waves as shown in figure 7. The first IG wave is a set-down wave that travels seawards in anti-phase with the wave group. Amplitudes of set-down waves depend on the beach slope, group frequency and mean break-point location (Symonds et al., 1982). The second IG wave is a setup wave, propagation shore-ward in phase with the wave group. The amplitude of this wave is relatively insensitive to incident wave height. Both waves have the same frequency as the wave group and originate at the sea-swell wave break-point (Symonds et al., 1982)

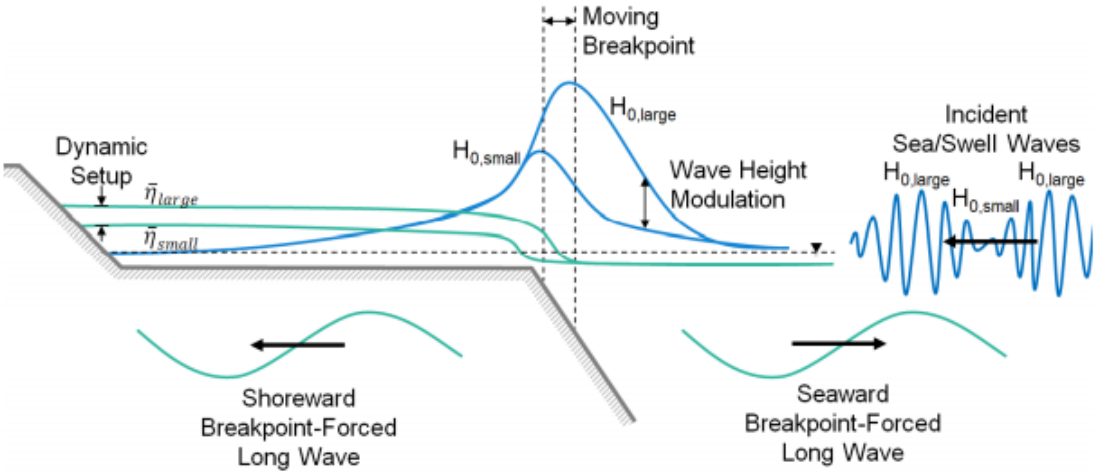

Figure 7: Generation of a bound long wave by a moving breakpoint (Pearson, 2016)

Bound long waves are dominant on mild sloping beaches and break-point forcing is dominant on steeper beaches (Van Dongeren et al., 2007)(Battjes et al., 2004). The steep reef crest makes that break-point forcing is an important mechanism on reef profiles.

Free IG waves

When incident short and bound IG waves reach shallow water and enter the surf-zone, they lose their group structure due to breaking and will propagate to the shore as free IG waves. When the free IG waves are released, they are reflected on the beach and radiate seawards into deep water "leaky mode", or the free IG waves get trapped in the surf zone and become an "edge wave". (Herbers et al., 1995b) found that although both bound and free IG energy levels increase with decreasing water depth and increasing short waves energy, free IG waves generally dominate the IG frequency band (Herbers et al., 1995b).

2.2.2 Wave transformation and propagation on reefs

Obtaining a good understanding of the influence of coral degradation on wave transformation requires a good understanding of wave transformation as waves propagate from the deep ocean, across a reef platform, towards the shore (Gourlay, 1992). Wave transformation across reefs is complex and includes processes of shoaling, breaking, energy dissipation, refraction and reflection (Monismith, 2007). This section describes the wave transformation and propagation over coral reef from offshore towards the beach.

Shoaling zone

When ocean waves travel from the open ocean, over a reef, to the shore, they first face the reef front. Here, waves enter the shoaling zone, where linear and non-linear wave processes transform the wave characteristics (Eldeberky, 1997). Due to the steep slope of the reef front, the waves start to interact with the rough bottom and slow down as the water depth decreases. The waves do not lose energy at this point. The decrease in wave group velocity is compensated with an increase in wave height, a process known as shoaling (Gourlay, 1994). The shoaling of waves can be defined as the change in wave properties such as wave height, length and celerity by the propagation of waves from deeper water into shallower water (Gourlay, 1994). During the shoaling process the wave peak is steepened and the wave through is flattened because of the generation of higher wave harmonics.

Breaker zone

When waves propagate through the shoaling zone, the wave height increases until the waves break. This is the point where the waves enter the breaker zone. In this region individual short waves lose energy due to breaking and long waves are generated due to moving break point (section 2.2.1) or the generation of bound long waves (section 2.2.1) (Symonds et al., 1982).

Most waves break on the steep fore reef and reef crest when propagation towards the shore. The breaking limit γ is used in shallow water to determine at what water depth wave breaking occurs, following:

$$\gamma = \frac{H}{h} \tag{1}$$

Equation 1 shows the relative submersion of the reef where H is the wave height at breaking point (Symonds et al., 1982).

Due to the abrupt change in water depth from deep water to the near horizontal reef flat, there is a great variation in γ. (Vetter et al., 2010) found values for y between 0.9 and 1.1 near the reef crest and values of y between 0.12 and 0.22 on the reef flat for fringing reefs. Research also showed that the incident wave height played a role in the magnitude of γ. Larger incident wave heights caused larger values of γ. (Young, 1989) found the breaking limit to be higher for higher slopes.

Surf zone

After the beaker zone, the waves enter the surf zone . The surf zone is an important region within coral reef zones that is usually located inside the lagoon. The roughness of the coral reefs have a profound effect on the near-shore hydrodynamics due to the shallow water levels inside the lagoon (Franklin et al., 2013). (Svendsen, 1984) found that the surf

zone can be divided into three regions: (1) the outer surf zone, (2) the inner surf zone and (3) the swash zone.

The outer surf zone is characterized by a constant setdown and a rapid change in wave shape due to the development of the surf roller. In this zone the potential energy of the waves is transformed into kinetic energy, leading to a decrease in wave height, but not to a significant change in momentum flux (Svendsen, 1984).

When the waves propagate into the inner surf zone, wave setup and the dissipation of wave energy starts. Furthermore, a seawards undertow is created and the wave roller that developed in the outer surf-zone continues to travel landwards and becomes a bore (breaking wave front, resembling to a hydraulic jump) (Svendsen, 1984)

After the inner surf zone, the waves move into the swash zone. This is the zone where runup and rundown occurs and is marked by an up-rush of water against the beach face after waves have broken. The swash zone moves as water levels vary (Svendsen, 1984).

Runup

The wave runup can be defined as the vertical distance between the still water level (SWL) and the maximum height reached by the up-rush of waves breaking on a beach or structure (Gourlay, 1994), and is often used to predict coastal inundation and extreme water levels (Rey, 2019).

(Stockdon et al., 2006) described the runup by dividing it into three different components: (1) setup η, (2) infra-gravity swash (S_{IG}), and (3) sea-well swash (S_{inc}). There currently is no empirical formula to predict runup on reef. The theory of (Stockdon et al., 2006) is based on data derived from 10 field experiments on sandy beaches, under different environmental conditions. This resulted in the following empirical relationship:

$$R_{(2\%)} = 1.1 \left[\bar{\eta} + \frac{S}{2} \right] \tag{2}$$

where,

$$\bar{\eta} = 0.35\beta\sqrt{H_0 L_0}$$
$$S = \sqrt{(S_{inc})^2 + (S_{IG})^2}$$
$$S_{inc} = 0.75\beta\sqrt{H_0 L_0}$$
$$S_{IG} = 0.06\sqrt{H_0 L_0}$$

Where β is the beach slope $\bar{\eta}$ is the time-averaged water level elevations at the shoreline (i.e. setup), H_0 is the deep water wave height, L_0 is the wave length, S is the total swash, S_{IG} is the IG swash and S_{inc} the incident swash (Stockdon et al., 2006) as shown in figure 8. The runup is commonly expressed as $R_{2\%}$, which shows the runup level that is exceeded by 2% of the waves. The relative contribution of each component to the total runup depends on the local bathymetry and offshore wave condition (Bertin et al., 2018).

Swash is the turbulent layer that washes up against the beach, while setup is static at short wave timescale. IG swash is an important mechanism at the beach, because IG waves dominate at the reef flat. IG swash can be caused by IG waves breaking or due to a water level change caused by the reflection of an IG wave on the beach (Baldock et al., 1998) (Raubenheimer et al., 1995). (Guza and Feddersen, 2012) established that IG

swash increases with increasing frequency spread and decreases with increasing directional spread.

Incident swash is caused by the collapse of a bore. Incident waves lose most of their energy due to breaking. The remaining energy forms a bore and travels to the shoreline where the bore and backwater accelerate and collapses. This collapse causes the potential energy to be transferred into kinetic energy, resulting in an up-rush of water against the beach (incident swash) (Beyer, 1994).

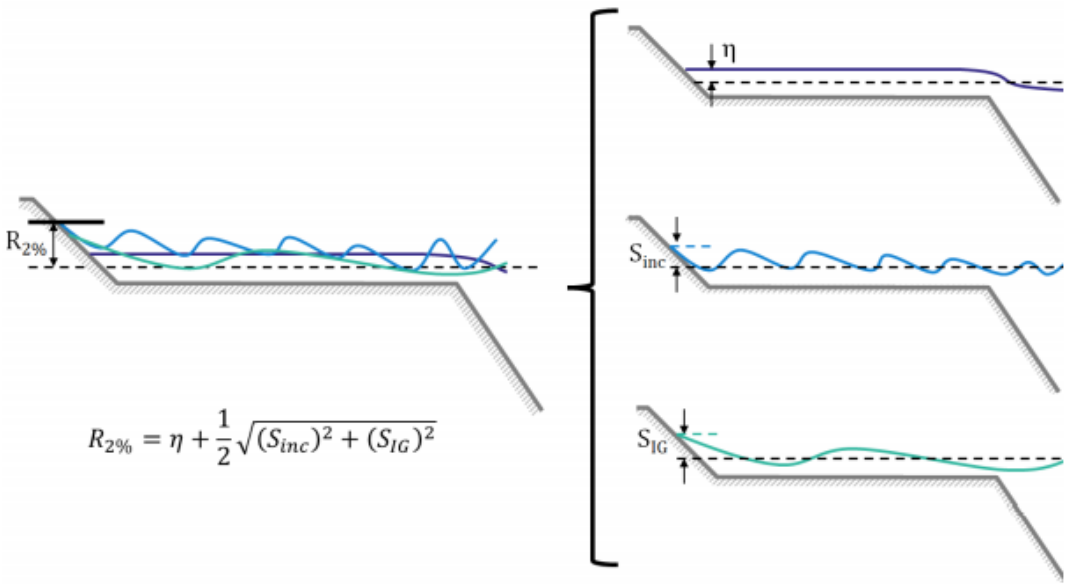

Figure 8: The total runup against a beach is shown left and the different components, setup, IG swash and incident swash are shown right (Pearson, 2016)

Setup

Wave setup is defined as the increase in mean water level (MWL) due to waves breaking (Gourlay, 1996). The breaking of waves causes an increase in radiation stress, which is balanced by a change in hydrostatic pressure i.e. by a change in MWL (Pearson, 2016). The maximum setup occurs at the intersection of the MWL and the beach face (Gourlay, 1992).

Similarly, the wave setdown is defined as the decrease in MWL during the process of shoaling (before the waves break). As the waves travel towards the shore, setdown occurs because the increasing wave trust is balanced by a change in hydrostatic pressure. This causes a decrease in MWL (Gourlay, 1996). The maximum setdown occurs near the breakpoint.

Linear wave theory

The principle of setup on reefs is similar to setup on sandy beaches. The main difference is the increased bottom roughness caused by reefs, which contributes to the wave-averaged cross-shore momentum balance. (Buckley et al., 2015) described the wave averages cross-shore momentum balance for linear or non-breaking waves on an alongshore uniform reef as:

$$\frac{\partial}{\partial_x} S_{xx} + \rho g(\bar{\eta} + d)\frac{\partial}{\partial_x}\bar{\eta} + \tau_b \tag{3}$$

where the over bars denote time averaging over many wave periods, S_{xx} is the cross-shore component of the wave radiation stress tensor (Longuet-Higgins and Stewart, 1964), where x is the cross-shore coordinate (positive onshore), d is the time-averaged still water depth, ρ is the water density and τ_b is the mean bottom stress (Buckley et al., 2015). In order to solve S_{xx} analytically, all wave orbital motions above η are neglected. The mean dynamic pressure above η is approximated as being hydrostatic, and the mean dynamic pressure below η is taken as $-\rho\overline{w'^2}$ (w' is the vertical component of the wave orbital velocity) (Apotsos et al., 2007). Under these assumptions, S_{xx} can be formulated as:

$$S_{xx} = E\left(2\frac{c_g}{c} - \frac{1}{2}\right) \tag{4}$$

where,

$$E_w = \frac{1}{8}\rho g H_{rms}^2 \tag{5}$$

where E is the wave energy density, c_g is the wave group velocity, and c is the wave celerity (Buckley et al., 2015), H_{rms} is the root-mean-square wave height (defined as $2\sqrt{2}$ times the standard deviation of the sea-surface elevation fluctuations) (Apotsos et al., 2007).

The second term (pressure gradient) of equation 3 results from the cross-shore gradient in setdown and setup. The interaction between the wave-current velocity field and the bottom roughness generates the third term (time-averaged bottom stress) and can be formulated by using the quadratic law as (Grant and Madsen, 1979) (Feddersen et al., 2000) (Monismith, 2007):

$$\bar{\tau}_b = \rho C_d \overline{|u_b| u_b} \tag{6}$$

where C_d is an empirical bulk bottom drag coefficient, and u_b is the instantaneous cross-shore free-stream velocity above the bottom roughness.

Non-linear wave theory

The breaking of waves is an important mechanism for setup in coastal area. The non-linearity of the waves increases as waves propagate from deep water over the reef crest to the reef flat and beach (Monismith et al., 2015).

(Govender et al., 2002) found that plunging (non-linear) wave had higher velocities in the reef crest compared to non-breaking (linear) waves. This, together with the presence of wave rollers, results in an local increase in kinetic energy when the waves enter the surf-zone. Rollers can also creating a lag between the dissipation of wave energy and the transfer of momentum to the water column (Svendsen, 1984). Equation 3 is true for situations where wave rollers, breaking and shoaling of waves is neglected. The rollers adds an additional source of radiations stress R_{xx} (Svendsen, 1984), which modifies equation 3 to (Buckley et al., 2015):

$$\frac{\partial(S_{xx} + R_{xx})}{\partial_x} + \rho g(\bar{\eta} + d)\frac{\partial}{\partial_x}\bar{\eta} + \tau_b = 0 \tag{7}$$

Equation 7 is based on the non-linear wave theory. The shoaling and breaking of waves result in the generation of kinetic and potential energy which creates a radiation stress gra-

dient (Buckley et al., 2015). The wave roller travelling with the breaking waves contributes to the kinetic energy and radiation stress and can be calculated by:

$$R_{xx} = 2E_r \tag{8}$$

where E_r is the kinetic energy of the wave roller modelled using an approximate energy balance following (Stive and De Vriend, 1995):

$$\frac{\partial}{\partial_x}(2E_r c) = D_{br} - \bar{\tau}_t c \tag{9}$$

Where

$$D_{br} = -\frac{\partial}{\partial_x}(E_w c_g \cos\bar{\theta}) \tag{10}$$

where D_{br} is the dissipation due to waves breaking, and τ_t is the mean shear stress at the boundary between the turbulent wave roller and the underlying organized wave motion which is approximated as:

$$\bar{\tau}_t = \frac{2gE_r}{c^2}\beta_D \tag{11}$$

where $\beta_D = \sin\theta_r \cos\theta_r$ is a dissipation coefficient that depends on the angle θ_r of inclination of the boundary between the turbulent wave roller and the underlying organized wave motion (Dally and Brown, 1995).

Equation 8, 9, 10, and 11 show the wave roller theory and implies that during the breaking of waves the kinetic energy is transferred into potential energy after which there is a momentum exchange where the kinetic energy is dissipated by shear stress (Buckley et al., 2015).

Reflection

Almost all the wave energy dissipates on either the reef front of reef flat due to frictional dissipation or dissipation due to waves breaking. The small amount of wave energy that remains may be reflected offshore the reef crest or at the shore. The reflection is expressed by the reflection coefficient Kr. This coefficient compares the outgoing and incoming energy fluxes and wave heights and is determined by a combination of hydrodynamic and morphological factors. Kr =1 means all the incoming wave energy is reflected (Van Dongeren et al., 2007).

Incoming waves that are reflected at the beach can form standing wave patterns over the reef(Nwogu and Demirbilek, 2010). When these reflected waves reach the reef crest they can then be reflected again, changing their direction back to the shore. This pattern of double reflection can lead to the trapping of wave energy on the reef flat. (Péquignet et al., 2009) found that the reflection of waves on reefs depended on the wave period, wave height and wave steepness. Waves with larger periods, wave height and wave steepness showed more reflection compared to wave with a smaller period, wave height and wave steepness. (Yao et al., 2017) conducted laboratory experiment and found that the amount of wave reflected depends on the slope of both the fore reef and the beach, with an increasing reflection on a fore reefs with slopes steeper than 1:4 [-].

Resonance

The trapping of low frequency wave near the beach can lead to resonance. Resonance can be defined as the amplifying of wave energy due to matching of external forces to the natural frequency on the reef area (Cheriton et al., 2016) (Péquignet et al., 2009) (Pomeroy et al., 2012). On a fringing reef, the wave resonance is controlled by morphological properties and hydrodynamic conditions and mainly depends on the width and water depth of the reef flat. Due to the higher reef crest, a fringing reef can be seen as a semi-enclosed basin where resonance periods are often in the order of tens of minutes (Péquignet et al., 2009). In the presence of resonance, reefs can amplify small waves, making these areas more prone to flooding.

(Buckley et al., 2018) found that there are two conditions under which the incoming low frequency waves will be in phase with the low frequency waves trapped on the reef flat after reflection on the beach or reef crest. (1) The energy trapped at the reef flats must be high enough. Wave energy with nearly the same frequency as the natural frequency will not always induce resonance because energetic forcing of those waves are required (Péquignet et al., 2009). (2) standing low-frequency waves must have a node (fixed water level) at the reef crest. The natural frequency needs to have a specific node location that is determined by:

$$f_{node} = \frac{1}{4}(2n-1)\left(\int_{c}^{xshoreline} \frac{1}{\sqrt{gh(x)}}dx\right)^{-1} \tag{12}$$

$$T_{N,n} = \frac{1}{f_{N,n}} \tag{13}$$

where, $x_{shoreline}$ is the point of reflection at the shoreline, n is the number of nodes from the reflection point, h(x) is the still water depth + wave setup and $T_{(N,n)}$ is the resonant (or natural) period (Péquignet et al., 2009).

The morphological properties that influence and control the resonance on a reef are: reef width, water depth and roughness, and the dissimilar effect on each other. A wider reef results in a greater resonant amplification, but waves also experience more frictional dissipation, which causes damping of the natural frequencies. The reef width also influences which low frequency waves experience resonance. IG waves are more likely to be resonated on a reef flat with a width smaller than 300 metres (Shimozono et al., 2015), whereas VLF wave resonance is found to be dominated on reef flats with a width between 250 and 500 metres (Pearson, 2016).

2.2.3 Wave dissipation

This section explores the wave dissipation mechanisms. Wave energy dissipation on reefs can be caused by wave breaking and bottom friction. Wave breaking on reefs is explained in section 2.2.2. The energy dissipation due to friction is explained below.

Frictional dissipation

As mentioned in chapter 2.2.2, wave breaking is the dominant dissipation mechanism along the fore reef and reef crest. Across the reef flat and lagoon frictional dissipation is dominant (Nepf and Vivoni, 2000). Both flow structures inside the reef and flow over canopies have a significant effect on the large-scale hydrodynamics in reef lined coasts.

Flow through a coral colony

The hydrodynamics in and around reef organisms depend on complex interactions between bottom roughness and the motion of the overlying water column (Lowe et al., 2005). Understanding flow dynamics in canopies has proven to be very difficult due to the highly variable spatial flow structures that arise in coral branches (Monismith, 2007). The flow in and around the canopy is slowed down by the drag force above the canopy. The total drag is a combination of the skin friction caused by flow in and around the canopy and in form drag resulting from the roughness and shape of the canopy (Lowe et al., 2005). (Raupach and Shaw, 1982) used a Raynolds-averaged Navier-Stokes momentum equation on a horizontal plane to describe the flow in and above a canopy:

$$\frac{\partial < u >}{\partial t} = -\frac{1}{\rho}\frac{\partial < P >}{\partial_x} + \frac{1}{\rho}\frac{\partial_{\tau_{xy}}}{\partial_z} - f_x \tag{14}$$

where x is the stream-wise direction, z is the vertical direction, u is the stream-wise velocity, P is the pressure, τ_{xy} is the shear stress, the brackets indicate spatially averaged variables and f_x represents a spatially averaged canopy resistance term that arises from forces exerted by the canopy onto the surrounding flow (Lowe et al., 2005). Equation 14 shows that the canopy flow acceleration is a combination of the pressure gradient and shear stress counterbalanced by the canopy resistance. The paragraphs below investigates different flow regimes.

Unidirectional flow

In the presence of an unidirectional flow or current, a discontinuity in form drag slows down the water above a submerged canopy. This creates a large velocity gradient perpendicular to the canopy (Lowe and Falter, 2015) together with a strong shear layer and a local peak in turbulent shear stress above the canopy (Ghisalberti, 2009). Turbulence just above and inside the canopy depends on the turbulence produced within the shear layer (Nepf and Vivoni, 2000). The shear layer typically has a length scale Ls similar to the canopy height (Raupach and Shaw, 1982). Turbulent stress vertically transfers momentum and energy from the overlying water column into the canopy. Together with the pressure gradient above the canopy and gravitational potential (bed slope) this creates a flow within the canopy.

The in-situ flow structure of an unidirectional flow over a canopy strongly depends on the ratio between the canopy height (h_c) and water depth (H), also known as depth of submergence. Three important things happen when the depth ration increases. First, the driving force for momentum transfer in the canopy shifts form predominantly pressure driven to stress driven. Second, two different zones distinguish themselves inside the canopy based on the exchange mechanism with the surrounding water column. A pressure gradient created by drag of vegetation controls the momentum transfer in the 'longitudinal advection zone'. In the 'vertical turbulent zone' momentum transfer is stress-driven. Third, the turbulence production shifts from the stem wakes to the shear layer on top of the canopy (Nepf and Vivoni, 2000).

(Lowe et al., 2008) defined three different classes of canopy flow based on the depth of submergence as shown in figure 9: (1) deeply submerged or unconfined flow ($H/h_c > 1$), (2) shallow submerged or depth limited flow ($H = h_c$) and (3) emergent flow ($H/h_c < 1$) as shown in figure 9.

An emergent flow is driven by the pressure gradient. Here the water exchange with the surrounding column is predominantly by longitudinal advection and all the turbulence is

produced at the wake of the stems (Nepf and Vivoni, 2000)

As the depth ratio increases, the canopy becomes submerged (depth limited). In this state there is a shift of turbulence production from the stem wakes to the top of the canopy and the contribution of the turbulent stress becomes more important and comparable to the pressure gradient within the canopy. As the turbulent stress increases, the water exchange mechanism with the surrounding column shifts from an exchange through longitudinal advection to a vertical turbulent exchange (Nepf and Vivoni, 2000).

Turbulent stress on top of the canopy is the driver for deeply submerged or unconfined flow within and around a canopy. The contribution of the pressure gradient is neglectable (Nepf, 2012). Turbulent stresses are mainly created by the large velocity gradient at the top of the reef as wake turbulence of individual coral branches only has a minor influence(Raupach and Shaw, 1982).

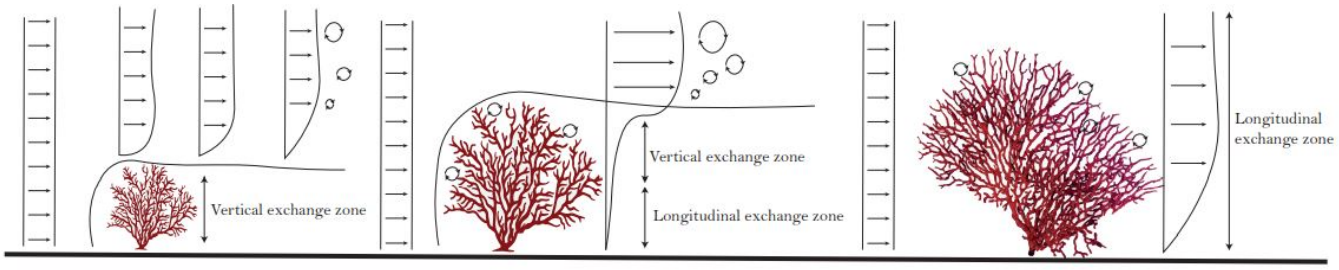

Figure 9: Effect of depth of submergion on the flow over a canopy adapted from (Roelvink, 2019)

Wave driven flow through canopy

Flow through a coral colony changes in the presence of waves. Dense canopies can cause a large velocity reduction in unidirectional flow. This is not the case for high frequency waves driven flow over a canopy. Unsteady flow beneath waves causes inertia forces that are comparable to or larger than the canopy drag (Lowe et al., 2005) (Luhar et al., 2010).

(Lowe, 2007)found two key differences between wave driven and unidirectional flow: (1) the former induces a large oscillatory pressure gradient, and (2) flow resistance in wave driven flow is increased by acceleration inside the canopy that adds an inertial force. (Lowe, 2007) also showed that flow within a submerged canopy in both unidirectional and oscillatory flow conditions can be predicted by depth integrating equation 14, giving by:

$$\frac{\partial \widehat{U}_w}{\partial t} = -\frac{1}{\rho}\frac{\partial P}{\partial x} + \frac{C_f}{2h_c}|U_{\infty,w}|U_{\infty,w} - \frac{C_d\lambda_f}{2h_c(1-\lambda_p)}|\widehat{U_w}|\widehat{U_w} - \frac{C_m\lambda_p}{1-\lambda_p}\frac{\partial \widehat{U}_w}{\partial t} \tag{15}$$

Where:

- U_w= spatially averaged in-canopy flow velocity
- C_f = a friction coefficient that relates the magnitude of the shear stress at the canopy interface to the free stream velocity $U_{\infty,w}$
- C_M=an inertial force coefficient
- C_d=an empirical canopy drag coefficient
- λ_f defined as the ratio of the total frontal area of the canopy elements to the total plan area occupied by the canopy

- λ_p defined as the ratio of the plan area occupied by the canopy elements to the total plan bed area (exposed bed + canopy elements) (Lowe et al. 2005b).
- $U_{\infty,w}$= free stream velocity

Surface waves experience resistance in a region near the bed called the wave boundary layer (Lowe et al., 2005) when propagating over a reef. Above the waves boundary layer it can be assumed that the wave do not experience resistance from the canopy. Inside the wave boundary layer it is assumed that the wave do experience resistance forces like shear stress and form drag due to the bottom roughness.

3 Objectives and thesis outline

This chapter states the aim of this research. To achieve this aim, one primary research question and 4 investigative questions are stated. Both the research aim and the research questions are based on the results of the literature review from chapter 2 and the motivation from chapter 1.1. Next, the outline of this thesis is given.

3.1 Research objective

This research aims to provide an observational study on the current state of coral reef in the study area, using structure for motion. In addition, numerical simulations are done to predict the wave propagation over the coral reefs in both its current state and in a further degraded state. (Van Dongeren et al., 2013) showed the importance of infragravity waves near the beach in coral reef lined coast. This research will therefor distinguish between short wave motion offshore and infragravity wave motion near the beach.

3.2 Research questions

Research question

What effect does the degradation of coral reef in the Whitehouse bay, Jamaica, have on the total wave energy dissipation and on the low frequency runup, considering hydrodynamic reef processes?

Investigative questions

1. How can the structural complexity of the coral reef near Whitehouse bay in Jamaica be quantified?
2. How and how much does coral degradation affect its structural complexity?
3. How much does the amount of coral degradation and erosion affect the dissipation due to vegetation?
4. How much does the low frequency wave height and low frequency runup increase or decrease due to coral degradation and full coral erosion?

3.3 Thesis outline

This thesis comprised of 10 different chapters that are structured on the research and investigative questions. Chapter 1 outlines the motivation of this study and chapter 2 summarizes the relevant background information and literature. Chapter 3 provides the aim and research questions. Chapter 4 gives a description of the field site. Chapter 5 focuses on mapping the structural complexity of the coral reef in the field site and determines the corresponding vegetation parameter that are used during the numerical simulations. These vegetation parameters are used for the calibration of the drag coefficient in chapter 6. Chapter 7 explains the method used for the numerical simulations to determine wave propagation over the coral reef. The results of which are shown in chapter 8. The results and methods are discussed in chapter 9. The key findings and answers to the research questions are given in chapter 10 (conclusions) and recommendations for further research.

4 Field site

The field site for this study is Whitehouse bay in Jamaica. Whitehouse bay is located in the South coast of Jamaica, next to an area of former salt marsh. The area is a popular tourist destination due to the Sandals Whitehouse resort. Figure 10 shows that the beaches along the Whitehouse bay mainly comprises debris and sand with sediment size of D15 = 0.0001 [m], D50 = 0.0002 [m], D90 = 0.0003 [m] (Daly and Nienhuis, 2018).

Figure 10: (a) shows the Whitehouse resort, (b) shows picture of the debris on the beach and [google earth] (c) shows a closeup of the sediment on the beach [google earth]

WaveWatch has collected the wave and tide statistics at several points along the coast of Jamaica, as shown in figure 11. The red dot shows the location closest to the Whitehouse bay, where WaveWatch collected data from 1979 to 2010 (Chawla et al., 2013).

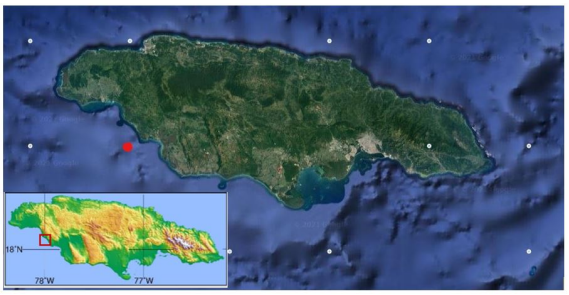

Figure 11: Location of the where the wave data shown in figure 11 is collected (Chawla et al., 2013)

Figure 12 shows the wave heights [mm], peak periods [ms] and directional spreading [centi/degrees] at this location. Here it can be seen that there is an average wave height of 716 [mm] and an average peak period of 746 [ms].

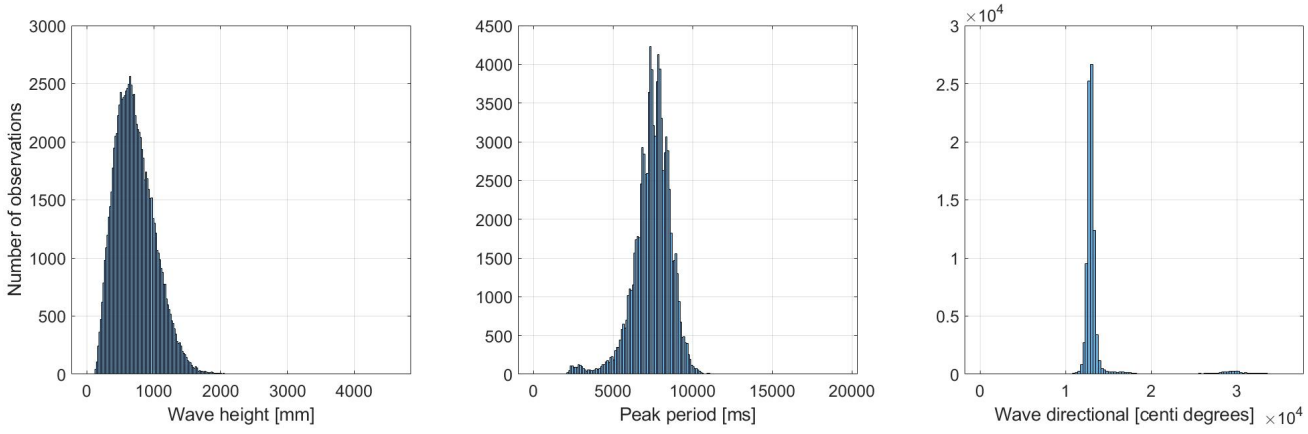

Figure 12: Wave height, Peak period and Wave direction from data point show in figure 11. Data collected from (Chawla et al., 2013)

5 Reef Structure

This chapter focuses on mapping the state of the coral reefs and sea-grass in the study area. First, an explanation of the Structure for motion (SfM) survey is given. After this, the results are shown. The results are then used to determine the vegetation height, stem thickness and vegetation density of both corals and sea-grass.

Vegetation

Chapter 2.2.3 discusses the influence of vegetation and in-canopy flow on the wave transformation and dissipation. Based on these findings, the effect of vegetation is accounted for by implementing the canopy model in Xbeach.

There are 2 different ways to implement the effect of vegetation, in our case sea-grass and coral, into Xbeach. The first involves adjusting the bottom friction coefficient (c_f). Second, canopy flow can be implemented into the model. The later solves the canopy flow in Xbeach based on the vegetation height (ah), stem thickness (bv), vegetation density (N) and drag coefficient (C_d). Although the bottom fiction approach is more validated by (e.g. (Pomeroy et al., 2015), (Quataert, 2015), (Roelvink, 2019)), (van Rooijen et al., 2016) implemented a canopy model into XB-NH. (van Rooijen et al., 2016) showed an increased accuracy for predicting wave height when using the canopy model compared to the bottom friction approach. (Lowe et al., 2005) and (Lowe et al., 2007) developed a canopy model with the ability to estimate dissipation rates due to coral canopies. The model by (Lowe et al., 2005) was assessed by (Wiechen, 2020), who found that the canopy model is in good agreement with the experimental results.

5.1 Structure for motion

Structure for motion (SfM) is used to determine the structural complexity of the corals and the sea-grass characteristics in the study area. SfM estimate 3D structures based on 2D images by using a photogrammetric range imaging technique (Luhmann et al., 2019) that estimates the motion and location of 2-dimensional images (Ozyesil et al., 2017).

The SfM survey comprises three phases. First is the collection of images, as described in section 5.1.1. Second, the images are processed using Agisoft Metashape to create a digital elevation model (DEM) of the coral reef and sea-grass, as described in section 5.1.2. Third, the results of the DEMs and the images of the coral reef and sea-grass are used to determine different vegetation parameters.

5.1.1 Data collection reef

The data collected during a fieldwork conducted between May 15, 2019 and May 25, 2019, by (Daly and Nienhuis, 2018) is used to determine structural complexity and the erosion of the reef and sea-grass. During this fieldwork, a diver swam across the sea floor along ground-control points (see figure 13 c), holding a drone with a camera (see figure 13 b) while making pictures. The photos from this underwater camera are used for Agisoft Metashape. 8 different areas of about 100 $[m^2]$ were surveyed. The results from survey 1 till 3 will not be used due to the poor quality of the images. Figure 14 shows the location of 5 different reef areas where the images of the reef were taken.

Figure 13: (a) Boad with a single beam echo sounder attached to a pole (b) Drone with a camera attached. A drone like this was used to create underwater images of the reef. (c) Ground control point at the location where the images were taken by a diver (Daly and Nienhuis, 2018)

In order to map the bathymetry of the study area, a single beam echo sounder was attached to a pole on the side of a boat (see figure 13 a). This boat sailed across the area and measured the horizontal position of the echo sounder. The collected data is interpolated to map the bathymetry of the study area, which is shown in figure 14. All coordinates are in UTM zone 18Q.

Figure 14: Locations of the SfM surveys [google earth]

5.1.2 Creating digital elevation model (DEM)

The images from the data collection are processed into DEMs with Agisoft Metashape. The following steps are taken to get from 2-dimensional images to a DEM, as shown in figure 15.

To start with, the images are loaded into Metashape, after which the images are tied together during the *Photo alignment*. Different matching points are detected during this step, after which the photos with matching point are paired together in order to make a *point cloud*. During the next step, pair-wise depth maps are computed for each image and combined into a *Dense point cloud*. From the point cloud, a *Mesh* is generated. *Textures* can then be added and a *orthophoto* can be generated from the Mesh. In order to create a *DEM*, several ground control points are added to the Mesh. The coordinates from the ground control point are added manually based on the bathymerty of the field site. These ground control points are 1 by 1 metre, and will determine the accuracy of the DEM.

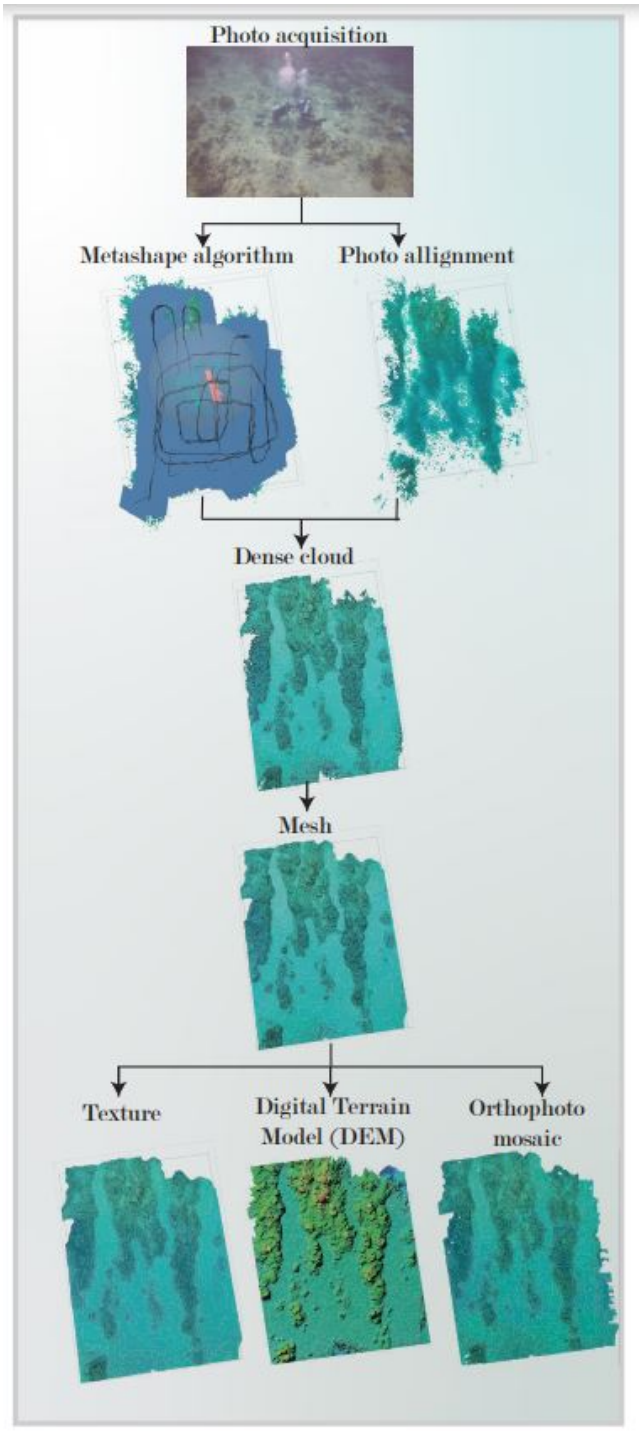

Figure 15: Method used to process reef images into a DEM, using Agisoft Metashape

Table 12 shows the size of the real ground control point (GCP) and the size of the GCP in the processed images per SfM. Here it can be seen that there is a large deviation between the DEM and the actual reef area. Metashape overestimates the dimensions of the different SfM areas. The DEMs are corrected based on the accuracy. The corrected DEM and the 3-dimensional images of the SfM locations can be found in appendix B.

Table 1: Accuracy of the SfM results

	width GCP in Metashape [m]	width GCP in field site [m]	accuracy [%]
SfM_4	1.5	1	67
SfM_5	2	1	50
SfM_6	2.2	1	45
SfM_7	1.69	1	59
SfM_8	1.2	1	83

5.1.3 Determining vegetation parameter

The corrected DEMs are used to determine the vegetation parameters for corals and sea-grass. Paragraph 5 explained that the canopy model is used to model vegetation during this study. This model uses 4 different vegetation input parameters. Vegetation height (ah) [m], stem thickness (bv) [m], vegetation density (N) [stems/m^2] and drag coefficient (C_d) [-].

To get ah, we calculated the average height of the adjusted DEMs.

Image processing is used to derive bv and N from the images for coral and sea-grass. To do this, the images are smoothed out to distinguish the stems from the background (see figure 16 b). After this, we locate the edges of the image, determine the stem thickness and count the amount of stems per square metre. This process is repeated for 5 different photos per SfM location, from which the average value is calculated.

The results from the SfM survey in appendix B show that the surveyed areas are not completely covered with vegetation. To account for this, the vegetation cover is calculated in %. N is assumed to be spread evenly throughout the total area by taking N*vegetation cover.

C_d is calculated during the calibration of the drag coefficient in chapter 6.

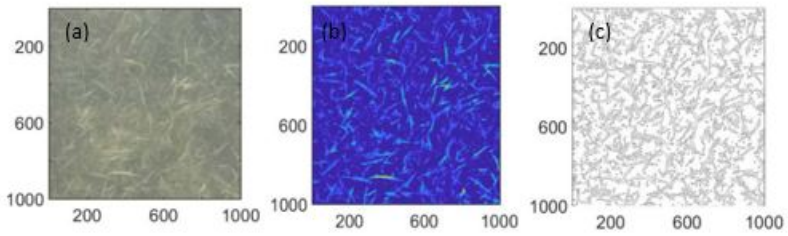

Figure 16: Steps used in photo processing to get bv an N from images. (a) shows the original images, (b) shows the smooth images and (c) is used to calculate the stems (Daly and Nienhuis, 2018)

	ah [m]	bv [m]	N [stems/m^2]
SfM_4	1.98	0.0082	5483
SfM_5	1.05	0.016	1248
SfM_6	0.2	0.0215	292
SfM_7	0.9	0.0182	329
SfM_8	0.97	0.0206	1199

Table 2: Vegetation parameter results from the DEMs and photo processing

6 Calibration of drag coefficient

This chapter describes the calibration of the drag coefficient (Cd) for coral and sea-grass. To do this, I used the observed wave height from transect 2 between May 21, 2019 and May 22, 2019.

The calibration is divided into two parts. During the first part, one type of vegetation representing coral is uniformly spread across the whole 1D transect from the offshore boundary until the beach. I then applied different drag coefficients to the simulations as shown in table 3. The coral drag coefficients are based on the results of (McDonald et al., 2006), who calculated the drag coefficient for 24 different flows over a submerged canopy. The vegetation height (ah), stem thickness (bv) and vegetation density are kept constant throughout the simulations and are based on the results of chapter 5

Table 3: Input parameters for coral and sea-grass: vegetation height ($ah[m]$), stem thickness ($bv[m]$), vegetation density ($N[corals/m^2]$), Drag coefficient ($Cd[-]$)

Coral input					Sea-grass input				
Simulation	**ah**	**bv**	**N**	**Cd**	**Simulation**	**ah**	**bv**	**N**	**Cd**
1	0.1	0.019	767	**0.13**	1	0.4	0.023	1051	**0.05**
2	0.1	0.019	767	**0.3**	2	0.4	0.023	1051	**0.18**
3	0.1	0.019	767	**0.5**	3	0.4	0.023	1051	**0.25**
4	0.1	0.019	767	**0.75**	4	0.4	0.023	1051	**0.40**
5	0.1	0.019	767	**1**	5	0.4	0.023	1051	**0.83**
6	0.1	0.019	767	**1.25**	6	0.4	0.023	1051	**1.22**
7	0.1	0.019	767	**1.68**	-	-	-	-	**-**

During the second part of the calibration, an extra vegetation type representing sea-grass is added to the simulations. The sea-grass is added on the reef flat as shown in Figure 17. The sea-grass drag coefficients are based on the results of different studies by (Cavallaro et al., 2018) (Mendez and Losada, 2004b) (Paul and Amos, 2011) (Sánchez-González et al., 2011) (Koftis et al., 2013) (Zeller et al., 2014).

For the calibration of the drag coefficient, a uniform grid-size of 5 metres is used. The calibration of the drag coefficient will be based on the wave height at the location of the pressure sensors. Because the pressure sensors are further offshore, a 5 metre grid will suffice.

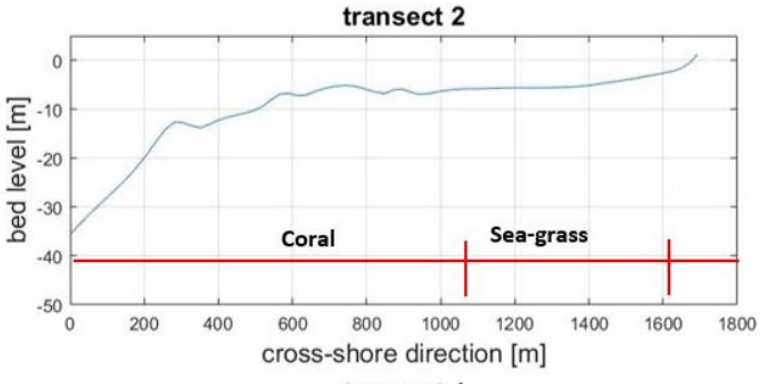

Figure 17: Location of coral and sea-grass on transects 2

The model output for part 1 and 2 comprises a wave height time series at the location of the different pressure sensors on transect 2. The simulations have a duration of 24 hours

+ 1 hour spin-up time. Tidal conditions and a varying offshore wave height are included in the simulations based on the data from pressure sensor $OSSI_{WH01}$ as shown in figure 53. The model output is calculated for 30 minute bins.

Figure 18: Location and names of the pressure sensors [google earth]

The results are compared to the field data from pressure sensor $PT2X_{WH13}$ (Before the reef crest), $OSSI_{WH15}$ (Reef crest), $PT2X_{WH17}$ (outer reef flat) and $PT2X_{WH19}$ (Reef flat) by calculation the bias, scatter index (SCI) and root-mean-square error (RMSE) according to equation 16, 17 and 18, where n is the number of data points (Roelvink, 2019). The drag coefficient with the lowest bias, SCI and RMSE is used during the numerical simulations of chapter 7.

$$Bias = \frac{1}{n}\sum_{i=1}^{n}(X^i_{modelled} - X^i_{measured}) \tag{16}$$

$$SCI = \frac{\sqrt{\frac{1}{n}\sum_{i=1}^{n}(X^i_{modelled} - X^i_{measured})^2}}{\frac{1}{n}\sum_{i=1}^{n} X^i_{measured}} \tag{17}$$

$$RMSE = \sqrt{\frac{1}{n}\sum_{i=1}^{n}(X^i_{modelled} - X^i_{measured})^2} \tag{18}$$

Figure 19 shows the results of part 1 in a scatter plot. Figure 20 shows the corresponding bias, SCI and RMSE. The best result is achieved for simulation 3 (Cd=0.5[-]), which gives an average bias of 0.025, a SCI of 0.534 and a RMSE of 0.064. Figure 20 shows the wave height is underestimated at the reef crest and that the largest overestimation is achieved before the reef crest.

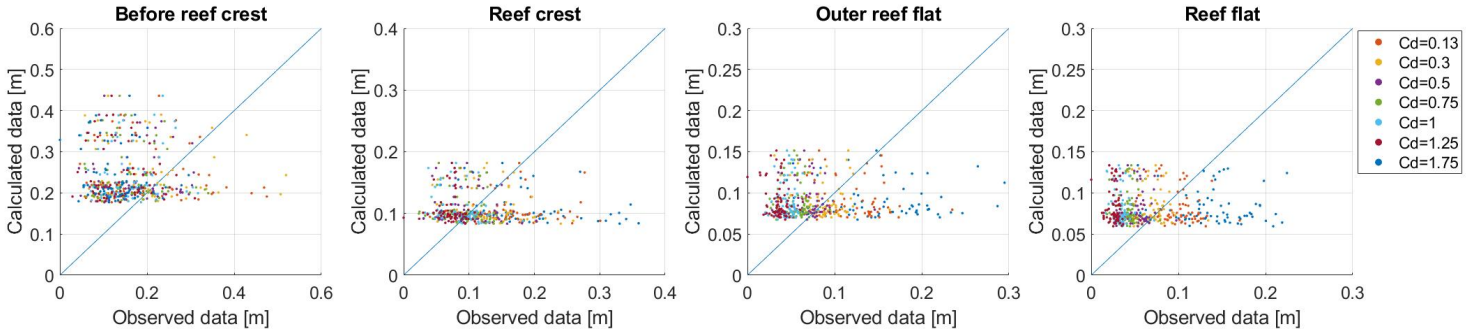

Figure 19: Observed vs measured data from part 1 of the calibration for different coral drag coefficients

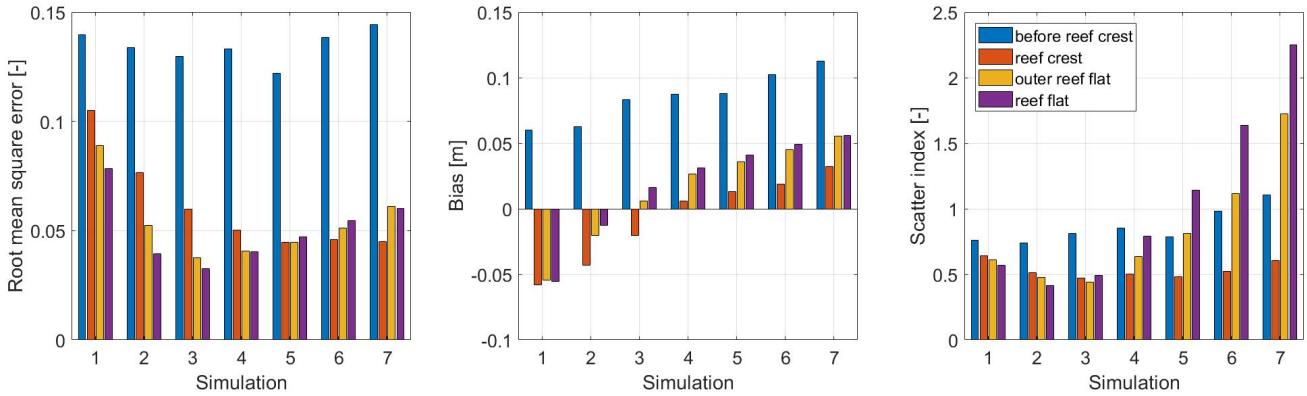

Figure 20: root-mean-square error [-], bias [-] and Scatter index [-] for part 1 of the calibration

Figure 21 shows the results of part 2 of the calibration in scatter plots. Figure 22 shows the corresponding bias, SCI and RMSE. The best result is achieved when a Cd of 0.05 applies to the sea-grass area. This gives a bias of 0.017, a SCI of 0.538 and a RMSE of 0.064. Figure 22 shows that the wave height is still underestimated at the reef crest and that the largest overestimation is still achieved before the reef crest.

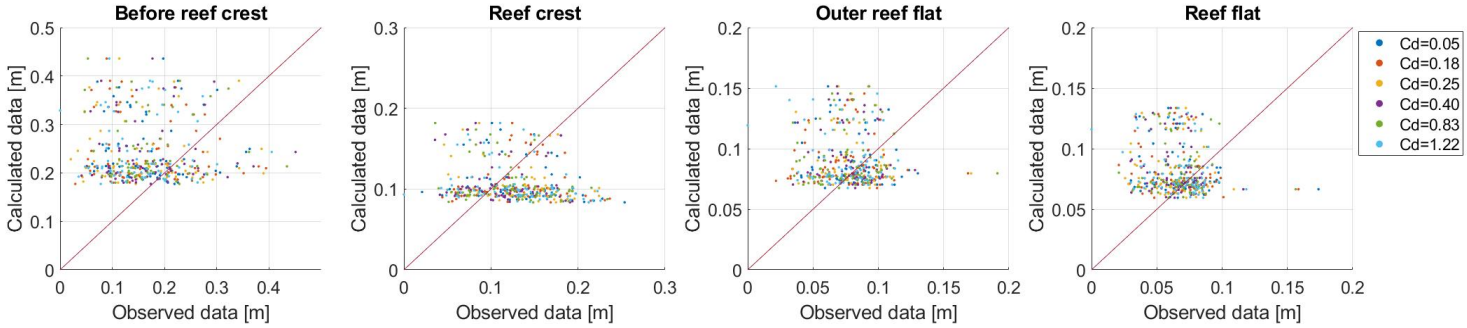

Figure 21: Observed vs measured data from part 2 of the calibration for different coral drag coefficients

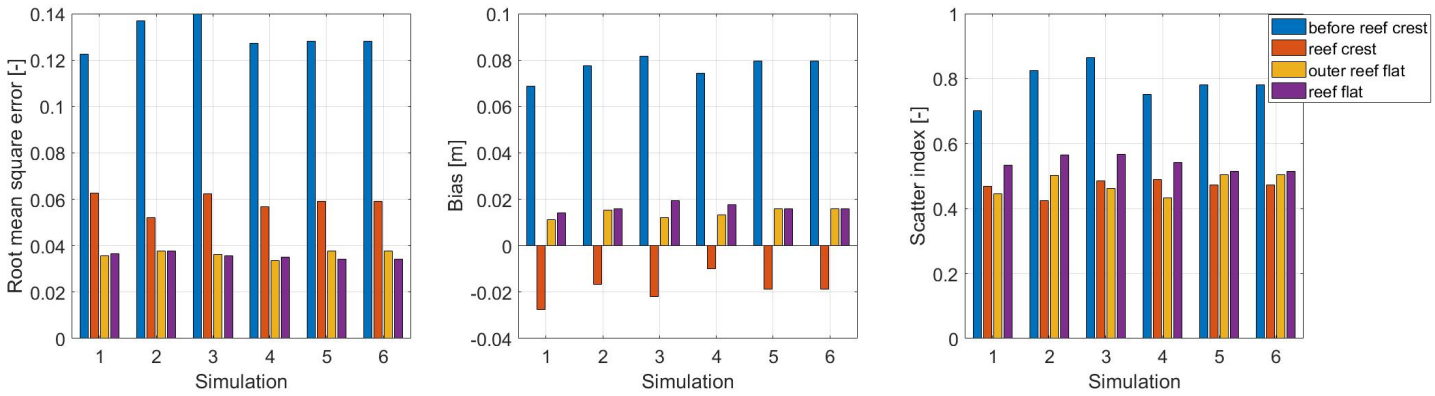

Figure 22: root-mean-square error [-], bias [-] and Scatter index [-] for part 2 of the calibration

7 Numerical simulation

This chapter describes how Xbeach is used to model the effect of reef degradation on the IG wave runup and the wave energy dissipation across a reef in Whitehouse bay Jamaica. First, the data collection is described. The next section provides the motivation on the chosen Xbeach model. In addition to this, the model formulations and physical processes used in Xbeach are elaborated. After this, the model set-up and input parameter are described. Last, the output selection and the post-processing method are given. The study will focus on a 1-dimensional model. Sediment transport and morphological changes are outside the scope of this research and will not be elaborated.

7.1 Methodology

7.1.1 Data collection

The data from a field campaign conducted in May 2019 by (Daly and Nienhuis, 2018) is used for the numerical model. During this campaign 9 pressure sensors (3 x OSSI-010-003B-1 @ 10Hz and 6 x PT2X @ 8Hz) and 3 tilt current meters (TCM4 @ 16Hz) were places along 4 different transect lines from the reef crest along the inner lagoon to the beach. Figure 23 show the location of the sensors. The pressure sensors and tilt current meters measure the current and free surface waves along the coast over an area spanning approximately 4 km and up to 2 km offshore, between depths of 2–50 m. The pressure sensors were first placed along transect 3 and 4 from May 17 till May 20, 2019 and were that transferred to transect 1 and 2 from May 20 till May 24. $OSSI_{WH01}$ is the most offshore pressure sensor location and its data will be used as an offshore reference point for all the four transects.

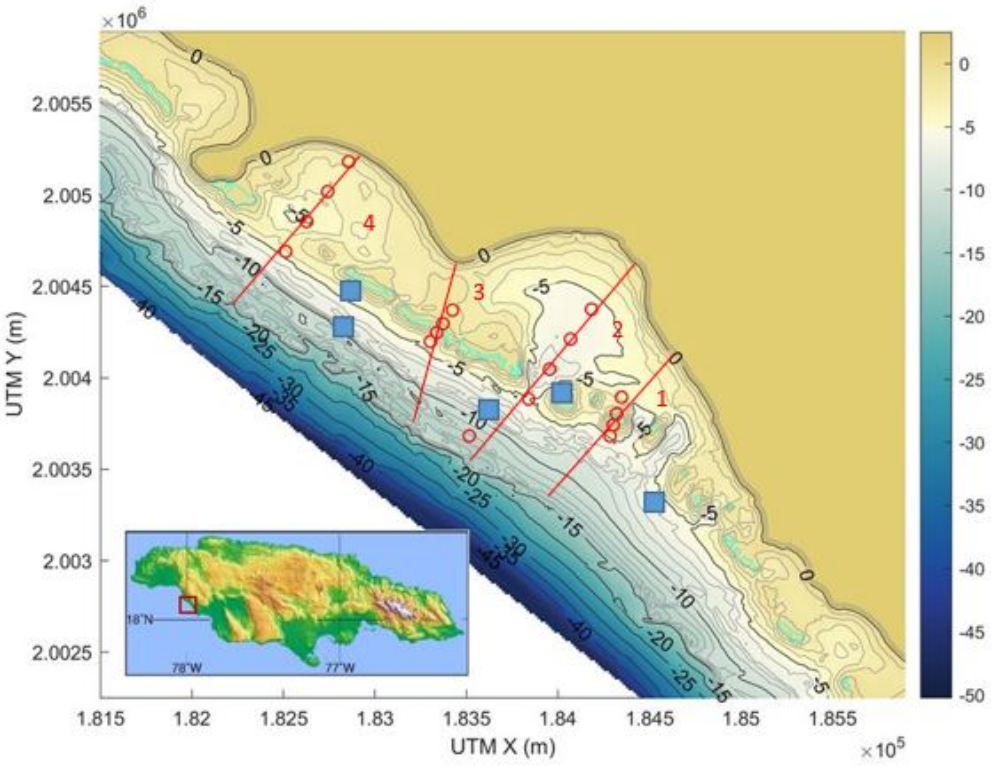

Figure 23: Study area. The red dots indicate the location of the pressure sensors and the blue squares represent the location of the structure for motion surveys. The red lines show the locations of transect 1, 2, 3 and 4 (Daly and Nienhuis, 2018)

7.1.2 Xbeach

Xbeach surfbeat (XB-SB) is used for the numerical simulations in this study. XB-SB is the short wave phase-averaging and long-wave resolving mode of Xbeach, where short wave height variation is solved on a group scale (Roelvink et al., 2010).

Xbeach is a numerical model that can simulate wave propagation for both long and short waves, current, flow, sediment transport and morphological changes in coastal areas. The model can predict an array of hydrodynamic processes, such as shoaling, refraction, breaking, propagation and dissipation of waves. Xbeach can also model the morphological changes, sediment transport and includes the effect of vegetation. Originally, the model was designed to simulate morphological and hydrodynamic processes on sandy beaches on a storm time scale but can also be applied to fringing reefs.

The choice to use XB-SB is based on the results of studies by (Van Dongeren et al., 2012) and (Lashley et al., 2018). (Van Dongeren et al., 2012) showed the accuracy of XB-SB in predicting both the generation mechanism and decay due to frictional wave dissipation, the runup and rundown of infragravity waves over reefs. (Lashley et al., 2018) compared Xbeach non-hydrostatic (XB-NH) and XB-SB in predicting runup over a 1D (alongshore uniform) fringing reef. He found that XB-NH accurately predicted the wave transformation while under-predicting the runup at the beach, while XB-SB over-predicted the wave height on the reef flat, which led to an over-prediction of the runup at the beach. Furthermore, he found that both XB-SB and XB-NH were able to accurately predict extreme runup events.

7.1.3 Model formulation

Dissipation

There are three types is dissipation processes that are implemented in our Xbeach model. This is dissipation due to wave breaking (D_w), bottom friction (D_f) and vegetation (D_v).

Dissipation due to waves breaking

For this study, the wave breaking formulation according to (Roelvink, 1993) extended is used. (Roelvink, 1993) used the fraction of waves breaking (Q_b) multiplied by the dissipation per breaking event to calculate the dissipation due to waves breaking (D_w) as shown in equation 19:

$$D_w = 2\frac{\alpha}{T_{rep}} Q_b E w \tag{19}$$

where α is a wave dissipation coefficient, T_{rep} is the wave period and E_w is the wave energy. The wave energy and fraction of waves breaking is calculated by equation 20 and 21 respectively:

$$E_w(x, y, t) = \int_0^{2\pi} S_w(x, y, t, \theta) d\theta \tag{20}$$

$$Q_b = 1 - exp(-(\frac{H_{rms}}{H_{max}})^n) \tag{21}$$

with:

$$H_{rms} = \sqrt{\frac{8E_w}{\rho g}} \tag{22}$$

$$H_{max} = \gamma(h + \delta H_{rms}) \tag{23}$$

where H_{max} is the maximum wave height, which is calculated as a ratio of water depth h and a fraction of wave height times the breaker index γ. H_{rms} is the root-mean-square wave height

Dissipation due to bed friction

Short wave dissipation due to bottom friction in Xbeach is modelled as:

$$D_f = \frac{2}{3\pi}\rho f_w(\frac{\pi H_{rms}}{T_{m01}\text{sinh}kh})^3 \tag{24}$$

where f_w is the short-wave bottom friction coefficient, k is the wave number.

Because the dissipation due to vegetation in this study is calculated according to the canopy model instead of the bottom friction approach, D_f is only calculated in the areas where there is no vegetation, such as near the beach.

Dissipation due to vegetation

The dissipation due to vegetation, D_v is calculated by using equation 25. (Suzuki et al., 2012) adjusted the model approach of (Mendez and Losada, 2004a), to consider vertically heterogeneous vegetation. According to this approach, D_v is calculated as a function of the local wave height and four different vegetation parameter (vegetation height ah, stem thickness bv, vegetation density N and drag coefficient C_D in the area of wave propagation.

$$D_{v,i} = A_v\frac{\rho C_{D,i} b_{v,i} N_{v,i}}{2\sqrt{\pi}}(\frac{kg}{2\sigma})^3 H^3_{rms} \tag{25}$$

with,

$$A_v = \frac{(\sinh^3 k\alpha_i h - \sinh^3 k\alpha_{i-1}h) + 3(\sinh k\alpha_i h - \sinh k\alpha_{i-1}h)}{3k\cosh^3 kh} \tag{26}$$

where α is the relative vegetation height ($= h_v/h$) and i is the amount of vegetation layers. For the sake of simplification and because of a lack of information about the structure of individual coral branches in the study area, the vegetation is assumed to be vertically uniform (i=1).

7.2 Model setup

7.2.1 Bathymetry

For the bathymetry, I used 4, 1-dimensional grids as shown in figure 24, where the computation x-as is approximately perpendicular to the coastline. The locations and bathymetry of the transects are based on the locations of the pressure sensors shown in figure 23, and results of the field work. I chose not to use a 2-dimensional grid due to the increased

computation time. A test run shows that using a 2-dimensional grid increased the computational time by 10 fouled.

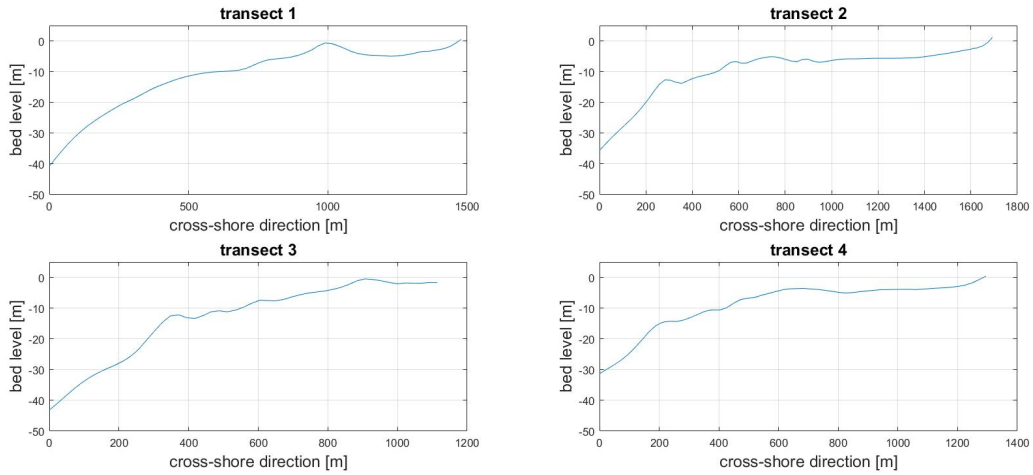

Figure 24: Bed profile of transect 1,2,3 and 4. The transects are perpendicular to the coast line and X is positive towards the shore.

7.2.2 Computational grid

The grid-size for numerical simulations will vary from 7 metres offshore to 0.5 metre onshore. A smaller grid-size onshore is important to get accurate runup predictions. The maximum grid-size ratio between adjacent cells is 5%. One of the test runs showed that an uniform grid-size of 0.5 metre caused a lot of noise between the reef crest and the beach. A uniform grid of 7 metres cancelled out most of this noise but did not give an accurate view of the low frequency waves and runup near the beach.

Choosing the gird-size is a trade-off between computation time and accuracy. Choosing a smaller grid-size will increase the accuracy, but will also increase the computation time. Reducing the grid-size by 50% means that double the amount of calculations will be made and thus doubling the computation time.

7.2.3 parameter settings

Appendix A shows the parameters settings used for the numerical simulations. Some important parameter settings are elaborated in section 7.3, the rest of the parameter setting are set at default setting. A detailed explanation of all the parameter setting can be found in (Roelvink et al., 2010).

7.3 Input selection

7.3.1 Boundary conditions

An artificial offshore boundary is set in Xbeach to show the location where the flow conditions are imposed. It is important that the boundary is set far enough offshore so that the waves can pass through this boundary to the deep sea with minimal reflection.

The offshore wave height and peak peak period measured by WaveWatch (Chawla et al., 2013) as shown in figure 11 and figure 12 are used as boundary conditions for the numerical simulations. Both the sensitivity analysis in appendix C and calibration 6 use the data from pressure sensor $OSSI_{WH01}$ as the input parameters for the offshore boundary. The results of which showed very small IG wave heights and IG runup. A higher offshore wave

height is chosen for the numerical simulations to ensure that the IG waves are high enough to contribute to the runup at the beach. Table 4 shows the offshore boundary wave height and period per simulation. These conditions are kept constant throughout the simulation, and the tidal effect is neglected.

Table 4: Offshore wave height and peak period for different simulations

Simulation	Wave height [m]	Peak period [s]
1	0.5	6.99
2	1	7.89
3	2	8.86
4	3	9.99
5	4	10.77
6	4.62	9.46

7.3.2 Scenarios

During this study, coral degradation is defined as: the point where corals are dead and no new growth occurs.

Four different scenarios (S1 till S4) are used during the simulation. The scenarios are based on the current and expected future state of the reef. Each scenario shows a different amount of coral erosion and presence of sea-grass. The four scenarios are:

- S1 models the wave transformation on the reef at its current state, with the assumption that both coral and sea-grass are present as shown in figure 15. The results of the structure for motion survey and calibration of the drag coefficient are used as vegetation parameters.
- For S2, a future scenario representing the state of coral reefs in 2100 is modelled. (Eakin, 1996) researched the erosion rate on stressed reefs and found a vertical erosion rate of 6 [mm/year]. This would result in a coral height of 0.304 [m] in 2100.

  (McDonald et al., 2006) studied the effect of water depth to coral height ratio on the drag coefficient and found that this correlation can be described by the power law: $C_d = 1.01(H : h)^{-}2.77 + 0.01$. If we look at transect 2 in figure 24 we can see that the highest point on the reef is the reef crest. This is also the point where the water depth to vegetation height changes the most with a decreasing vegetation height. The power law given above results in a drag coefficient reduction of 34% when the vegetation height is reduced from 0.78 [m] to 0.304 [m]. This results in a drag coefficient of 0.33 [-]. The vegetation density, stem thickness and the presence of sea-grass are assumed to remain the same.
- S3 shows a scenario where the coral reefs are completely gone due to erosion but where the sea-grass is still present.
- S4 models the wave transformation when both the coral reef and sea-grass are completely gone. This scenario represents a sandy beach.

Figure 25 shows the location of the vegetation for the different transects. As discussed in chapter 6, vegetation representing coral will be placed from the offshore boundary until the shore side of the reef crest, and vegetation representing sea-grass will be placed along the reef flat. Table 5 shows the vegetation input parameters for each transect and scenario.

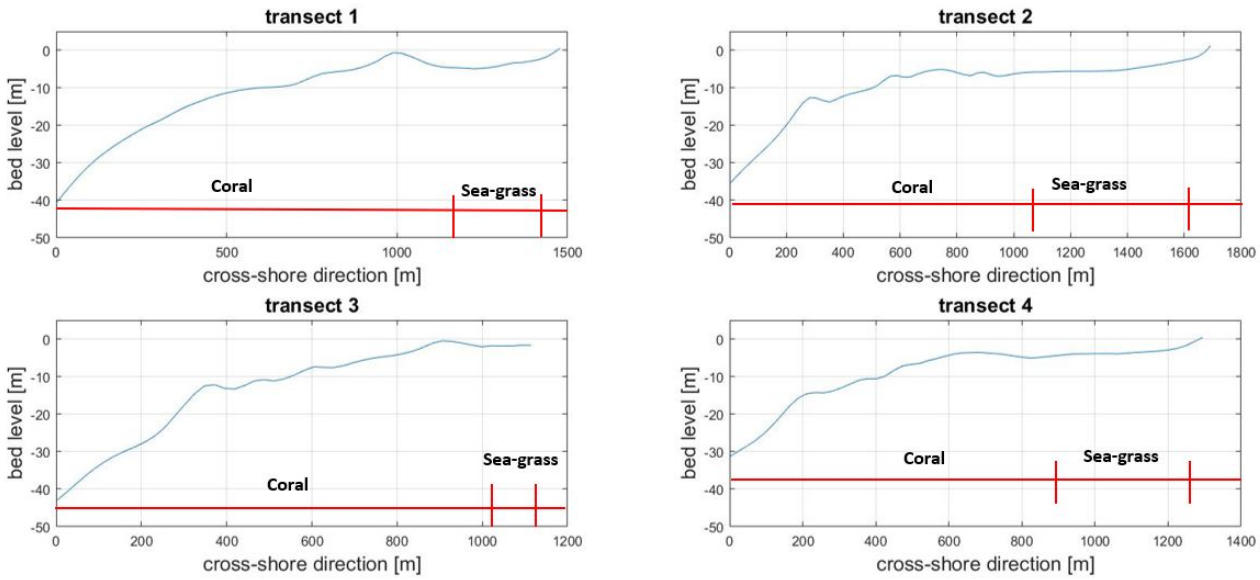

Figure 25: Location of coral and sea-grass along the 4 different transects

Table 5: Vegetation input, vegetation height (ah) [m], stem thickness (bv) [m],

	Scenario 1		Scenario 2		Scenario 3		Scenario 4	
	coral	sea-grass	coral	sea-grass	coral	sea-grass	coral	sea-grass
ah	0.78	0.4	0.304	0.4	-	0.4	-	-
bv	0.019	0.023	0.019	0.023	-	0.023	-	-
N	767	1051	767	1051	-	1051	-	-
Cd	0.5	0.05	0.33	0.05	-	0.05	-	-

7.4 Output selection

Four different outputs are selected in Xbeach: 1) instantaneous spatial output 2) time-averaged spatial output 3) fixed point output or 4) runup gauge output (Roelvink et al., 2010). For this study instantaneous spatial output is used to generate a time series at each x-grid location at a time interval of 240 seconds. Time-averaged spatial output is used to generate a time series at each x-grid location at a time interval of 18000 seconds. Point output is used to generate a time series at a time interval of 100 seconds. The runup is determined by the runup gauge that describes a time-series of different variables at the moving water line. Table 6 shows the x-location of the point output and runup gauge of each transect. The following output variables are selected for the instantaneous spatial-, time-averaged spatial-, and fixed point output:

- Hrms wave height based on instantaneous wave energy (H) $[m]$
- Water level (zs) $[m]$
- Glm velocity in cell centre, x-component (u) $[m/s]$
- Wave energy (E) $[Nm/m^2]$
- Fraction breaking waves (Qb) $[-]$
- Dissipation (D) $[W/m^2]$
- Dissipation due to short wave attenuation by vegetation (Dveg) $[W/m^2]$

Table 6: X-locations of the point output and the runup gauge for each of the four transects. The locations are positive onshore

Transect 1	**Transect 2**	**Transect 3**	**Transect 4**
0	0	0	0
282	282	282	282
588	588	588	588
750	750	750	750
894	894	894	894
1044	1044	1044	1044
1375	1375	1110 (runup)	1290 (runup)
1460 (runup)	1650		
	1680 (runup)		

7.5 Post-Processing

The Xbeach simulations are post-processed to determine the effect of coral degradation on the wave energy dissipation and IG runup. To determine the contribution of SS and IG waves, the detrended time series of the water level and wave height are filtered based on the SS en IG frequencies, where the cutoff frequency between SS and IG waves is at 0.04 Hz. The water level time series at the runup location is sorted in ascending order, where-after the 2% exceeding value is calculated to get $R_{2\%}$. The setup is obtained by extracting the offshore water level from the mean water level.

8 Results

This chapter presents the results of the numerical simulations from chapter 7. The paragraphs below show the IG wave height, total wave energy, IG runup, IG R2% and the setup. The figures display the different scenarios, corals and sea-grass (S1), reduced corals and sea-grass (S2), only sea-grass (S3) and no coral or sea-grass (S4) for different offshore wave height (H_{m0}). Appendix D shows the propagation of these parameters over the reef profiles.

8.1 IG wave height

Figure 26, 27, 28 and 29 shows the average IG wave height and the change in average wave height compared to S1 for the different scenarios and offshore wave heights (H_{m0}), per transect.

Table 7 show per transect for what scenario and at what offshore wave height the maximum increase in IG wave height is achieved.

Table 7: Maximum increase in IG wave height for each transect

Transect	Scenario	H_{m0}	$\%increase$
1	S4	0.5	1490
2	S4	2	1094
3	S3	0.5	1230
4	S4	1	1335

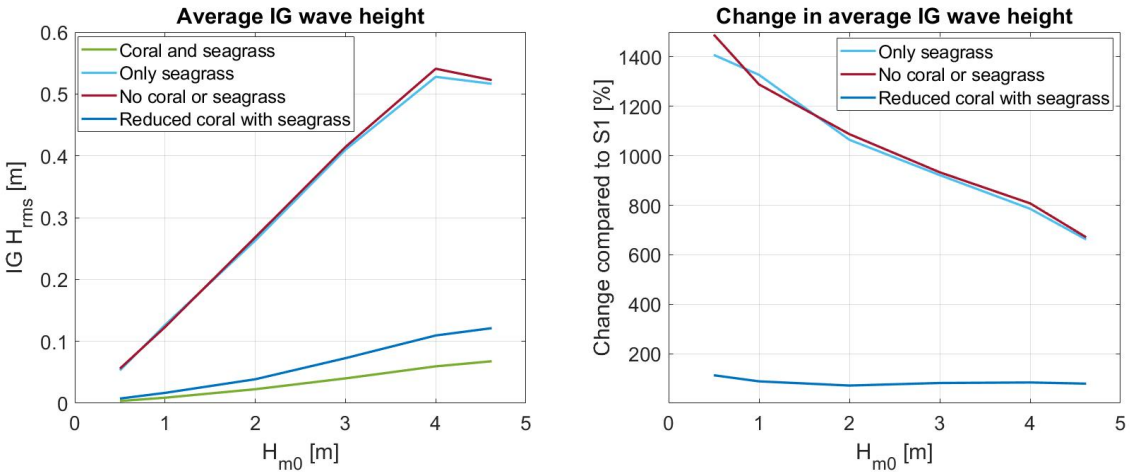

Figure 26: Average low frequency (IG) wave height [m] for scenario S, S2, S3 and S4. Transect 1

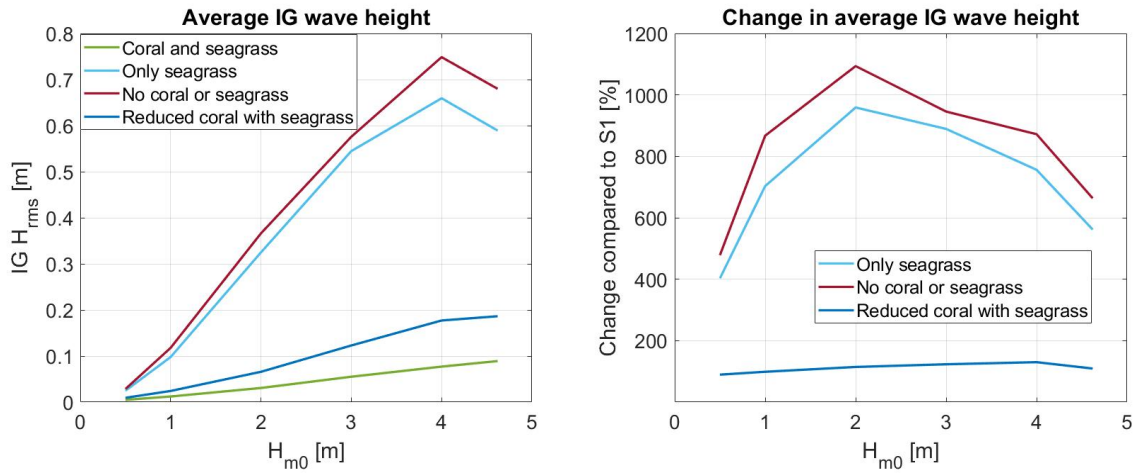

Figure 27: Average low frequency (IG) wave height [m] for scenario S, S2, S3 and S4. Transect 2

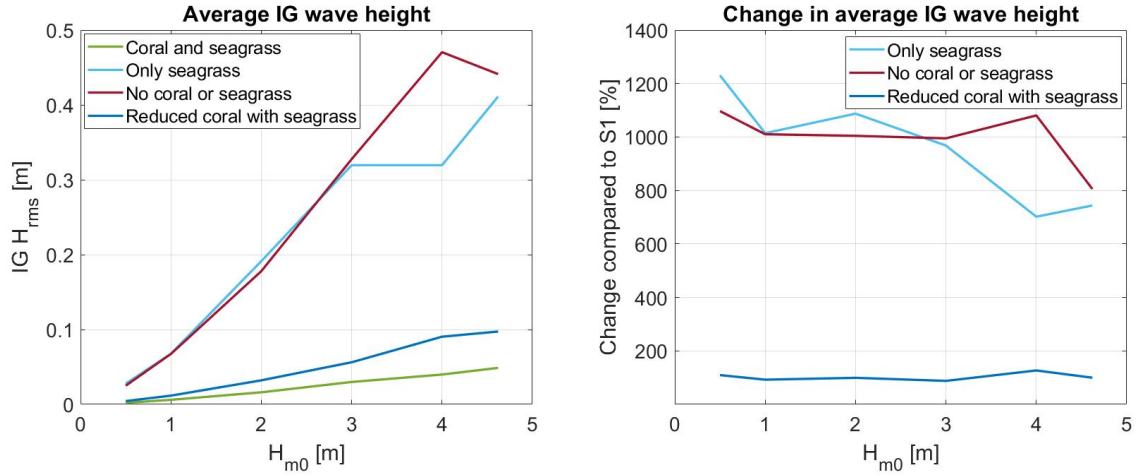

Figure 28: Average low frequency (IG) wave height [m] for scenario S, S2, S3 and S4. Transect 3

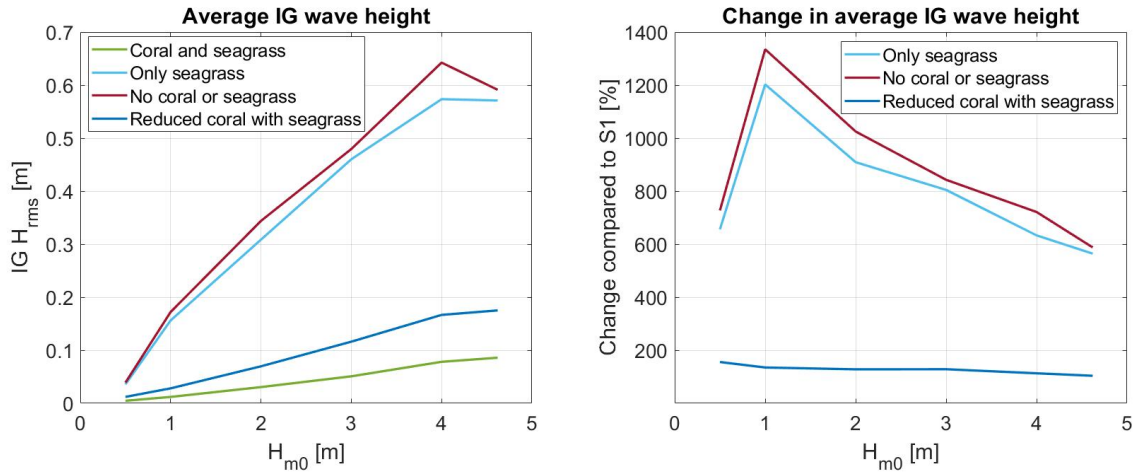

Figure 29: Average low frequency (IG) wave height [m] for scenario S, S2, S3 and S4. Transect 4

8.2 Wave energy

Figure 30, 31, 32 and 33 shows the average total wave energy and the change in average total wave energy compared to S1 for the different scenarios and offshore wave heights (H_{m0}), per transect.

Table 8 show per transect for what scenario and at what offshore wave height the maximum increase in total wave energy is achieved.

Table 8: Maximum increase in total wave energy for each transect

Transect	Scenario	H_{m0}	$\%increase$
1	S4	4	182
2	S4	2	535
3	S4	4	172
4	S4	2	450

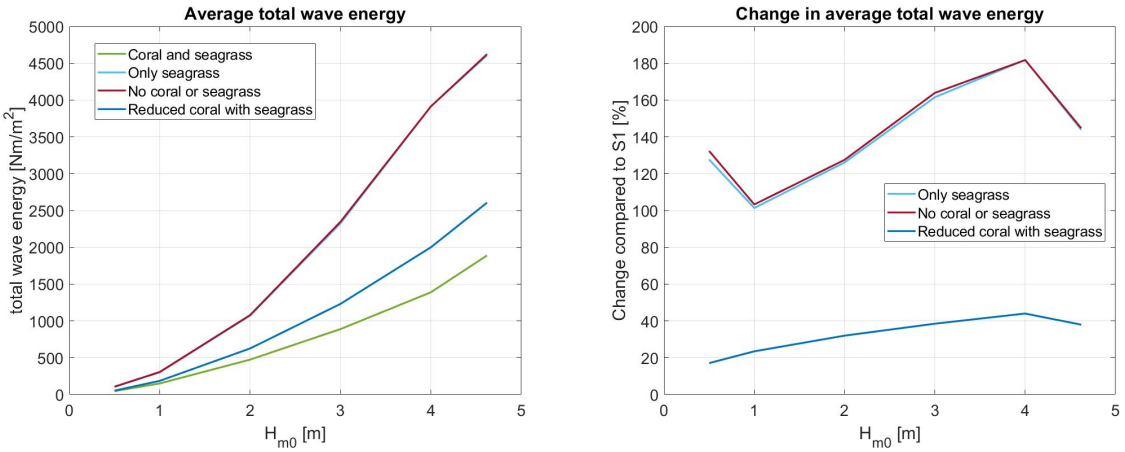

Figure 30: Average wave energy [Nm/m^2] for scenario S1, S2, S3 and S4. Transect 1

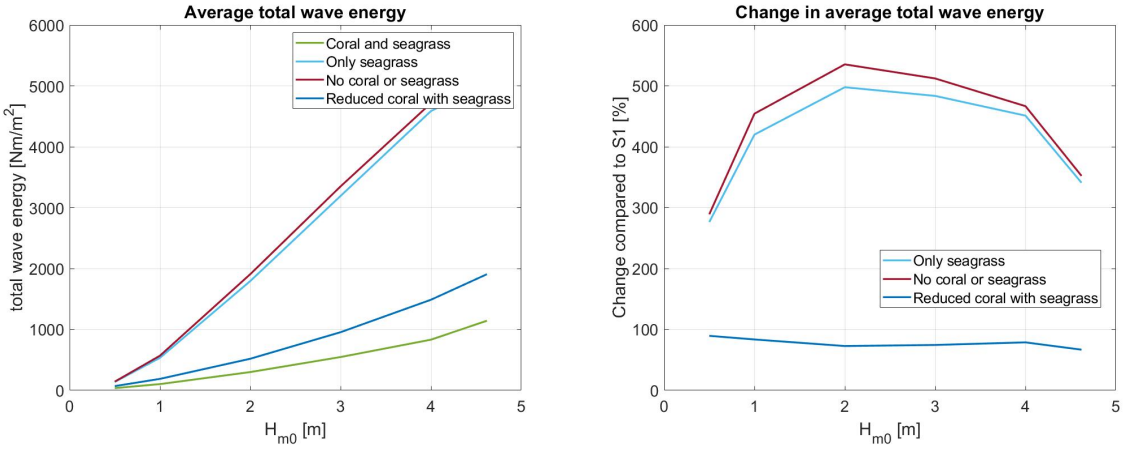

Figure 31: Average wave energy [Nm/m^2] for scenario S1, S2, S3 and S4. Transect 2

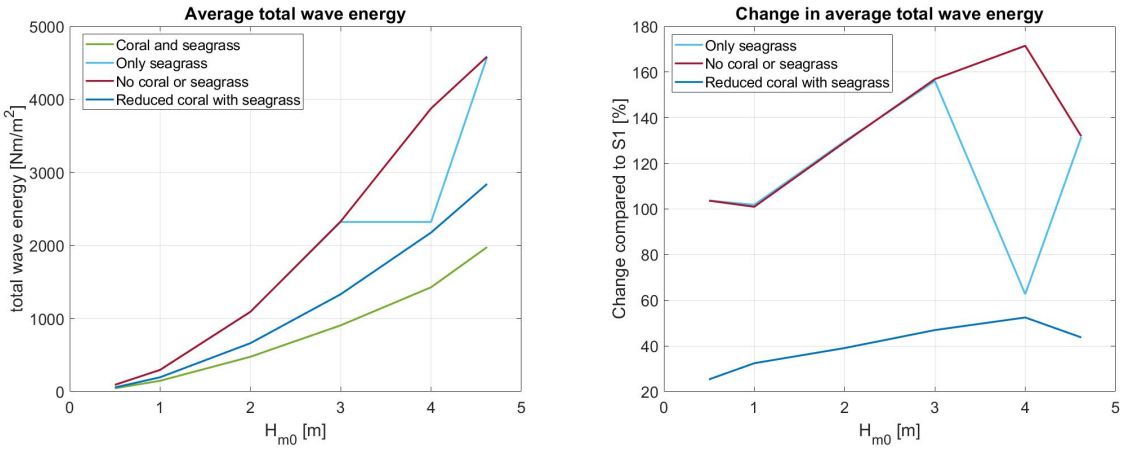

Figure 32: Average wave energy [Nm/m^2] for scenario S1, S2, S3 and S4. Transect 3

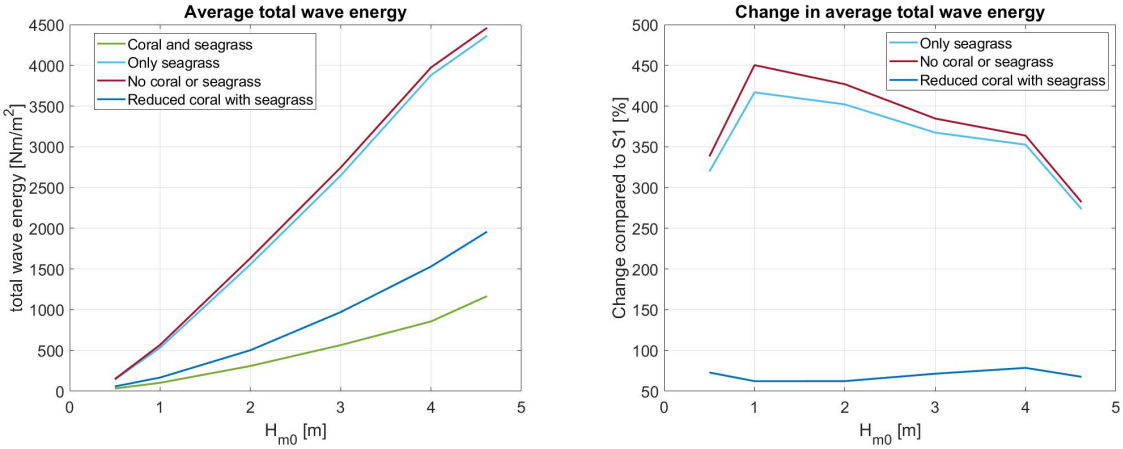

Figure 33: Average wave energy [Nm/m^2] for scenario S1, S2, S3 and S4. Transect 4

8.3 IG runup

Figure 34, 35, 36 and 37 show the average runup, $R2\%$, setup and the change in average runup, $R2\%$ and setup compared to S1 for the different scenarios and offshore wave heights (H_{m0}), per transect.

Tables 9, 10 and 11 show per transect for what scenario and at what offshore wave height the maximum increase in average runup, $R2\%$ and setup is achieved.

Table 9: Maximum increase in IG runup for each transect

Transect	Scenario	H_{m0}	$\%increase$
1	S4	1	1112
2	S4	0.5	-200
3	S4	3	55409
4	S4	1	284

Table 10: Maximum increase in IG $R2\%$ for each transect

Transect	Scenario	H_{m0}	$\%increase$
1	S4	2	1720
2	S3	2	760
3	S4	4.62	12315
4	S4	0.5	305

Table 11: Maximum increase in setup for each transect

Transect	Scenario	H_{m0}	$\%increase$
1	S4	4	137
2	S4	4	328
3	S4	4	123
4	S5	4	286

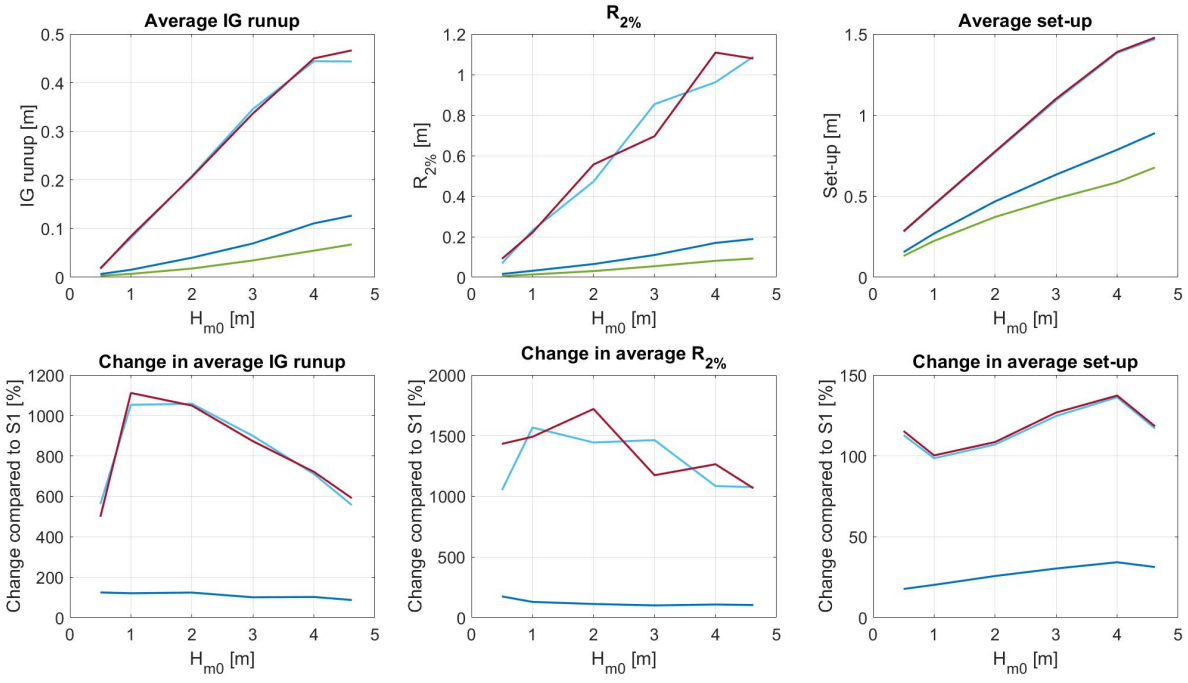

Figure 34: Average IG runup and $R_{2\%}$ for scenario S, S2, S3 and S4. Transect 1

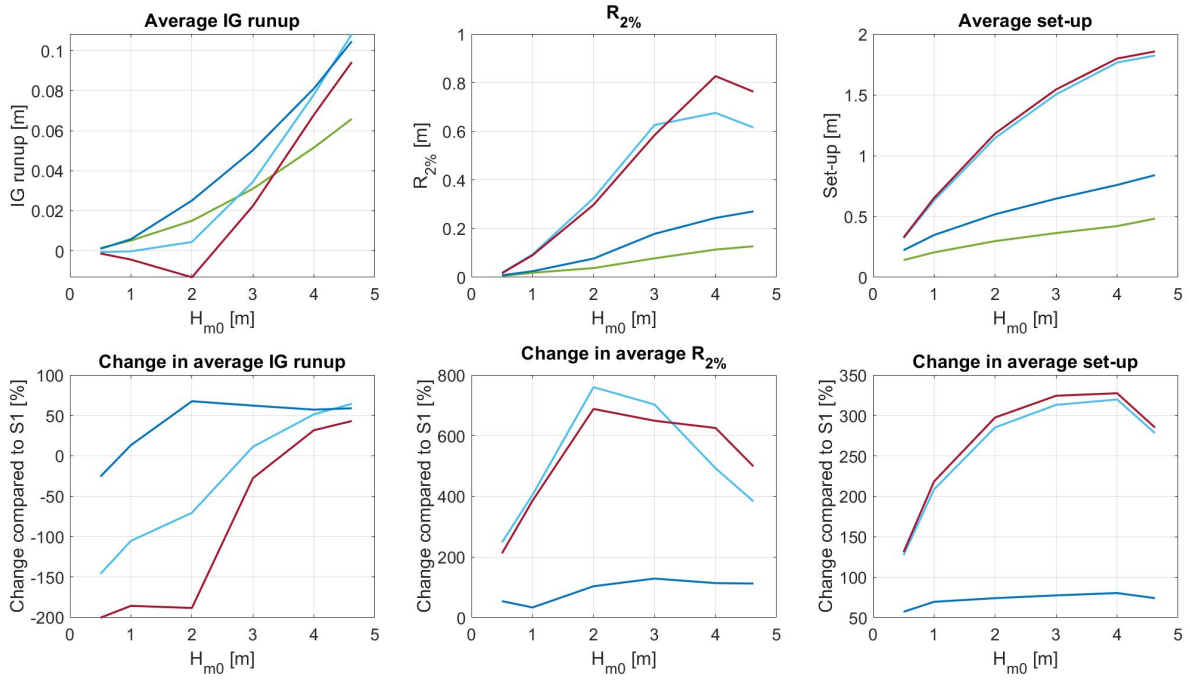

Figure 35: Average IG runup and $R_{2\%}$ for scenario S, S2, S3 and S4. Transect 2

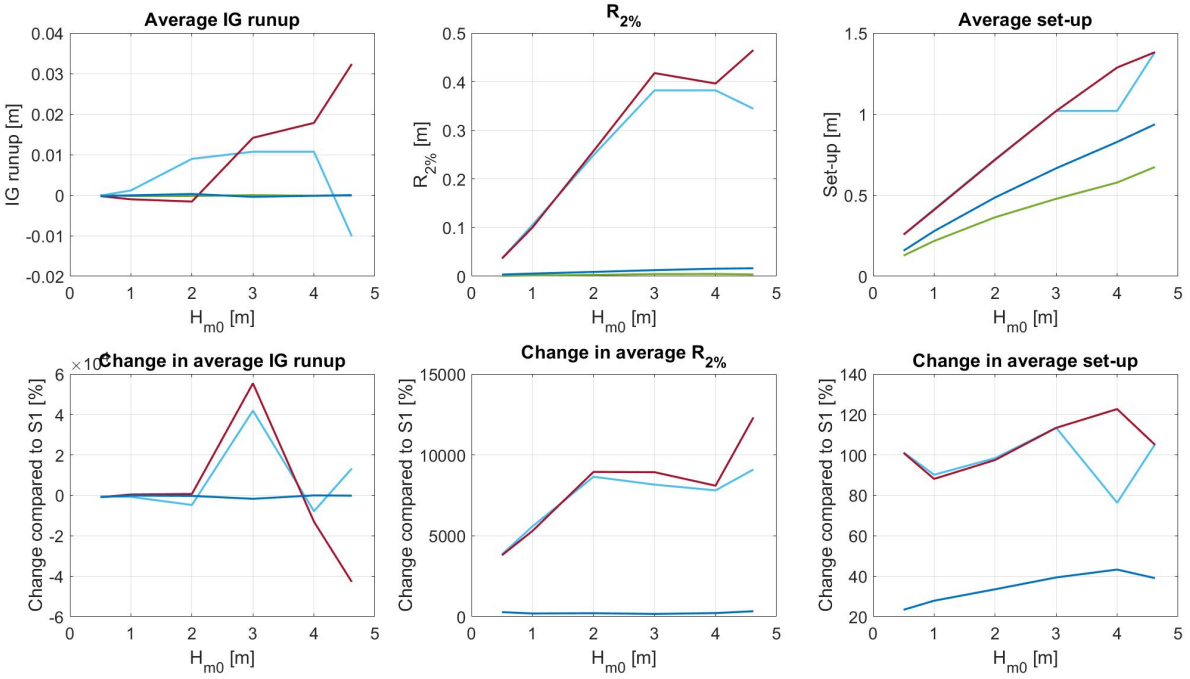

Figure 36: Average IG runup and $R_{2\%}$ for scenario S, S2, S3 and S4. Transect 3

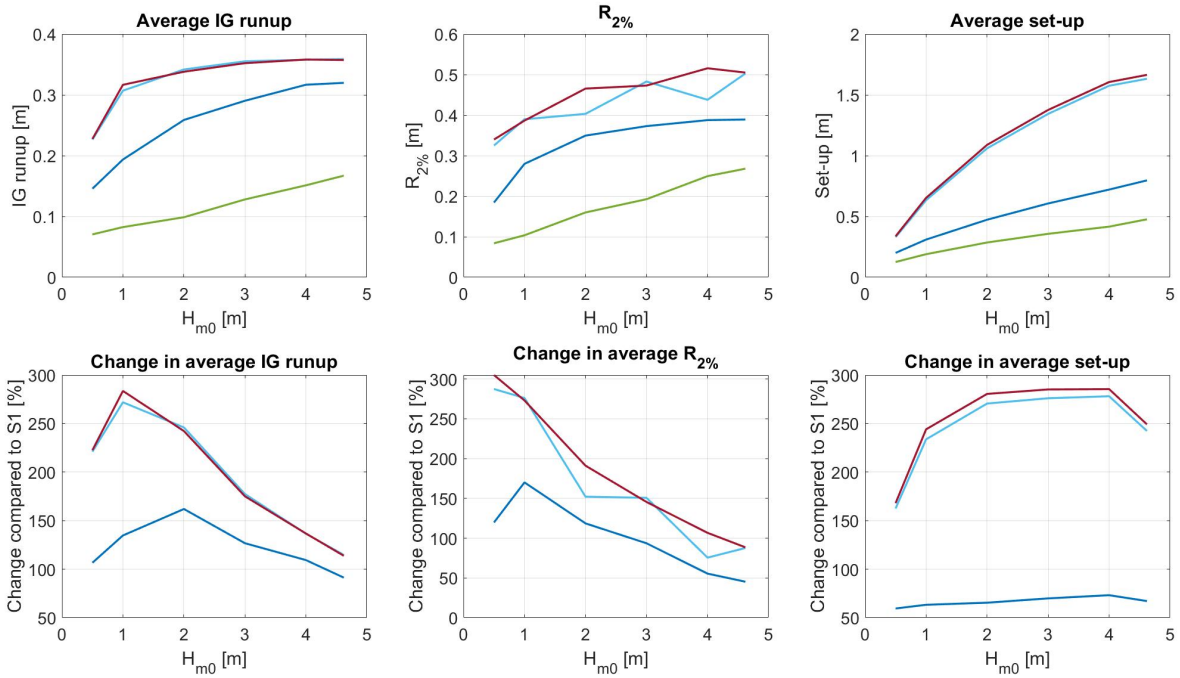

Figure 37: Average IG runup and $R_{2\%}$ for scenario S, S2, S3 and S4. Transect 4

9 Discussion

This chapter discusses the results that were found during this study. This study covers the following aspects:

- The structural complexity of corals and sea-grass is quantified using a structure for motion survey.
- The drag coefficient of corals and sea-grass is calibrated based on the results of the structure for motion survey and field data.
- The numerical model Xbeach surfbeat is used to model the wave propagation over a coral reef in its current state and in a future degraded state.
- The results of the numerical model are processed to quantify the effect of coral degradation on the wave propagation and transformation on the fringing reef in the Whitehouse bay, Jamaica.

The results, uncertainties and limitation of each aspect is discussed below.

Structure for motion

For this study, SfM is used on 5 different reef areas. The results of the SfM survey showed high quality 3-dimensional images of the reef areas. The results from chapter 5 as shown in appendix B show well-defined individual corals, textures and clear areas of vegetation cover and sediment. However, the SfM shows low accuracy in term of dimensions. Table 12 shows that the 3-dimensional images in Metashape are 20% to 120% larger that in reality.

The DEM of SfM 7 in figure 50 shows a very clear Acropora hyacinthus (see figure 38). On the adjusted DEM this coral reaches around 1.2 metres in height. (Kerry and Bellwood, 2015) research the structures of Acropora hyacinthus and found that these coral have an average height of around 0.43 [m]. Compared to this, the coral height in DEM 7 seems to be over-predicted in height. However, (Kinch et al., 2008) showed that the Acropora hyacinthus can grow up to a view metres in diameter, which shows that the width of this coral is accurately predicted.

Figure 38: Acropora hyacinthus coral

The limitation of using SfM during this study is the high computational time and storage space. To achieve the highest quality during all the steps shown in figure 15, a computational time of 14 days and a storage space of 35 GB is required per SfM. By choosing a lower quality, the computational time and storage space could be reduced to 3 days and 20 GB per SfM.

Vegetation density

I used the canopy model to account for the effect of vegetation. This model uses the vegetation height, stem thickness, vegetation density and drag coefficient of the corals and sea-grass in the study area.

Using the stem thickness and vegetation density is a commonly used method for sea-grasses, as this type of vegetation has a clear stem. The results of the photo processing showed an average vegetation density for sea-grass of 1051 $[stems/m^2]$. This vegetation density is in line with the vegetation density used by (Adhitya et al., 2014). (Adhitya et al., 2014) compared the influence of low density sea-grasses (400 $[stems/m^2]$) to high density sea-grasses ([1100 $stems/m^2$]) on the flow within a sea-grass meadow. The sea-grass density of 1051 $[stems/m^2]$ that I used during my thesis indicates high density sea-grass. This is also confirmed when we look at the pictures of the sea-grass patches.

Using the stem thickness and vegetation density for coral is less validate by previous research. However, (Lowe et al., 2005) used the density of coral to evaluate the canopy model of (Lowe et al., 2005) and (Lowe et al., 2007), and found that the results of his experiment were in good agreement with the results of research by (Lowe et al., 2005) and (Lowe et al., 2007).

The choice to use the stem thickness and vegetation density for corals is based on the 3-dimensional structures of the corals in the study area and the results of the sensitivity analysis. After photo-processing the photos with corals, the photos show the individual coral fragments that were sticking out. These individual coral fragments have a low thickness which results in a high vegetation density. The results of the SfM survey show larger rocks and corals, which would results in a large stem thickness and a low vegetation density.

The results of the sensitivity analysis show that a reduction in stem thickness of 50% and a reduction in vegetation density in 50% both cause the same increase or decrease in water-level, wave height, dissipation due to vegetation and IG runup. This would mean that the effect of a 50% increase in stem thickness combined with a 50% decrease in vegetation density would result a water-level, wave height, dissipation due to vegetation or IG runup change of around 0%.

Based on these results, the assumption is made that an under-prediction in stem thickness would lead to an over-prediction in vegetation density, which would eventually cancel each other out during the simulations.

Calibration of drag coefficient

A calibration was used to determine the drag coefficient of both the coral and sea-grass along the 1-dimensional grids. The results of the literature study showed that knowledge on how to accurately determine drag or friction coefficients from coral reefs is sorely lacking.

6 different drag coefficients were used in phase 1 of the calibration. The coral drag coefficient ranged from 0.13 to 1.68 and were based on the results of a study by (McDonald et al., 2006). The best fit was achieved for a drag coefficient of 0.5[-]. This is a relatively low drag coefficient compared to the results of (McDonald et al., 2006). (McDonald et al., 2006) determined these drag coefficients by conducting different flum experiments for uni-directional flow over corals. Our calibration also represents a flum experiment because we used a 1-dimensional grid with one directional bin. The difference is in the flow condition.

For the calibration we used wave driven flow. This could explain why the calibration resulted in a relatively low coral drag coefficient.

The sea-grass drag coefficient used in the calibration ranged from 0.05 to 1.22 and were based on the results of different studies (Cavallaro et al., 2018) (Mendez and Losada, 2004b) (Paul and Amos, 2011) (Sánchez-González et al., 2011) (Koftis et al., 2013) (Zeller et al., 2014). The best fit was achieved for a sea-grass coefficient of 0.05. This is a very low drag coefficient compared to the results of the above-mentioned studies. One reason for this is that the sea-grass was only placed in the reef flat. If we look at the propagation of the waves, we see that most of the wave height is lost on the reef crest before the waves come in contact with the sea-grass. When the wave reached the sea-grass area, they have very little energy left to be dissipated by the sea-grass. If we chose a lower coral drag coefficient, the sea-grass drag coefficient is expected to be higher.

The accuracy of the calibration is limited by the location of the pressure sensors. 18 show that the sensors on transect 2 are about 350 metres offshore and that only pressure sensor $PT2X_{19}$ and $PT2X_{17}$ are inside the area where the sea-grass is placed. This means that the adding of sea-grass only has a large effect on these two pressure sensors.

1-dimensional grid

To minimise the computational time and storage, 4, 1-dimensional grid were used instead of 1, 2-dimensional grid. The 1-dimensional reef profile with a single directional bin excludes certain reef processes, such as the directional spreading, diffraction and refraction. It also excludes the alongshore variations in bathymetry. The results from the SfM survey showed well-defined grooves and spurs. These grooves and spurs will also influence the wave propagation and are neglected during this study.

The results are in line with the expectations and existing research. It showed that the IG wave height and IG runup increased significantly with a degraded coral reef. Furthermore, the results show that wave breaking is the dominant dissipation mechanism for the scenarios with no coral reef, and that dissipation due to vegetation was dominant for the scenarios where coral reefs were still present.

Results

Incoming sea- and swell waves are subject to a range of processes when they propagate over a reef area. Many studies have shown that XB-SB can model the wave propagation of low frequency waves over reef areas.

The results of chapter 8 shows the maximum IG wave height is achieved for scenario 4 (no coral or sea-grass). These results are in line with the results of the dissipation due to waves breaking from appendix D. Section 2.2.1 explained that IG waves are generated by moving break point and the breaking of sea-swell waves. This explains that an increase in waves breaking results in an increase in IG wave generation and thus in a higher IG wave height.

The results of the wave total wave energy are also in line with the expectations. Scenario S4 shows the highest wave energy and also shows the lowest dissipation due to vegetation.

When we look at the results of the average IG runup we can see that transect 1 and 4 have highest average IG runup. This is in line with equation 2. This equation shows that the IG runup is a function of of the beach slope. Transect 1 and 4 shows a larger beach slope.

The results of this study are in line with the expectations and existing research. It showed that the IG wave height and IG runup increased significantly with a degraded coral reef. Furthermore, the results show that wave breaking is the dominant dissipation mechanism for the scenarios with no coral reef, and that dissipation due to vegetation was dominant for the scenarios where coral reefs were still present.

A limitation of using XB-SB during this study is that it only showed the effect of coral degradation on low frequency wave height under storm condition. The offshore boundary conditions from the fieldwork (sensor $OSSI_{WH01}$) were used during the sensitivity analysis and calibration. The results of these simulation showed very small low frequency wave height where the effect of coral degradation was not visible. This study also revealed the importance of further research and a better understanding of reef processes.

10 Conclusion & Recommendations

The aim of this research is to provide both an observational study on the current state of coral reefs in the study area and numerical simulations of the wave propagation over the coral reefs in both its current state and in a further degraded state. This chapter answers the research question from chapter 3. Recommendations for further research are given based on the conclusions.

10.1 Conclusion

The main question of this study is *"What effect does the degradation of coral reefs in the Whitehouse bay, Jamaica, have on the total wave energy dissipation and on the low frequency runup, considering hydrodynamic reef processes?"*. The answer to this question is given below. Because this answer is based on the answers to the different investigative questions. The Investigative questions will first be elaborated.

Investigative questions

1. *How can the structural complexity of the coral reef near Whitehouse bay in Jamaica be quantified?*

   The structural complexity of coral during this study in defined as the physical 3-dimensional structure of the coral branches or coral reefs (Jones et al., 1994). The structural complexity in this study is quantified by determining the vegetation height, stem thickness and the vegetation density.

   The following steps are taken to determine the coral height: 1) get images from the coral reef, 2) process images using Metashape and create a 3-dimensional image of the reef area, 3) create a DEM from the 3-dimensional image by adding ground control points, 4) use the ground control points to calculate the accuracy of the DEM, 5) adjust the DEM based on the accuracy and 6) use the adjusted DEM to determine the coral height.

   The following steps are taken to quantify stem thickness and vegetation density: 1) get images from the coral reef, 2) use photo processing in Matlab to highlight the coral branches, 3) calculate the thickness of the coral branches (stem thickness) and the vegetation density.

2. *How and how much does coral degradation affect its structural complexity?*

   Paragraph 2.1.4 discusses that the dying of corals or coral degradation does not automatically lead to a change in structural complexity. Degraded corals that live in areas with very low to no human- and wave impact can maintain their structural complexity until erosion occurs. If erosion of the coral branches occur, the vertical erosion rate can reach 6 [mm/year]

3. *How much does the amount of coral erosion affect the dissipation due to vegetation (Dveg)?*

   Table 16 shows that a decrease in vegetation height from 1.6 [m] to 0.1 [m] results in a decrease in Dveg of 46%. A decrease in stem thickness from 0.4[m] to 0.025 [m] results in a decrease in Dveg of 49%. A decrease in vegetation density from 2400 [corals/m^2] to 150 [corals/m^2] also results in 49% Dveg decrease. Lastly, a decrease in drag coefficient from 4 [-] to 0.25 [-] results in a decrease in Dveg of 48%.

4. *How much does the low frequency (IG) wave height and low frequency (IG) runup increase or decrease due to coral degradation and full coral erosion?*

   When we compare scenario S1 to scenario S3 a maximum increase in IG wave height of 1408% is achieved for $H_{m0} = 0.5$ on transect 1, 1094% for $H_{m0} = 2$ on transect 2, 1230% for $H_{m0} = 0.5$ on transect 3 and 1202 % for $H_{m0} = 1$ on transect 4. When we compare scenario S1 to scenario S4 a maximum increase in IG wave height of 1490% is achieved for $H_{m0} = 0.5$ on transect 1, 1094% for $H_{m0} = 2$ on transect 2, 1097% for $H_{m0} = 0.5$ on transect 3 and 1335% for $H_{m0} = 1$ on transect 4.

   The same is done for the IG runup. When we compare scenario S1 to scenario S3 we get an average increase in IG runup of 1058% for $H_{m0} = 2$ on transect 1, -146% for $H_{m0} = 0.5$ on transect 2, 41938% for $H_{m0} = 3$ on transect 3 and 272% for $H_{m0} = 1$ on transect 4. When we compare scenario S1 to scenario S4 we get an average increase in IG runup of 1112% for $H_{m0} = 1$ on transect 1, -200% for $H_{m0} = 0.5$ on transect 2, 55409% for $H_{m0} = 3$ on transect 3 and 284% for $H_{m0} = 1$ on transect 4.

The conclusion of the investigative questions are used to answer the main question:

"What effect does the degradation of coral reefs in the Whitehouse bay, Jamaica, have on the total wave energy dissipation and on the low frequency runup, considering hydrodynamic reef processes?".

Based on the results of this study we can conclude that the following things happen due to coral degradation in Whitehouse bay, Jamaica:

- The dissipation due to vegetation decreases.
- When there are no corals on the reef crest, more wave energy dissipates on the sea-grass.
- The dissipation due to waves breaking increases.
- The total wave energy increases, with a maximum of 535% when all coral and sea-grass are gone.
- The low frequency runup increases, with a maximum of 55409% when all coral and sea-grass are gone.

10.2 Recommendations

This study gives insight into the wave transformation over coral reefs in the Whitehouse bay, Jamaica. To better understand the implications of the results, future studies could address:

2-dimensional grid

First, it is recommended to investigate the wave propagation in Whitehouse bay in a 2-dimensional space. This study focuses on the wave transformation and runup of 4, 1-dimensional transects, using a single directional bin. This means that the longshore gradient is ignored and the waves are modelled perpendicular to the coast without refraction. Wave propagation over coral reefs is sensitive to the dimensional space due to a change in alongshore bathymetry. Using a 2-dimensional will result in a varying incoming short wave energy along the seaward boundary. It would be interesting to see how the IG wave transformation changes across the reef on a 2-dimensional grid where the refraction is taken into account.

The main challenge with using a 2-dimensional grid is the increased computational time and storage space. This could be resolved by using a computer with a stronger processor.

Using Xbeach non-hydrostatic (XB-NH)

The next recommendation is to use Xbeach non-hydrostatic (XB-NH) to model the wave propagation across the reef. Xbeach surf beat (XB-SB) was used for this study. The main advantage of XB-SB compared to XB-NH is the reduced computation time and storage.

It would be interesting to use XB-NH to see what the impact of coral degradation on the runup would be under normal wave conditions. The results of the sensitivity analysis and calibration of the drag coefficient showed a very small runup under normal conditions. This is because XB-SB does not solve individual short waves and does not show the contribution of incident waves to the runup.

If XB-NH is used to model the effect of coral degradation on the runup, one should keep in mind the results of (Lashley et al., 2018). (Lashley et al., 2018) found that XB-NH under-predicted the runup at the beach.

Including the effect of sea level rise

To model the effect of coral degradation on the wave transformation, 4 different future scenarios were made based on the predicted coral erosion rate. The scenarios only covered the expected vertical coral erosion in 2100 and did not consider the expected sea level rise in 2100. Sea level rise will alter the offshore water level drastically. Therefore, it is recommended to investigate the effect of a changing sea level on the wave transformation and runup in Whitehouse bay Jamaica. To do this, different scenarios must be made based on the predicted sea level rise. These scenarios can compare the highest and lowest expected sea level rise in 2100.

11 Bibliography

References

Adhitya, A., Bouma, T., Folkard, A., Van Katwijk, M., Callaghan, D., De Iongh, H., and Herman, P. (2014). Comparison of the influence of patch-scale and meadow-scale characteristics on flow within seagrass meadows: a flume study. *Marine Ecology Progress Series*, 516:49–59.

Aldred, J. (2014). Caribbean coral reefs 'will be lost within 20 years' without protection. *The Guardian http://www. theguardian. com/environment/2014/jul/02/caribbean-coralreef-lost-fishing-pollution-report*.

Apotsos, A., Raubenheimer, B., Elgar, S., Guza, R., and Smith, J. A. (2007). Effects of wave rollers and bottom stress on wave setup. *Journal of Geophysical Research: Oceans*, 112(C2).

Baldock, T. (2012). Dissipation of incident forced long waves in the surf zone—implications for the concept of "bound" wave release at short wave breaking. *Coastal Engineering*, 60:276–285.

Baldock, T., Holmes, P., Bunker, S., and Van Weert, P. (1998). Cross-shore hydrodynamics within an unsaturated surf zone. *Coastal Engineering*, 34(3-4):173–196.

Battjes, J., Bakkenes, H., Janssen, T., and van Dongeren, A. R. (2004). Shoaling of subharmonic gravity waves. *Journal of Geophysical Research: Oceans*, 109(C2).

Bertin, X., De Bakker, A., Van Dongeren, A., Coco, G., André, G., Ardhuin, F., Bonneton, P., Bouchette, F., Castelle, B., Crawford, W. C., et al. (2018). Infragravity waves: From driving mechanisms to impacts. *Earth-Science Reviews*, 177:774–799.

Beyer, D. (1994). Energy dissipation in random breaking waves: the probability of breaking.

Block, H. (2008). John bruno (topic editor). 2008.".

Bruckner, A. (2011). Khaled bin sultan living oceans foundation 2011 coral reef assessment cay sal.

Buckley, M. L., Lowe, R. J., Hansen, J. E., and Van Dongeren, A. R. (2015). Dynamics of wave setup over a steeply sloping fringing reef. *Journal of Physical Oceanography*, 45(12):3005–3023.

Buckley, M. L., Lowe, R. J., Hansen, J. E., van Dongeren, A. R., and Storlazzi, C. D. (2018). Mechanisms of wave-driven water level variability on reef-fringed coastlines. *Journal of Geophysical Research: Oceans*, 123(5):3811–3831.

Cavallaro, L., Viviano, A., Paratore, G., and Foti, E. (2018). Experiments on surface waves interacting with flexible aquatic vegetation. *Ocean Science Journal*, 53(3):461–474.

Chawla, A., Spindler, D. M., and Tolman, H. L. (2013). Validation of a thirty year wave hindcast using the climate forecast system reanalysis winds. *Ocean Modelling*, 70:189–206.

Cheriton, O. M., Storlazzi, C. D., and Rosenberger, K. J. (2016). Observations of wave transformation over a fringing coral reef and the importance of low-frequency waves and offshore water levels to runup, overwash, and coastal flooding. *Journal of Geophysical Research: Oceans*, 121(5):3121–3140.

Dally, W. R. and Brown, C. A. (1995). A modeling investigation of the breaking wave roller with application to cross-shore currents. *Journal of Geophysical Research: Oceans*, 100(C12):24873–24883.

Daly, C. and Nienhuis, J. (2018). Effect of reef degradation on sediment flushing through reef gaps: Whitehouse, jamaica. In *AGU Fall Meeting Abstracts*, volume 2018, pages OS11E–1449.

Eakin, C. (1996). Where have all the carbonates gone? a model comparison of calcium carbonate budgets before and after the 1982–1983 el nino at uva island in the eastern pacific. *Coral Reefs*, 15(2):109–119.

Eldeberky, Y. (1997). Nonlinear transformation of wave spectra in the nearshore zone. *Oceanographic Literature Review*, 4(44):297.

Erickson, J. and Kusky, T. M. (2009). *Marine geology: exploring the new frontiers of the ocean*. Infobase Publishing.

Evans, D. and Jones, A. J. (2002). A proof of the gamma test. *Proceedings of the Royal Society of London. Series A: Mathematical, Physical and Engineering Sciences*, 458(2027):2759–2799.

Feddersen, F., Guza, R., Elgar, S., and Herbers, T. (2000). Velocity moments in alongshore bottom stress parameterizations. *Journal of Geophysical Research: Oceans*, 105(C4):8673–8686.

Franklin, G., Mariño-Tapia, I., and Torres-Freyermuth, A. (2013). Effects of reef roughness on wave setup and surf zone currents. *Journal of Coastal Research*, (65):2005–2010.

Ghisalberti, M. (2009). Obstructed shear flows: similarities across systems and scales. *Journal of Fluid Mechanics*, 641:51.

Goreau, T. J. and Hilbertz, W. (2012). Reef restoration using seawater electrolysis in jamaica. *Innovative Methods of Marine Ecosystem Restoration, CRC Press, Boca Raton*, pages 35–45.

Gourlay, M. (1994). Wave transformation on a coral reef. *Coastal engineering*, 23(1-2):17–42.

Gourlay, M. (1996). Wave set-up on coral reefs. 2. set-up on reefs with various profiles. *Coastal Engineering*, 28(1-4):17–55.

Gourlay, M. R. (1992). Wave set-up, wave run-up and beach water table: Interaction between surf zone hydraulics and groundwater hydraulics. *Coastal engineering*, 17(1-2):93–144.

Govender, K., Mocke, G., and Alport, M. (2002). Video-imaged surf zone wave and roller structures and flow fields. *Journal of Geophysical Research: Oceans*, 107(C7):9–1.

Graham, N. and Nash, K. (2013). The importance of structural complexity in coral reef ecosystems. *Coral reefs*, 32(2):315–326.

Grant, W. D. and Madsen, O. S. (1979). Combined wave and current interaction with a rough bottom. *Journal of Geophysical Research: Oceans*, 84(C4):1797–1808.

Guza, R. and Feddersen, F. (2012). Effect of wave frequency and directional spread on shoreline runup. *Geophysical Research Letters*, 39(11).

Herbers, T., Elgar, S., and Guza, R. (1995a). Generation and propagation of infragravity waves. *Journal of Geophysical Research: Oceans*, 100(C12):24863–24872.

Herbers, T., Elgar, S., Guza, R., and O'Reilly, W. (1995b). Infragravity-frequency (0.005–0.05 hz) motions on the shelf. part ii: Free waves. *Journal of physical oceanography*, 25(6):1063–1079.

Houthuys, R., Trentesaux, A., and De Wolf, P. (1994). Storm influences on a tidal sandbank's surface (middelkerke bank, southern north sea). *Marine Geology*, 121(1-2):23–41.

Jones, C. G., Lawton, J. H., and Shachak, M. (1994). Organisms as ecosystem engineers. In *Ecosystem management*, pages 130–147. Springer.

Kerry, J. T. and Bellwood, D. R. (2015). Do tabular corals constitute keystone structures for fishes on coral reefs? *Coral Reefs*, 34(1):41–50.

Kinch, J., Purcell, S., Uthicke, S., Friedman, K., et al. (2008). Population status, fisheries and trade of sea cucumbers in the western central pacific. *Sea cucumbers. A global review of fisheries and trade. FAO Fisheries and Aquaculture Technical Paper*, 516:7–55.

King, C. A. M. and Schwartz, M. L. (2019). Lagoon. https://www.britannica.com/science/lagoon-geography. Accessed: December 24, 2020.

Klomp, K., Clarke, K., Marks, K., and Miller, M. (2003). Condition of reef fish on jamaica's north coast signals late stages of overexplotation.

Koehl, M. and Hadfield, M. (2004). Soluble settlement cue in slowly moving water within coral reefs induces larval adhesion to surfaces. *Journal of Marine Systems*, 49(1-4):75–88.

Koftis, T., Prinos, P., and Stratigaki, V. (2013). Wave damping over artificial posidonia oceanica meadow: A large-scale experimental study. *Coastal Engineering*, 73:71–83.

Lashley, C. H., Roelvink, D., van Dongeren, A., Buckley, M. L., and Lowe, R. J. (2018). Nonhydrostatic and surfbeat model predictions of extreme wave run-up in fringing reef environments. *Coastal Engineering*, 137:11–27.

Leal, M. C., Ferrier-Pagès, C., Petersen, D., and Osinga, R. (2016). Coral aquaculture: applying scientific knowledge to ex situ production. *Reviews in Aquaculture*, 8(2):136–153.

Longuet-Higgins, M. S. and Stewart, R. (1964). Radiation stresses in water waves; a physical discussion, with applications. In *Deep sea research and oceanographic abstracts*, volume 11, pages 529–562. Elsevier.

Lowe, R. (2007). Jr koseff, sg monismith, and mj atkinson. 2007. spectral wave flow attenuation within submerged canopies: implications for wave energy dissipation. *J. Geophys. Res*, 112:C05018.

Lowe, R. J. and Falter, J. L. (2015). Oceanic forcing of coral reefs. *Annual review of marine science*, 7:43–66.

Lowe, R. J., Falter, J. L., Koseff, J. R., Monismith, S. G., and Atkinson, M. J. (2007). Spectral wave flow attenuation within submerged canopies: Implications for wave energy dissipation. *Journal of Geophysical Research: Oceans*, 112(C5).

Lowe, R. J., Koseff, J. R., and Monismith, S. G. (2005). Oscillatory flow through submerged canopies: 1. velocity structure. *Journal of Geophysical Research: Oceans*, 110(C10).

Lowe, R. J., Shavit, U., Falter, J. L., Koseff, J. R., and Monismith, S. G. (2008). Modeling flow in coral communities with and without waves: A synthesis of porous media and canopy flow approaches. *Limnology and Oceanography*, 53(6):2668–2680.

Luhar, M., Coutu, S., Infantes, E., Fox, S., and Nepf, H. (2010). Wave-induced velocities inside a model seagrass bed. *Journal of Geophysical Research: Oceans*, 115(C12).

Luhmann, T., Robson, S., Kyle, S., and Boehm, J. (2019). *Close-range photogrammetry and 3D imaging*. de Gruyter.

McDonald, C., Koseff, J., and Monismith, S. (2006). Effects of the depth to coral height ratio on drag coefficients for unidirectional flow over coral. *Limnology and oceanography*, 51(3):1294–1301.

Mendez, F. and Losada, I. (2004a). Transformation of random and non-random breaking waves over vegetation fields. *Coast. Eng*, 51:103–118.

Mendez, F. J. and Losada, I. J. (2004b). An empirical model to estimate the propagation of random breaking and nonbreaking waves over vegetation fields. *Coastal Engineering*, 51(2):103–118.

Monismith, S. G. (2007). Hydrodynamics of coral reefs. *Annu. Rev. Fluid Mech.*, 39:37–55.

Monismith, S. G., Rogers, J. S., Koweek, D., and Dunbar, R. B. (2015). Frictional wave dissipation on a remarkably rough reef. *Geophysical Research Letters*, 42(10):4063–4071.

Moyle, P. B. and Cech, J. J. (2004). *Fishes: an introduction to ichthyology*. Number 597 MOY.

Munk, W. H. (1951). Origin and generation of waves. Technical report, Scripps Institution of Oceanography La Jolla Calif.

Munk, W. H., Miller, G., Snodgrass, F., and Barber, N. F. (1963). Directional recording of swell from distant storms. *Philosophical Transactions of the Royal Society of London. Series A, Mathematical and Physical Sciences*, 255(1062):505–584.

Munk, W. H. and Sargent, M. C. (1954). Bikini and nearby atolls, marshall islands; oceanography (physical): Adjustment of bikini atoll to ocean waves. Technical report.

Nelson, R. C. (1994). Depth limited design wave heights in very flat regions. *Coastal Engineering*, 23(1-2):43–59.

Nepf, H. and Vivoni, E. (2000). Flow structure in depth-limited, vegetated flow. *Journal of Geophysical Research: Oceans*, 105(C12):28547–28557.

Nepf, H. M. (2012). Flow and transport in regions with aquatic vegetation. *Annual review of fluid mechanics*, 44:123–142.

Network, R. R. (2010). Recruitment — reef resilience.

NOAA (2020). What are Coral Reefs. [Accessed: December 24, 2020].

Nwogu, O. and Demirbilek, Z. (2010). Infragravity wave motions and runup over shallow fringing reefs. *Journal of waterway, port, coastal, and ocean engineering*, 136(6):295–305.

Nyström, M., Folke, C., and Moberg, F. (2000). Coral reef disturbance and resilience in a human-dominated environment. *Trends in ecology & evolution*, 15(10):413–417.

Ozyesil, O., Voroninski, V., Basri, R., and Singer, A. (2017). A survey of structure from motion. *arXiv preprint arXiv:1701.08493*.

Paul, M. and Amos, C. (2011). Spatial and seasonal variation in wave attenuation over zostera noltii. *Journal of Geophysical Research: Oceans*, 116(C8).

Pearson, S. G. (2016). Predicting wave-induced flooding on low-lying tropical islands using a bayesian network.

Péquignet, A. C. N., Becker, J. M., Merrifield, M. A., and Aucan, J. (2009). Forcing of resonant modes on a fringing reef during tropical storm man-yi. *Geophysical Research Letters*, 36(3).

Phinney, J. T., Hoegh-Guldberg, O., Kleypas, J., Skirving, W., and Strong, A. (2006). and estuarine studies.

Plass-Johnson, J., Cardini, U., van Hoytema, N., Bayraktarov, E., Burghardt, I., Naumann, M., and Wild, C. (2015). *Coral Bleaching*, pages 117 – 146.

Pomeroy, A., Lowe, R., Symonds, G., Van Dongeren, A., and Moore, C. (2012). The dynamics of infragravity wave transformation over a fringing reef. *Journal of Geophysical Research: Oceans*, 117(C11).

Pomeroy, A. W., Lowe, R. J., Van Dongeren, A. R., Ghisalberti, M., Bodde, W., and Roelvink, D. (2015). Spectral wave-driven sediment transport across a fringing reef. *Coastal Engineering*, 98:78–94.

Quataert, E. (2015). Wave runup on atoll reefs.

Raubenheimer, B., Guza, R., Elgar, S., and Kobayashi, N. (1995). Swash on a gently sloping beach. *Journal of Geophysical Research: Oceans*, 100(C5):8751–8760.

Raupach, M. R. and Shaw, R. (1982). Averaging procedures for flow within vegetation canopies. *Boundary-Layer Meteorology*, 22(1):79–90.

Rey, A. (2019). Wave runup on fringing reefs with paleo-stream channels.

Roelvink, D., Reniers, A., Van Dongeren, A., Van Thiel de Vries, J., Lescinski, J., and McCall, R. (2010). Xbeach model description and manual. *Unesco-IHE Institute for Water Education, Deltares and Delft University of Tecnhology. Report June*, 21:2010.

Roelvink, F. (2019). Coral restoration for coastal hazard risk reduction: The effect of coral restoration on wave transformation over various reef morphologies and the resulting runup.

Roelvink, J. (1993). Dissipation in random wave groups incident on a beach. *Coastal Engineering*, 19(1-2):127–150.

Sánchez-González, J. F., Sánchez-Rojas, V., and Memos, C. D. (2011). Wave attenuation due to posidonia oceanica meadows. *Journal of Hydraulic Research*, 49(4):503–514.

Shimozono, T., Tajima, Y., Kennedy, A. B., Nobuoka, H., Sasaki, J., and Sato, S. (2015). Combined infragravity wave and sea-swell runup over fringing reefs by super typhoon haiyan. *Journal of Geophysical Research: Oceans*, 120(6):4463–4486.

Smithers, S. (2011). Fringing reefs. Springer.

Sous, D., Tissier, M., Rey, V., Touboul, J., Bouchette, F., Devenon, J.-L., Chevalier, C., and Aucan, J. (2019). Wave transformation over a barrier reef. *Continental Shelf Research*, 184:66–80.

Stive, M. J. and De Vriend, H. J. (1995). Shear stresses and mean flow in shoaling and breaking waves. In *Coastal Engineering 1994*, pages 594–608.

Stockdon, H. F., Holman, R. A., Howd, P. A., and Sallenger Jr, A. H. (2006). Empirical parameterization of setup, swash, and runup. *Coastal engineering*, 53(7):573–588.

Storlazzi, C. D., Gingerich, S. B., van Dongeren, A., Cheriton, O. M., Swarzenski, P. W., Quataert, E., Voss, C. I., Field, D. W., Annamalai, H., Piniak, G. A., et al. (2018). Most atolls will be uninhabitable by the mid-21st century because of sea-level rise exacerbating wave-driven flooding. *Science Advances*, 4(4):eaap9741.

Suzuki, T., Zijlema, M., Burger, B., Meijer, M. C., and Narayan, S. (2012). Wave dissipation by vegetation with layer schematization in swan. *Coastal Engineering*, 59(1):64–71.

Svendsen, I. A. (1984). Wave heights and set-up in a surf zone. *Coastal engineering*, 8(4):303–329.

Symonds, G., Black, K. P., and Young, I. R. (1995). Wave-driven flow over shallow reefs. *Journal of Geophysical Research: Oceans*, 100(C2):2639–2648.

Symonds, G., Huntley, D. A., and Bowen, A. J. (1982). Two-dimensional surf beat: Long wave generation by a time-varying breakpoint. *Journal of Geophysical Research: Oceans*, 87(C1):492–498.

Van Dongeren, A., Battjes, J., Janssen, T., Van Noorloos, J., Steenhauer, K., Steenbergen, G., and Reniers, A. (2007). Shoaling and shoreline dissipation of low-frequency waves. *Journal of Geophysical Research: Oceans*, 112(C2).

Van Dongeren, A., Lowe, R., Pomeroy, A., Duong, T. M., Roelvink, D., Symonds, G., and Ranasinghe, R. (2012). Modelling infragravity waves and currents across a fringing coral reef. *Coastal Engineering Proceedings*, 1(33):currents–29.

Van Dongeren, A., Lowe, R., Pomeroy, A., Trang, D. M., Roelvink, D., Symonds, G., and Ranasinghe, R. (2013). Numerical modeling of low-frequency wave dynamics over a fringing coral reef. *Coastal Engineering*, 73:178–190.

Van Dongeren, A., Reniers, A., Battjes, J., and Svendsen, I. (2003). Numerical modeling of infragravity wave response during delilah. *Journal of Geophysical Research: Oceans*, 108(C9).

van Rooijen, A. A., Lowe, R., Ghisalberti, M., Hansen, J., McCall, R., and Van Dongeren, A. (2016). Physical and numerical modelling of wave transformation through a coastal canopy. In *20th Australian Fluid Mechanics Conference*, pages 1–4.

Vetter, O., Becker, J. M., Merrifield, M. A., Pequignet, A.-C., Aucan, J., Boc, S. J., and Pollock, C. E. (2010). Wave setup over a pacific island fringing reef. *Journal of Geophysical Research: Oceans*, 115(C12).

Webb, P. (2020). Coral Reefs. [Online; accessed 2021-03-29].

Wiechen, P. (2020). Wave dissipation on a complex coral reef.

Woodroffe, C. D. and Biribo, N. (2011). Atolls.

Yao, Y., He, W., Du, R., and Jiang, C. (2017). Study on wave-induced setup over fringing reefs in the presence of a reef crest. *Applied Ocean Research*, 66:164–177.

Young, I. R. (1989). Wave transformation over coral reefs. *Journal of Geophysical Research: Oceans*, 94(C7):9779–9789.

Zeller, R. B., Weitzman, J. S., Abbett, M. E., Zarama, F. J., Fringer, O. B., and Koseff, J. R. (2014). Improved parameterization of seagrass blade dynamics and wave atten-

uation based on numerical and laboratory experiments. *Limnology and Oceanography*, 59(1):251–266.

Zijlema, M. (2012). Modelling wave transformation across a fringing reef using swash. In *ICCE 2012: Proceedings of the 33rd International Conference on Coastal Engineering, Santander, Spain, 1-6 July 2012*. Coastal Engineering Research Council.

Part I

Appendix

12 Appendix A 'parm.file'

```
%%%%%%%%%%%%%%%%%%%%%%%%%%%%%%%%%%%%%%%%%%%%%%%%%%%%%%%%%%%%%%%%%%%%%%%%%%%%
%%%                                                                       %%%
%%%          XBeach parameter settings input file                         %%%
%%%          Location: Whitehouse                                         %%%
%%%          File ID:  wh03_real                                          %%%
%%%                                                                       %%%
%%%%%%%%%%%%%%%%%%%%%%%%%%%%%%%%%%%%%%%%%%%%%%%%%%%%%%%%%%%%%%%%%%%%%%%%%%%%

%%% Grid parameters %%%%%%%%%%%%%%%%%%%%%%%%%%%%%%%%%%%%%%%%%%%%%%%%%%%%%%%%

depfile     = bed.dep
posdwn      = 1
nx          = 374
ny          = 0
alfa        = 0
vardx       = 1
xfile       = x.grd
yfile       = y.grd
xori        = 0
yori        = 0
thetamin    = -90
thetamax    = 90
dtheta      = 180
thetanaut     1
mpiboundary   man
nmpi          1
mmpi          1

%%% Processes %%%%%%%%%%%%%%%%%%%%%%%%%%%%%%%%%%%%%%%%%%%%%%%%%%%%%%%%%%%%%

swave       = 1
lwave       = 1
flow        = 1
sedtrans    = 0
morphology  = 0
avalanching = 0
nonh        = 0
gwflow      = 0
```

Figure 39: parm.file Xbeach part 1

```
%%% General constants %%%%%%%%%%%%%%%%%%%%%%%%%%%%%%%%%%%%%%%%%%%%%%%%%%%%%%%%

rho         = 1025
g           = 9.81

%%% Flow boundary conditions %%%%%%%%%%%%%%%%%%%%%%%%%%%%%%%%%%%%%%%%%%%%%%%%%%

front       = abs_1d
back        = abs_1d
left        = neumann
right       = neumann
cyclic      = 0
order       = 2
secorder    = 1
nuh         = 0.1
zs0         = 0

%%% Wave boundary condition parameters %%%%%%%%%%%%%%%%%%%%%%%%%%%%%%%%%%%%%%%%

instat      = jons_table
bcfile      = jonswap.txt
Rt          = 1200
taper       = 10
dtbc        = 0.5
fnyq        = 5
lateralwave = wavecrest
waveform    = ruessink_vanrijn

%%% Wave breaking %%%%%%%%%%%%%%%%%%%%%%%%%%%%%%%%%%%%%%%%%%%%%%%%%%%%%%%%%%%%%

break       = roelvink1
bedfriction = manning
bedfriccoef = 0.02
```

Figure 40: parm.file Xbeach part 2

```
%%% Vegetation %%%%%%%%%%%%%%%%%%%%%%%%%%%%%%%%%%%%%%%%%%%%%%%%%%%%%%%%%%%%%%%

nveg          = 2
vegcanflo     = 1
vegetation    = 1
veggiefile    = vegetation.txt
veggiemapfile = coralbed.txt

%%% Model time %%%%%%%%%%%%%%%%%%%%%%%%%%%%%%%%%%%%%%%%%%%%%%%%%%%%%%%%%%%%%%%

tstart      = 0
tstop       = 18000
taper       = 3600
start on dd mmm yyyy and run for 4h + 1h spinup
```

Figure 41: parm.file Xbeach part 3

```
%%% Output variables %%%%%%%%%%%%%%%%%%%%%%%%%%%%%%%%%%%%%%%%%%%%%%%%%%%%%%%%

tintg       = 240
nglobalvar  = 9
H
zs
u
v
E
Qb
D
Df
Dveg

tintp = 100
npointvar = 2
H
zs

npoints = 9
0. 0.
282. 0.
588. 0.
750. 0.
894. 0.
1044. 0.
1375. 0.
1650. 0.
1691. 0.

nrugauge    = 1
1650. 0.
```

Figure 42: parm.file Xbeach part 4

13 Appendix B Results DEM

Table 12: Accuracy of the SfM results

	width GCP in Metashape [m]	width GCP in field site [m]	accuracy [%]
SfM_4	1.5	1	67
SfM_5	2	1	50
SfM_6	2.2	1	45
SfM_7	1.69	1	59
SfM_8	1.2	1	83

Figure 43, 44, 45, 46 and 47 show the results from the SfM survey processed in Metashape. Figure 43, 44 and 47 show very clear grooves and spurs and 45 shows large amounts of sea-grass.

Figure 48, 49, 50, 51 and 52. show the DEM, adjusted DEM and the slopes of SfM 4, 5, 6, 7 and 8 respectively.

Figure 43: Reef structure on location SfM_4

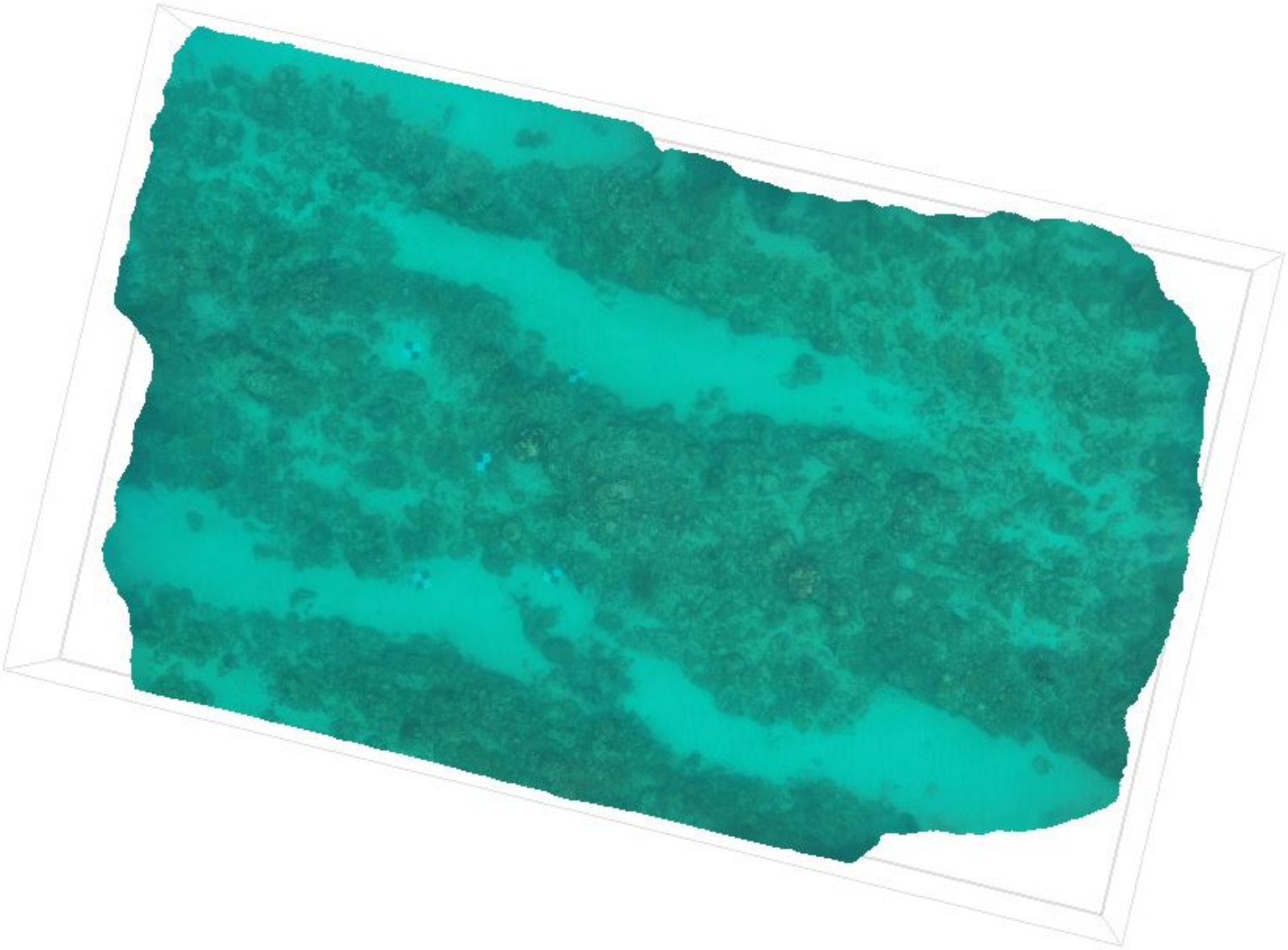

Figure 44: Reef structure on location SfM_5

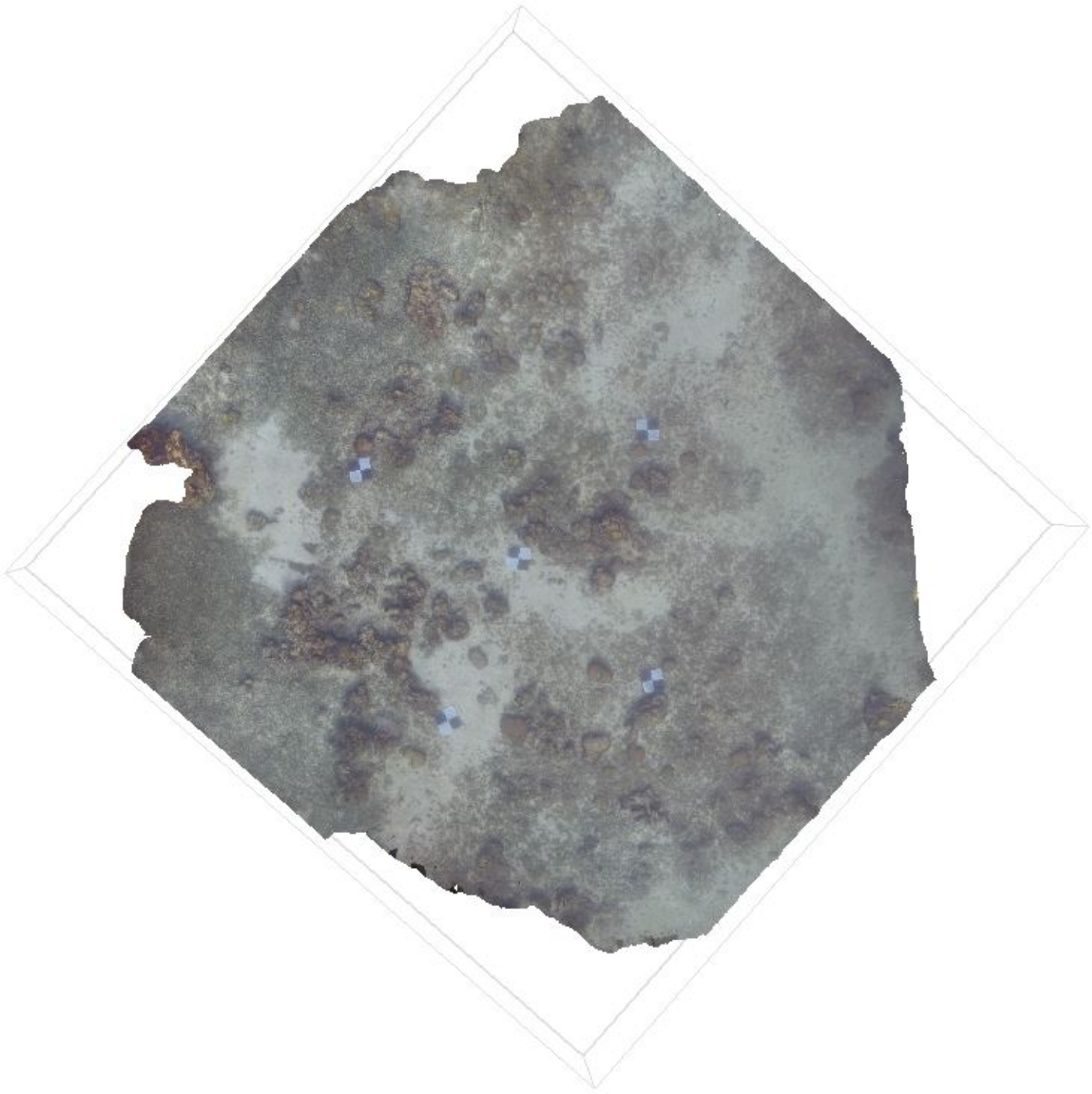

Figure 45: Reef structure on location SfM_6

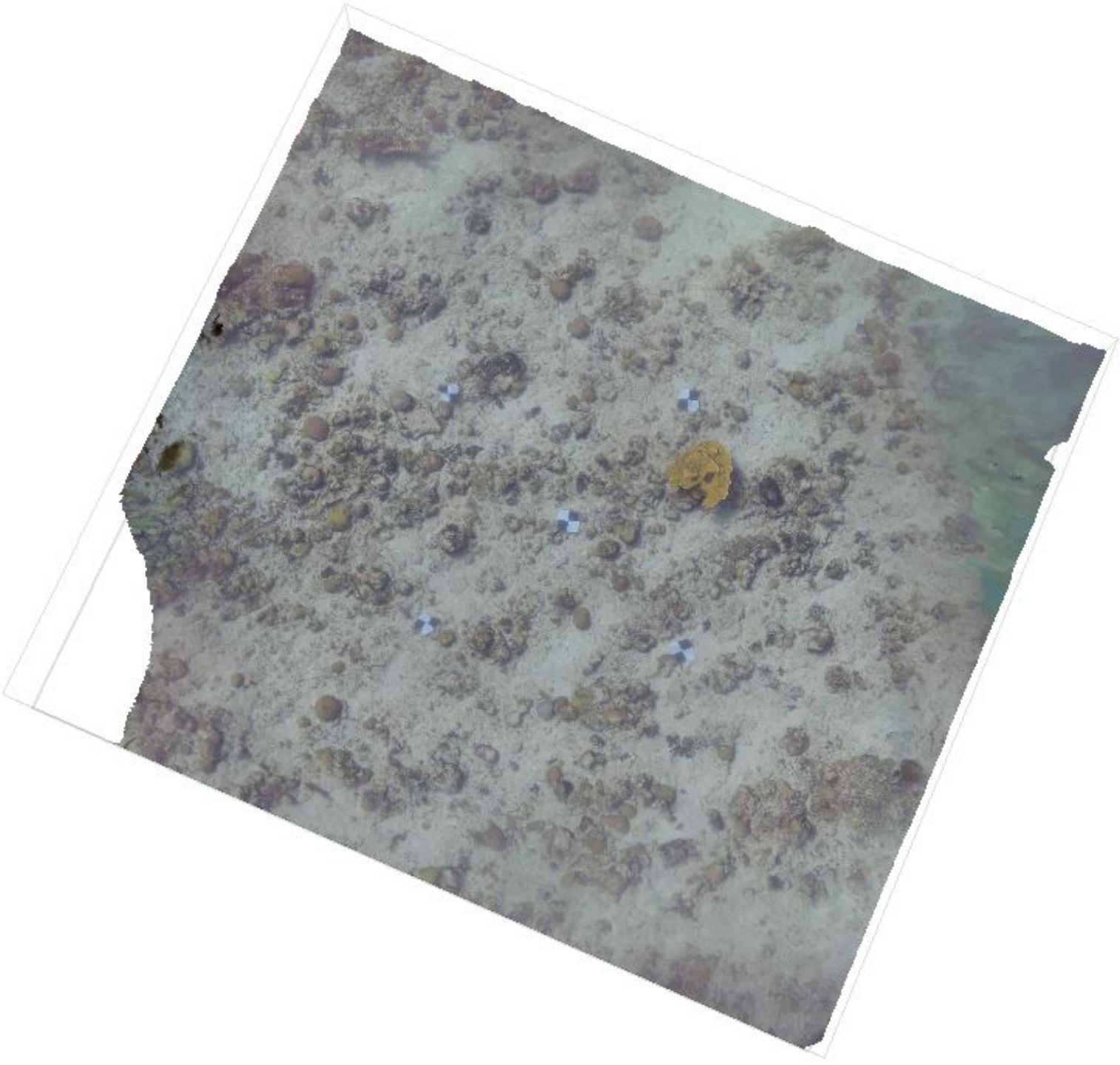

Figure 46: Reef structure on location SfM_7

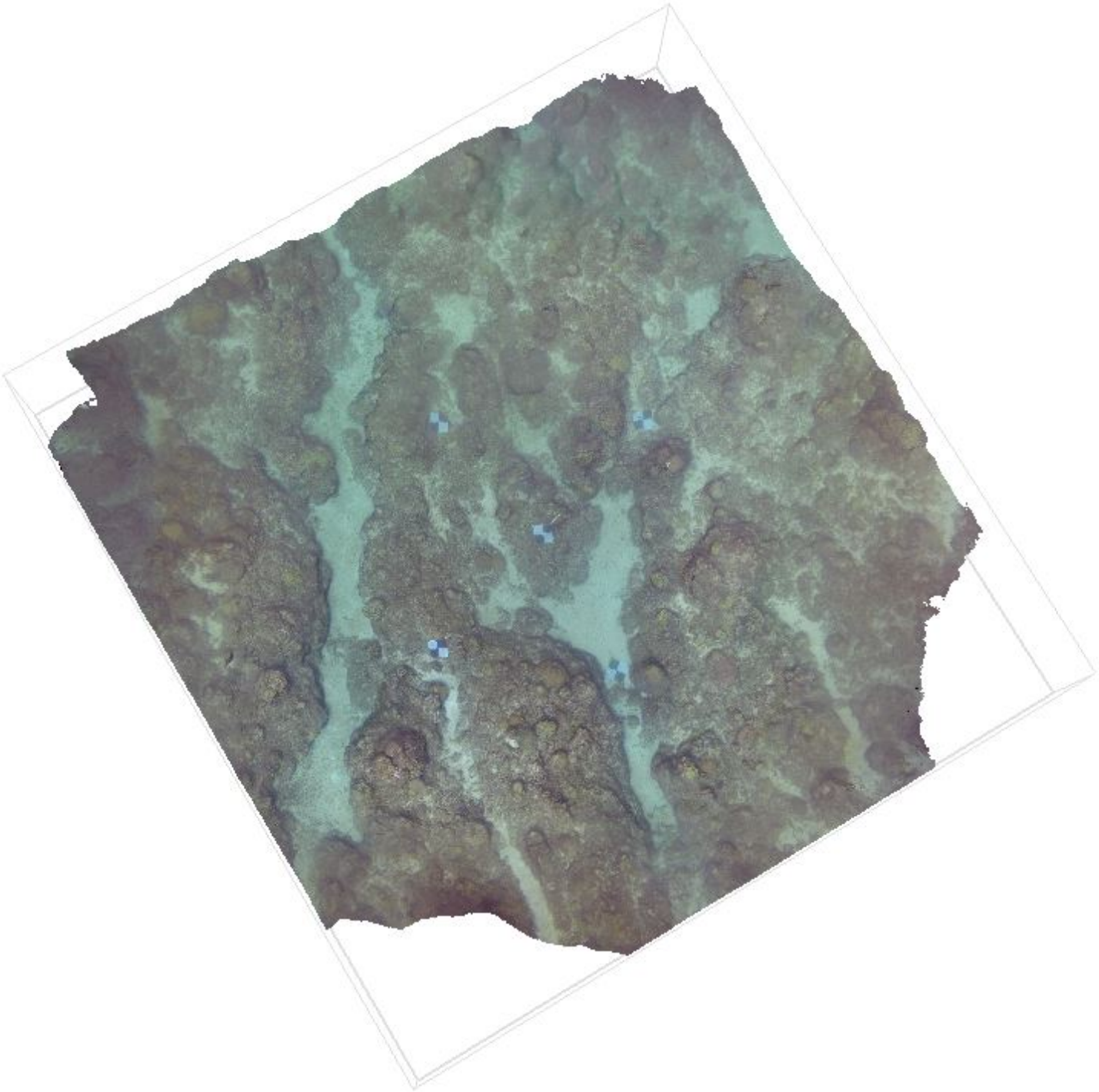

Figure 47: Reef structure on location SfM_8

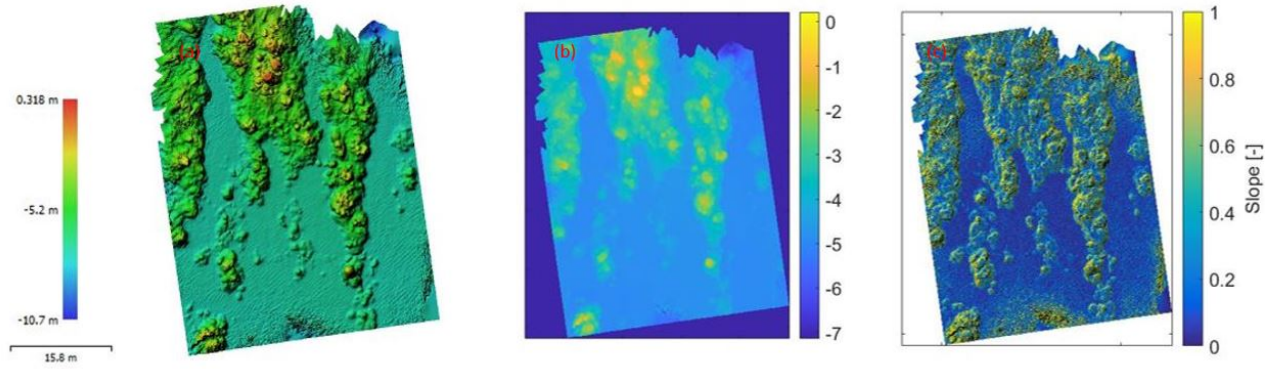

Figure 48: (a) DEM results from the structure for motion survey processed in Agisoft Metashape, for location SfM_4. (b) Adjusted DEM (c) slope

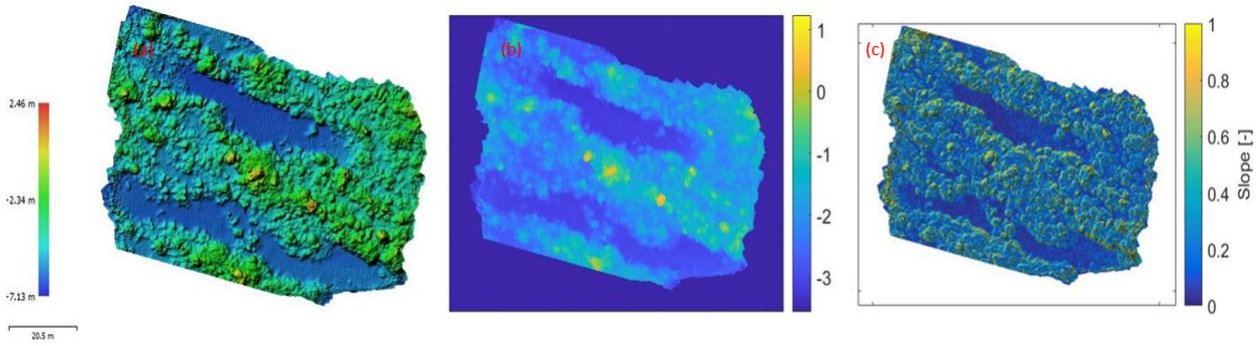

Figure 49: (a) DEM results from the structure for motion survey processed in Agisoft Metashape, for location SfM_5. (b) Adjusted DEM (c) slope

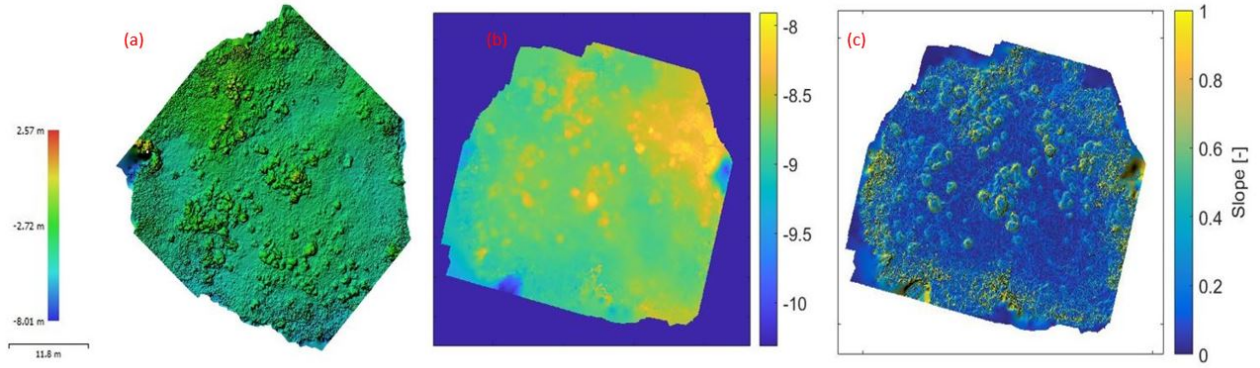

Figure 50: (a) DEM results from the structure for motion survey processed in Agisoft Metashape, for location SfM_6. (b) Adjusted DEM (c) slope

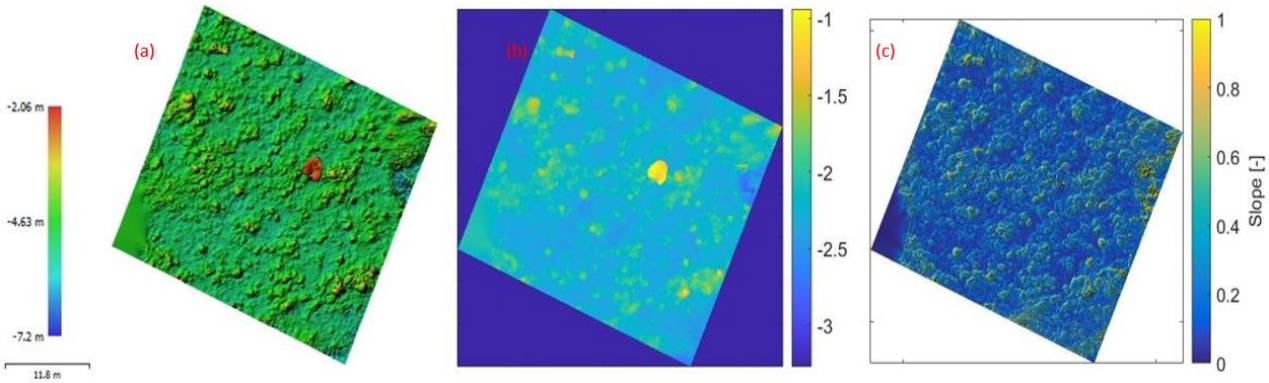

Figure 51: (a) DEM results from the structure for motion survey processed in Agisoft Metashape, for location SfM_7. (b) Adjusted DEM (c) slope

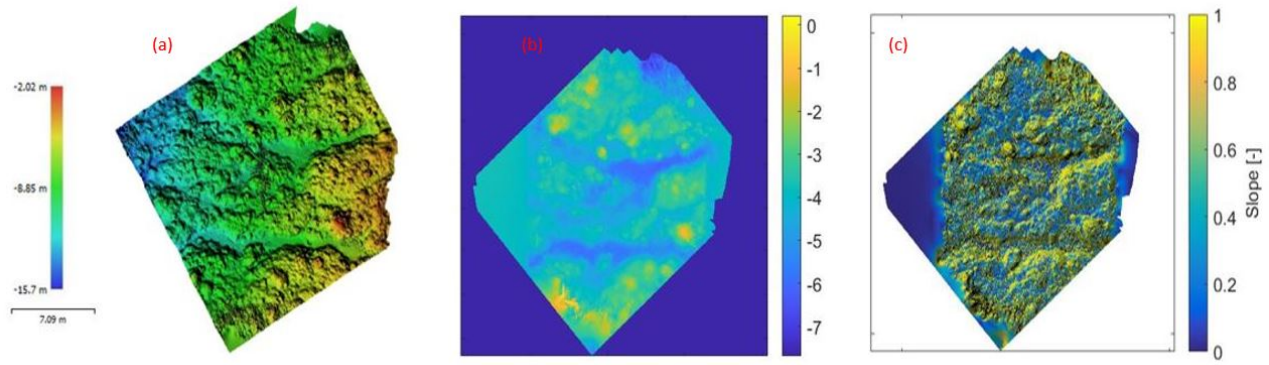

Figure 52: (a) DEM results from the structure for motion survey processed in Agisoft Metashape, for location SfM_8. (b) Adjusted DEM (c) slope

14 Appendix C Sensitivity analysis

Investigative question two of this study aims to determine the relationship between the wave transformation and the amount of coral degradation. Chapter 5 explained that the canopy model is used to account for the effect of vegetation. This sensitivity analysis evaluates the influence of the four different vegetation parameters: vegetation density (N), stem thickness (bv), relative vegetation height (av) and drag coefficient (Cd), on the following output parameters:

- Water level [m]
- Total Wave height [m]
- Dissipation due to vegetation [W/m2]
- IG Runup [m]

Similar to the calibration and numerical simulation, Xbeach surfbeat is used for the sensitivity analysis.

A constant wave height, wave period and water level from a height energy even between May 19 and May 20 at pressure sensor $OSSI_{WH01}$, as shown in 53, is used as input data for the sensitivity analysis. I used the high energy event to ensure a high enough wave height. This will prevent all incoming waves from breaking on the reef crest and gives a more detailed view on the effect of the vegetation input parameters on dissipation throughout the whole 1D transect. The influence of tide is not considered.

To minimize the simulation time and needed storage capacity, a uniform computational grid of 5 metres is chosen across the transect. The computation time for the sensitivity test is 3 hours plus an additional 30 minutes spin up time. 3 out of 4 vegetation parameters are kept at a constant value during each run and one parameter is increased. Table 13 shows the standard input parameters.

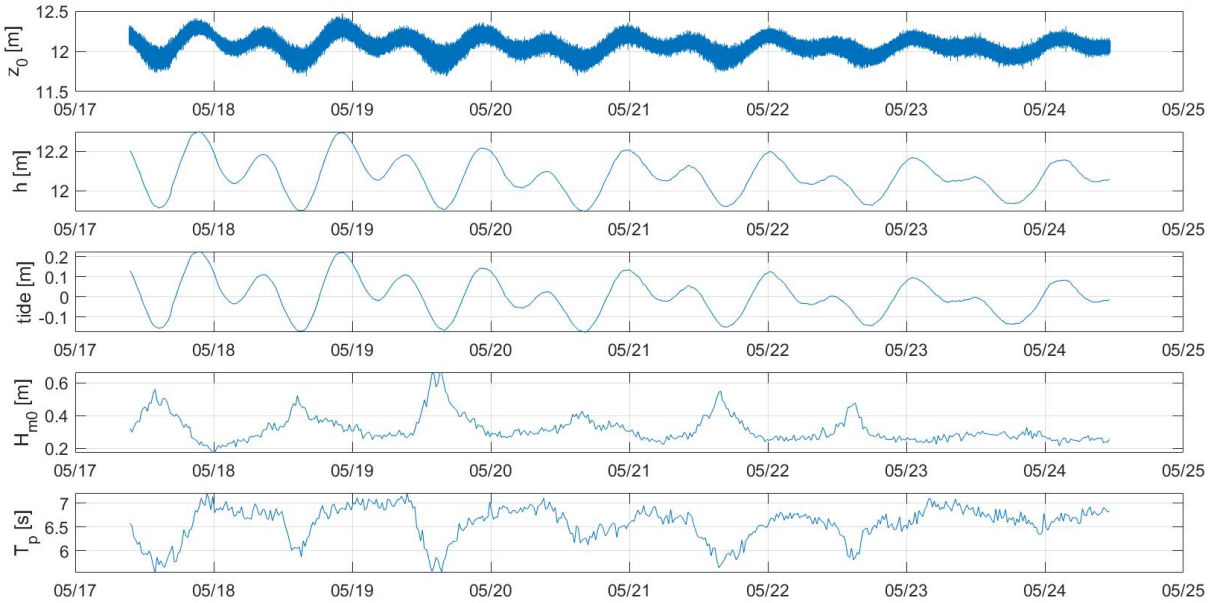

Figure 53: water level (z_0) [m], water depth (h) [m], tidal level (tide) [m], wave height (H_{m0}) [m] and peak period (T_p) [s] data from offshore pressure sensor $OSSI_{WH01}$

Table 13: Standard input parameters for the sensitivity analysis

Vegetation height [m]	Stem thickness [m]	Drag coefficient [-]	vegetation density [corals/m^2]
0.1	0.025	0.25	150

Figure 55, 56, 57 and 58 show the results of the sensitivity analysis. The results are also shown in table 14, 15, 16 and 17. Here it can be seen that an increase in vegetation density has the largest effect on the water level, wave height and dissipation due to vegetation. A doubling of vegetation density will cause an average water level increase of 143%, an average wave height decrease of 7.12 % and an average dissipation due to vegetation increase of 20.20%. The largest effect in the runup is caused by an increase in vegetation height, with an average decrease in runup of 56.10 %.

Table 14: Results of the sensitivity analysis for water level [m]. The table shows the water level when each of the four vegetation parameters are increased. It also shows the water level decrease in %, where - means there is an increase. This decrease is compared to the previous simulation

Water level [m]						
Simulation	**1**	**2**	**3**	**4**	**5**	Average
ah	-0.00037	-0.00017	0.00020	0.00057	0.00094	0.00023
% decrease	-	-54.30	-218.70	-185.86	-64.98	-131
bv	-0.00041	-0.00017	0.00020	0.00057	0.00094	0.00022
% decrease	-	-57.62	-214.86	-185.90	-65.19	-131
N	-0.00039	-0.00017	0.00016	0.00058	0.00092	0.00022
% decrease	-	-57.25	-196.51	-256.45	-60.06	-143
Cd	-0.00045	-0.00017	0.00019	0.00057	0.00092	0.00021
% decrease	-	-62.59	-209.55	-208.77	-60.61	-135

Table 15: Results of the sensitivity analysis for wave height [m]. The table shows the wave height when each of the four vegetation parameters are increased. It also shows the wave height decrease in %, where - means there is an increase. This decrease is compared to the previous simulation

wave height [m]						
Simulation	**1**	**2**	**3**	**4**	**5**	Average
ah	0.39	0.38	0.36	0.33	0.29	0.35
% decrease	-	2.96	5.08	8.62	11.52	7.05
bv	0.39	0.38	0.36	0.33	0.29	0.35
% decrease	-	3.58	5.36	7.66	10.91	6.88
N	0.39	0.38	0.36	0.33	0.29	0.35
% decrease	-	3.25	5.25	8.65	11.34	7.12
Cd	0.39	0.38	0.36	0.33	0.29	0.35
% decrease	-	3.32	5.88	8.10	11.65	7.24

Table 16: Results of the sensitivity analysis for dissipation due to vegetation [W/m^2]. The table shows the dissipation due to vegetation when each of the four vegetation parameters are increased. It also shows the dissipation due to vegetation decrease in %, where - means there is an increase. This decrease is compared to the previous simulation

Dissipation due to vegetation [W/m^2]						
Simulation	**1**	**2**	**3**	**4**	**5**	Average
ah	0.32	0.45	0.55	0.58	0.59	0.50
% decrease	-	-42.61	-22.00	-6.12	-1.47	-18.050
bv	0.31	0.46	0.56	0.60	0.61	0.51
% decrease	-	-46.40	-22.90	-6.00	-2.47	-19.442
N	0.31	0.46	0.55	0.61	0.61	0.51
% decrease	-	-49.03	-20.12	-11.47	-0.19	-20.202
Cd	0.32	0.45	0.56	0.60	0.61	0.51
% decrease	-	-39.85	-23.15	-8.04	-1.41	-18.113

Table 17: Results of the sensitivity analysis for runup [m]. The table shows the runup when each of the four vegetation parameters are increased. It also shows the runup decrease in %, where - means there is an increase. This decrease is compared to the previous simulation

runup [m]						
Simulation	**1**	**2**	**3**	**4**	**5**	Average
ah	0.121	0.021	0.010	0.005	0.003	0.032
% decrease	-	82.36	54.13	52.00	35.92	56.10
bv	0.119	0.027	0.010	0.007	0.005	0.034
% decrease	-	77.22	63.09	33.85	24.56	49.68
N	0.119	0.018	0.010	0.007	0.005	0.032
% decrease	-	85.02	42.41	35.86	24.36	46.91
Cd	0.119	0.017	0.010	0.007	0.005	0.031
% decrease	-	85.61	41.21	33.42	26.36	46.65

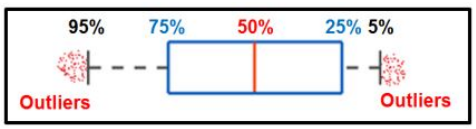

Figure 54: The red centre line denotes the median value (50th percentile) The blue box marks the 25th to 75th percentiles, while black whiskers mark the 5th and 95th percentiles.

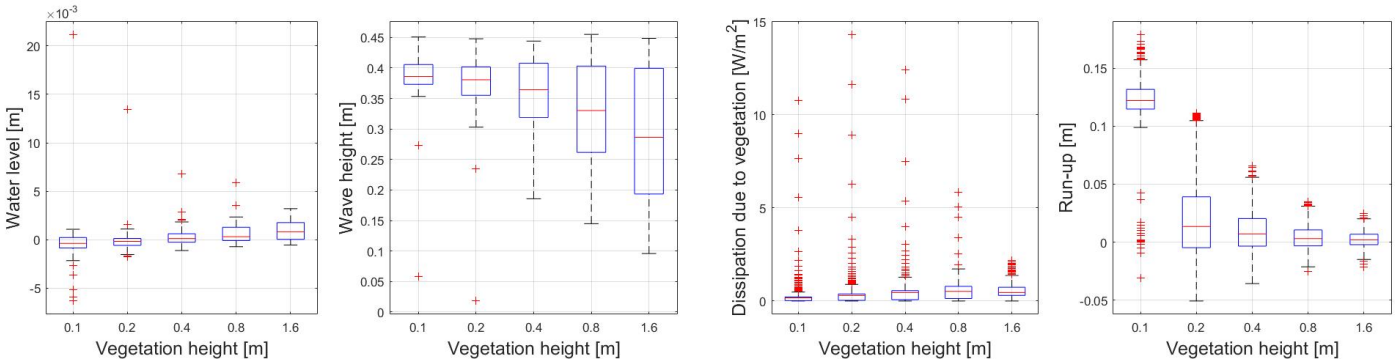

Figure 55: Influence of the vegetation height, stem thickness, drag coefficient and vegetation density respectively on the runup

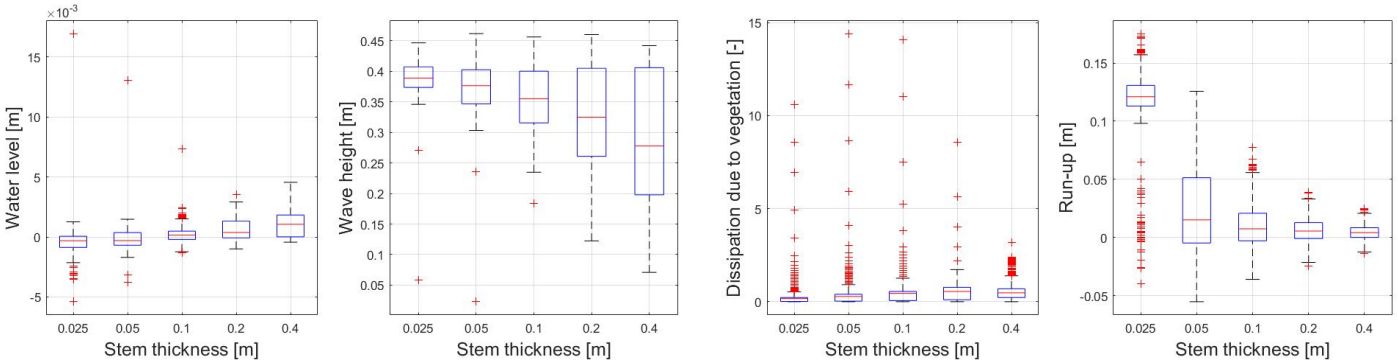

Figure 56: Influence of the Stem thickness, stem thickness, drag coefficient and vegetation density respectively on the runup

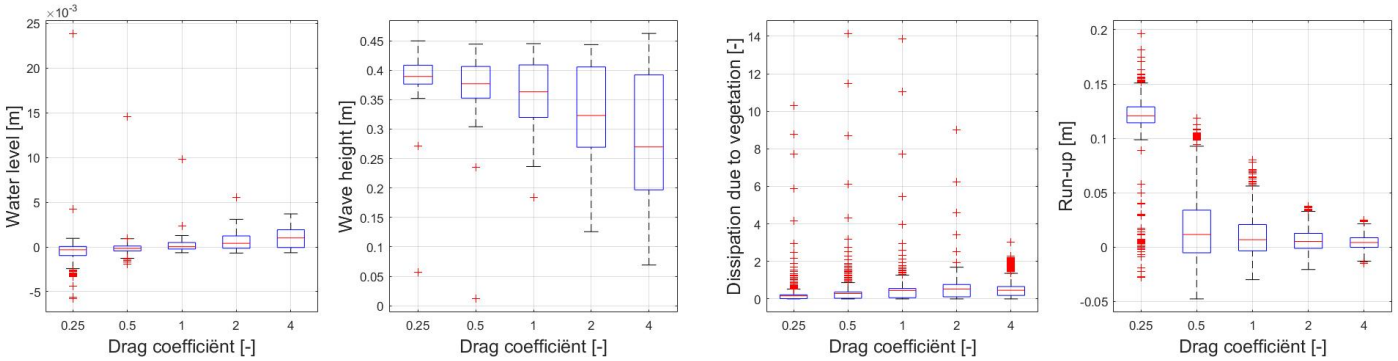

Figure 57: Influence of the drag coefficient, stem thickness, drag coefficient and vegetation density respectively on the runup

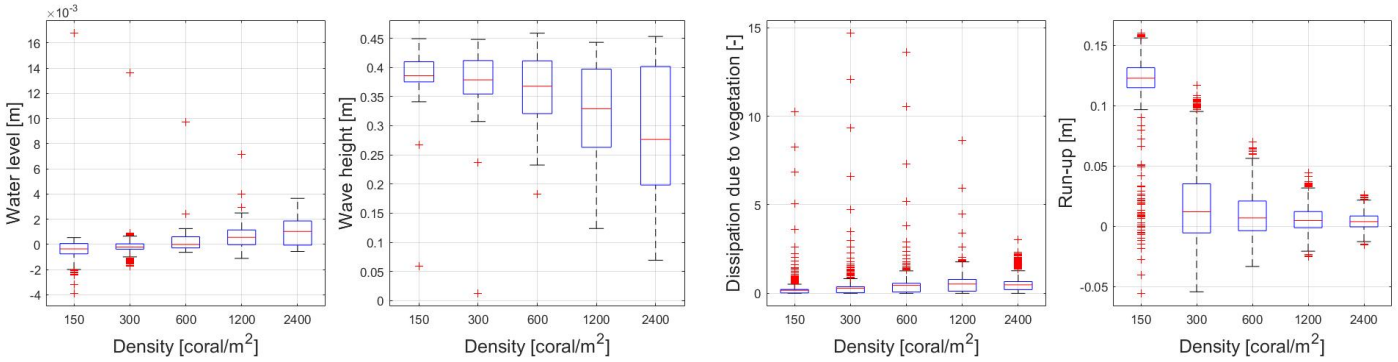

Figure 58: Influence of the vegetation density , stem thickness, drag coefficient and vegetation density respectively on the runup

15 Appendix D Wave propagation

15.1 IG wave height

Figure 59, 60, 61 and 62 show the propagation of the low frequency wave height [m] for transect 1, 2, 3 and 4 respectively. Here it can be seen that for scenario S3 and S4 the low frequency wave height increases from the point where the bed level increases. The wave height reached a peak at the location of the reef crest. The wave height for scenario S1 and S2 slightly increases with an increase in bed level and then experiences a rapid decrease at the reef crest.

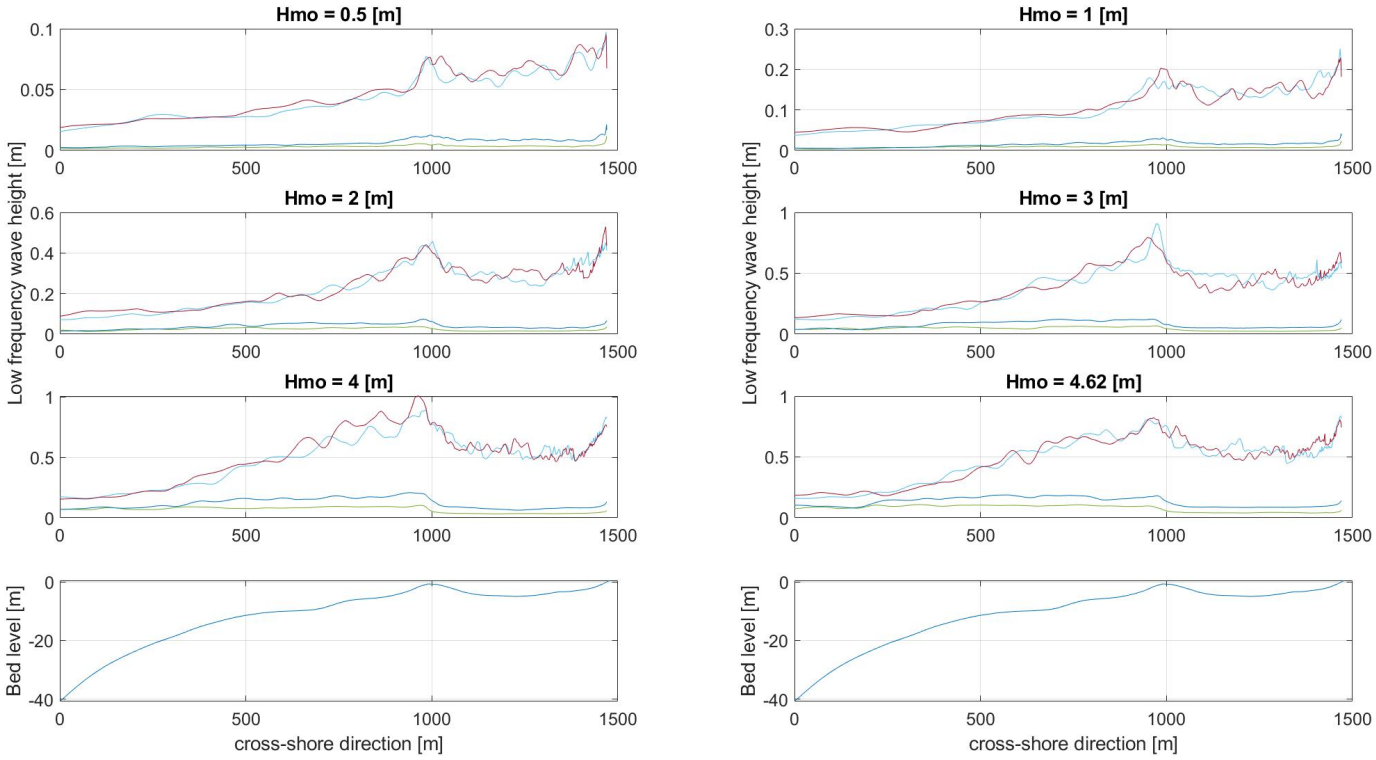

Figure 59: Propagation of the low frequency wave height [m] for scenario S, S2, S3 and S4. Transect 1

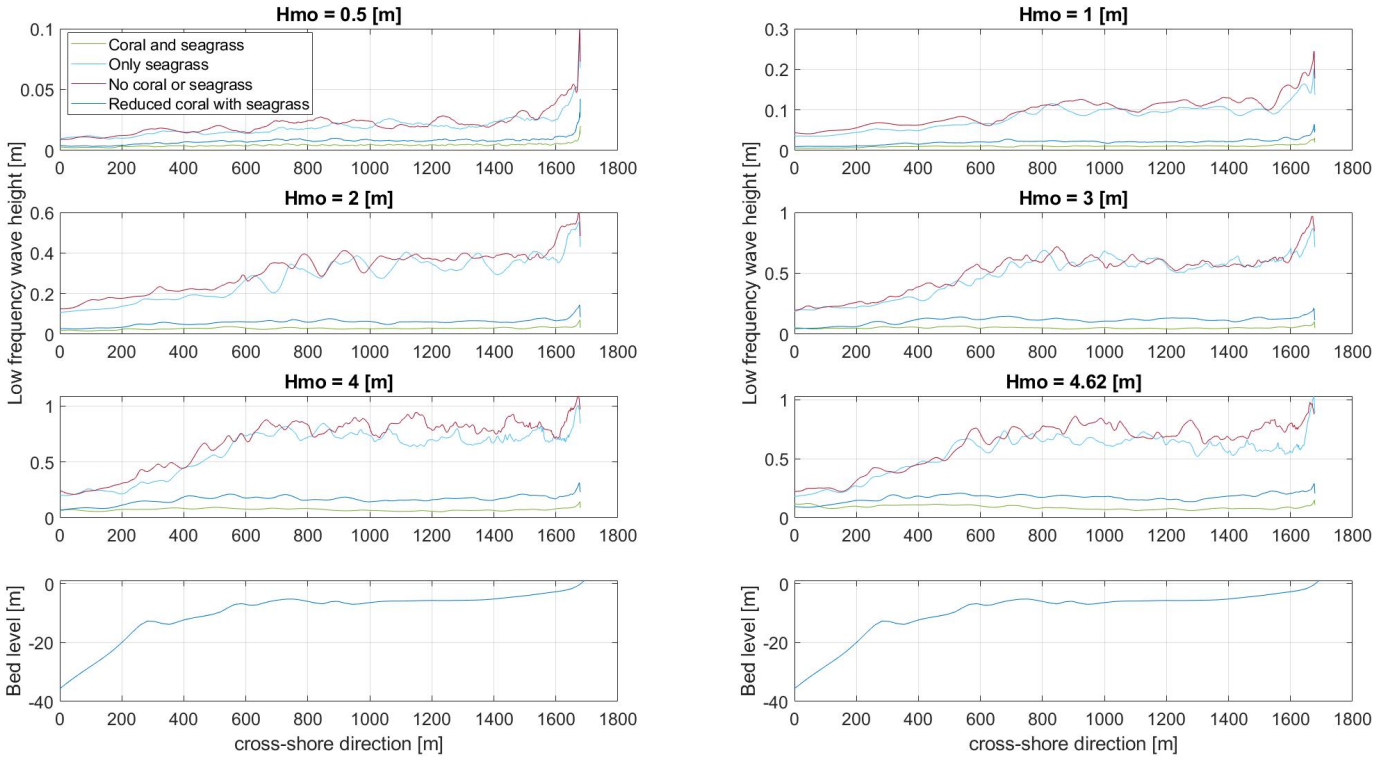

Figure 60: Propagation of the low frequency wave height [m] for scenario S, S2, S3 and S4. Transect 2

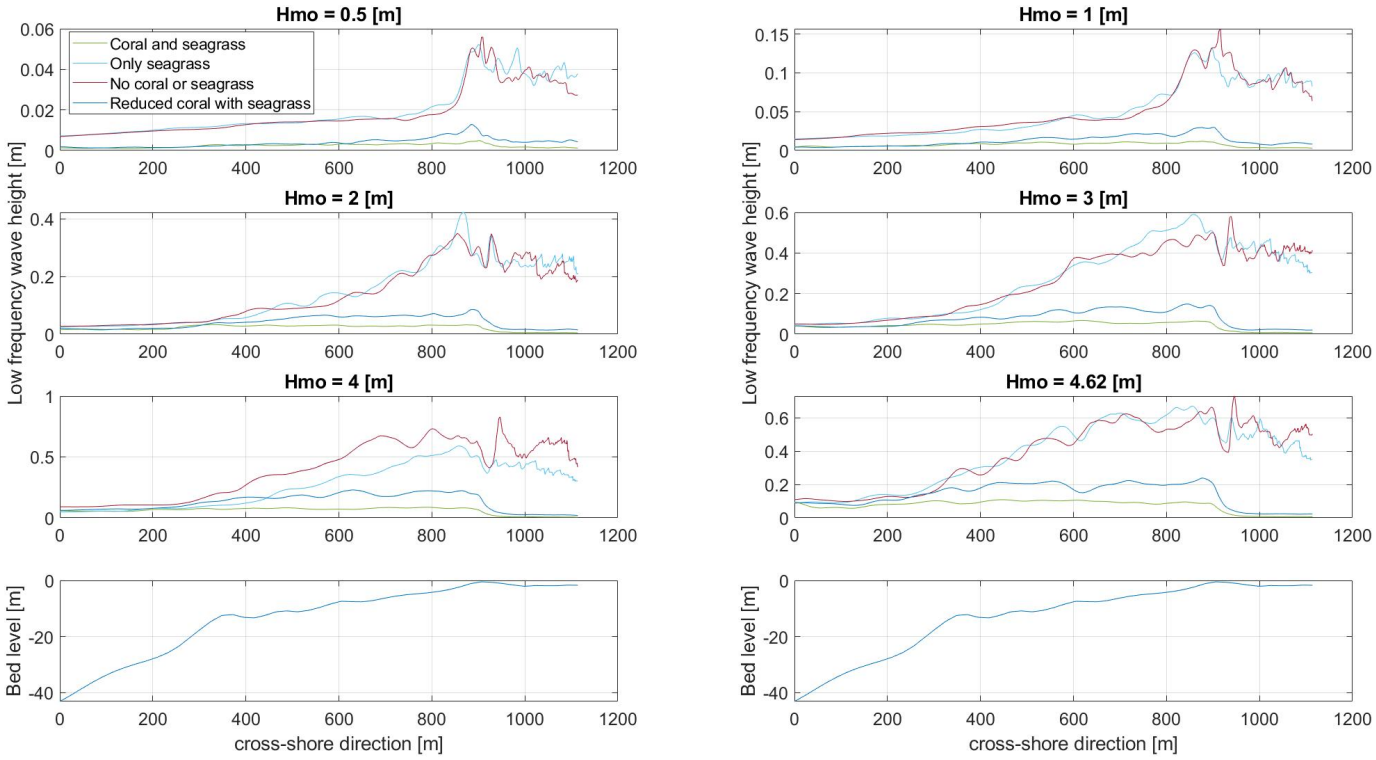

Figure 61: Propagation of the low frequency wave height [m] for scenario S, S2, S3 and S4. Transect 3

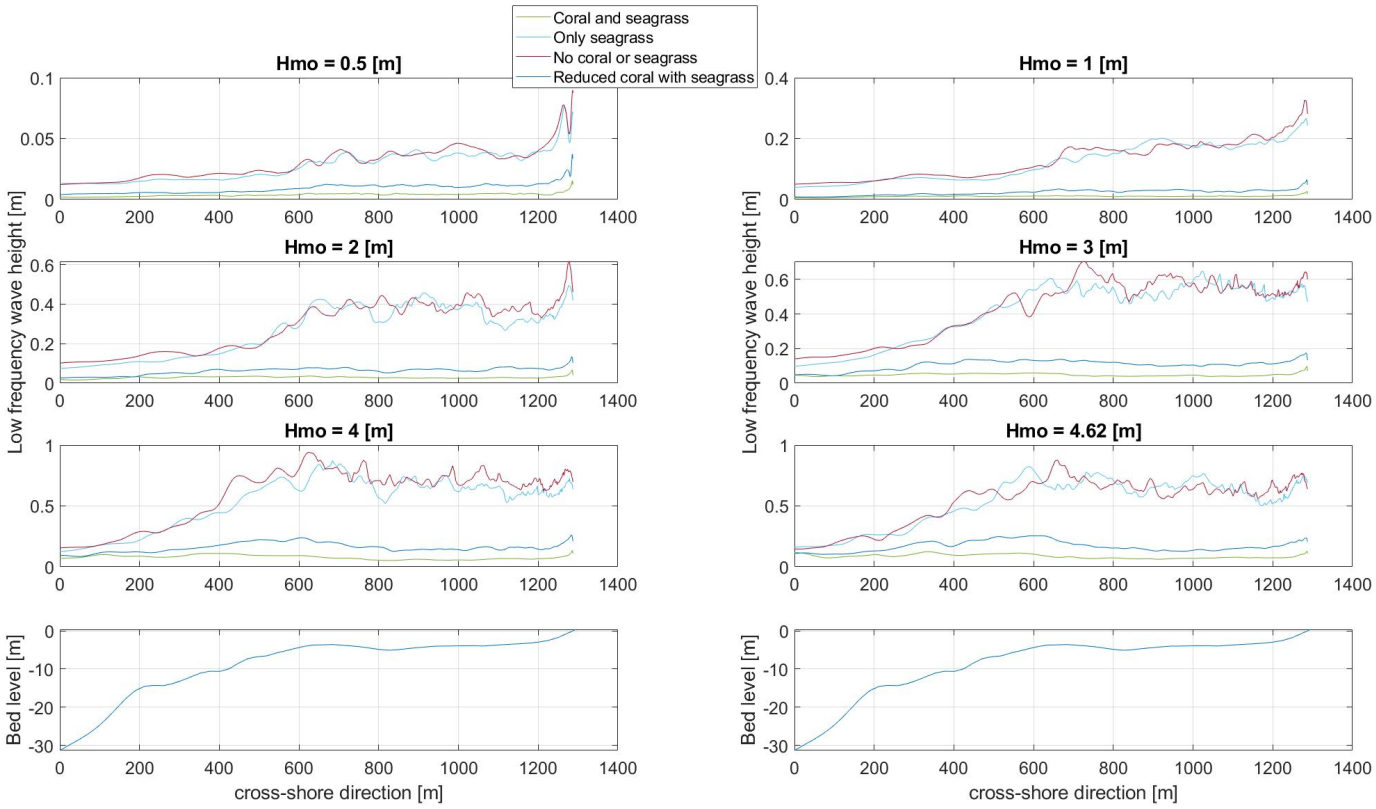

Figure 62: Propagation of the low frequency wave height [m] for scenario S, S2, S3 and S4. Transect 4

15.2 Dissipation due to waves breaking and vegetation

Figure 63, 64, 65, **??**, 67, **??**, 69 and 70 show the dissipation due to waves breaking (Dbr) and due to vegetation (Dveg) for transect 1, 2, 3 and 4.

The transect with a less profound reef crest (transect 2 and 4) shows a higher Dveg on the reef flat for scenario S3. This shows that the sea-grass can help to reduce the residual wave energy after the waves are broken. It can also be seen that not all waves break on the reef crest, but that for lower offshore wave heights waves also break onshore. This is especially true for scenario S1 and S2. For these scenarios the waves either break onshore or the energy is lost due to the interaction with vegetation offshore and on the reef crest. The transects with a more profound reef crest (transect 1 and 3) shows that for scenario S3 and S4 almost all the energy dissipation is caused by the breaking of waves on the reef crest.

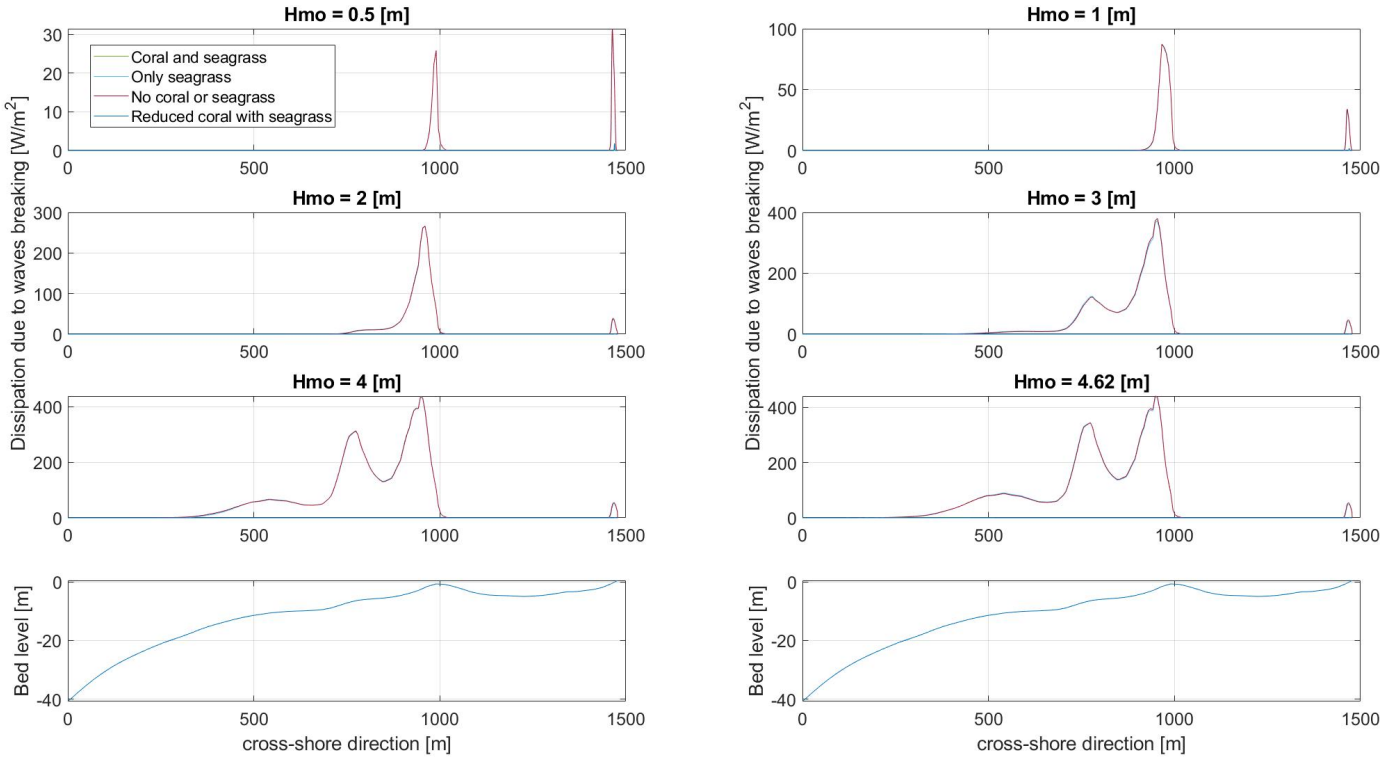

Figure 63: Dissipation due to waves breaking [W/m^2] for scenario S, S2, S3 and S4. Transect 1

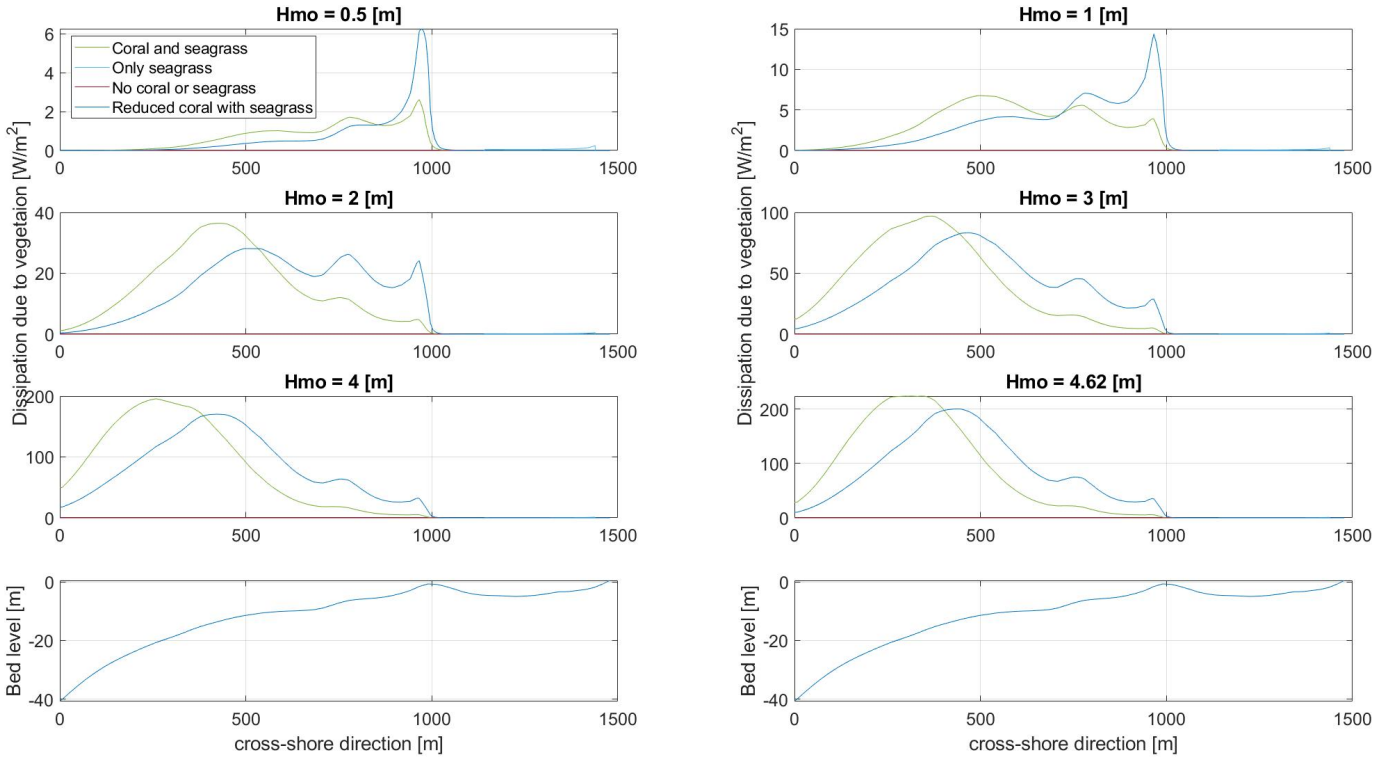

Figure 64: Dissipation due to vegetation [W/m^2] for scenario S, S2, S3 and S4. Transect 1

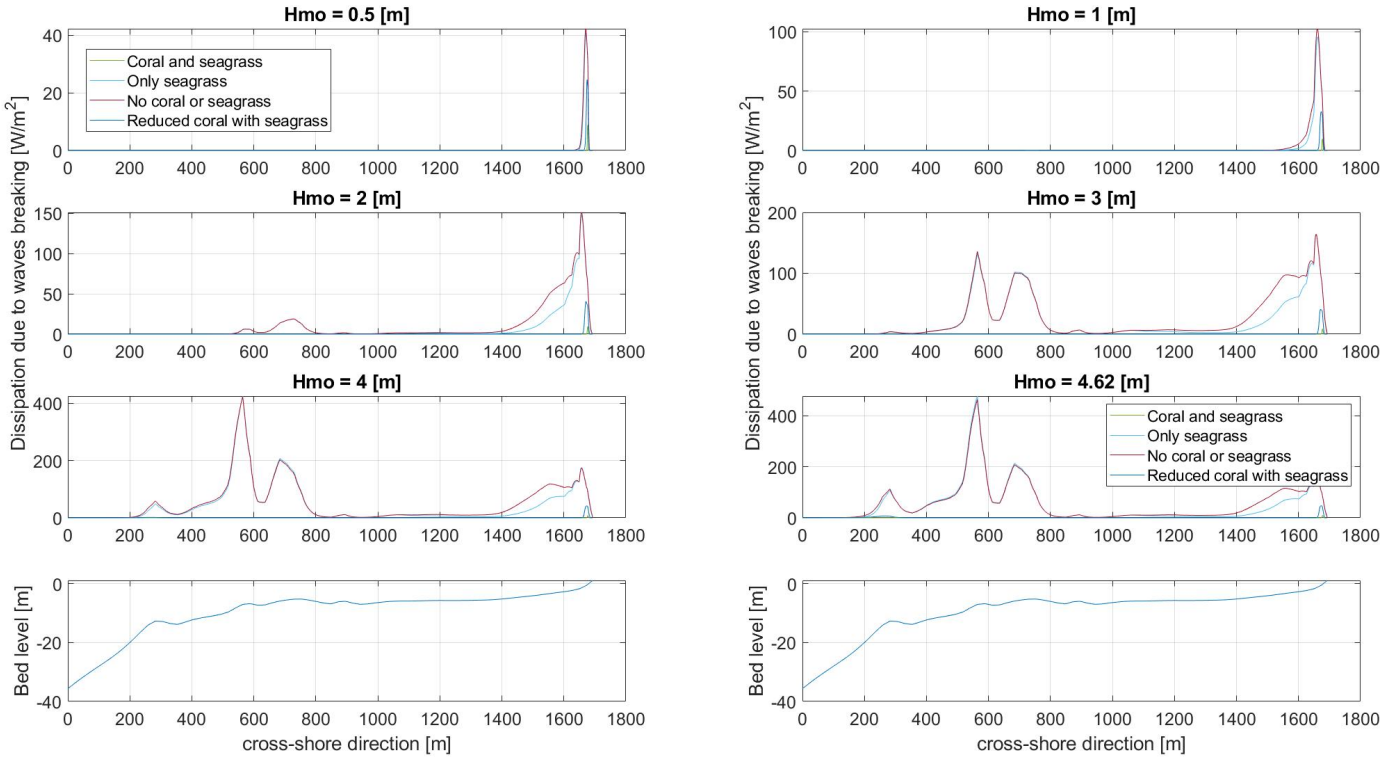

Figure 65: Dissipation due to waves breaking [W/m^2] for scenario S, S2, S3 and S4. Transect 2

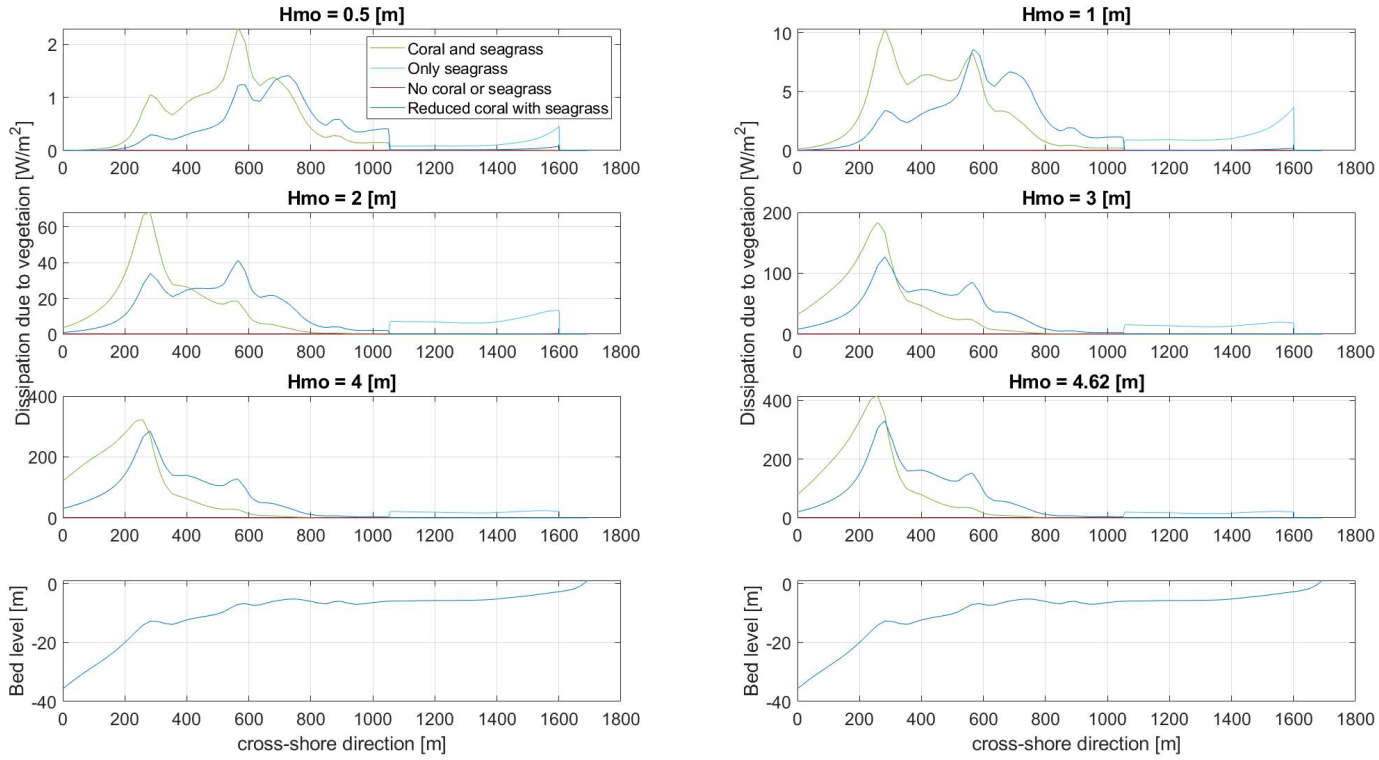

Figure 66: Dissipation due to vegetation [W/m^2] for scenario S, S2, S3 and S4. Transect 2

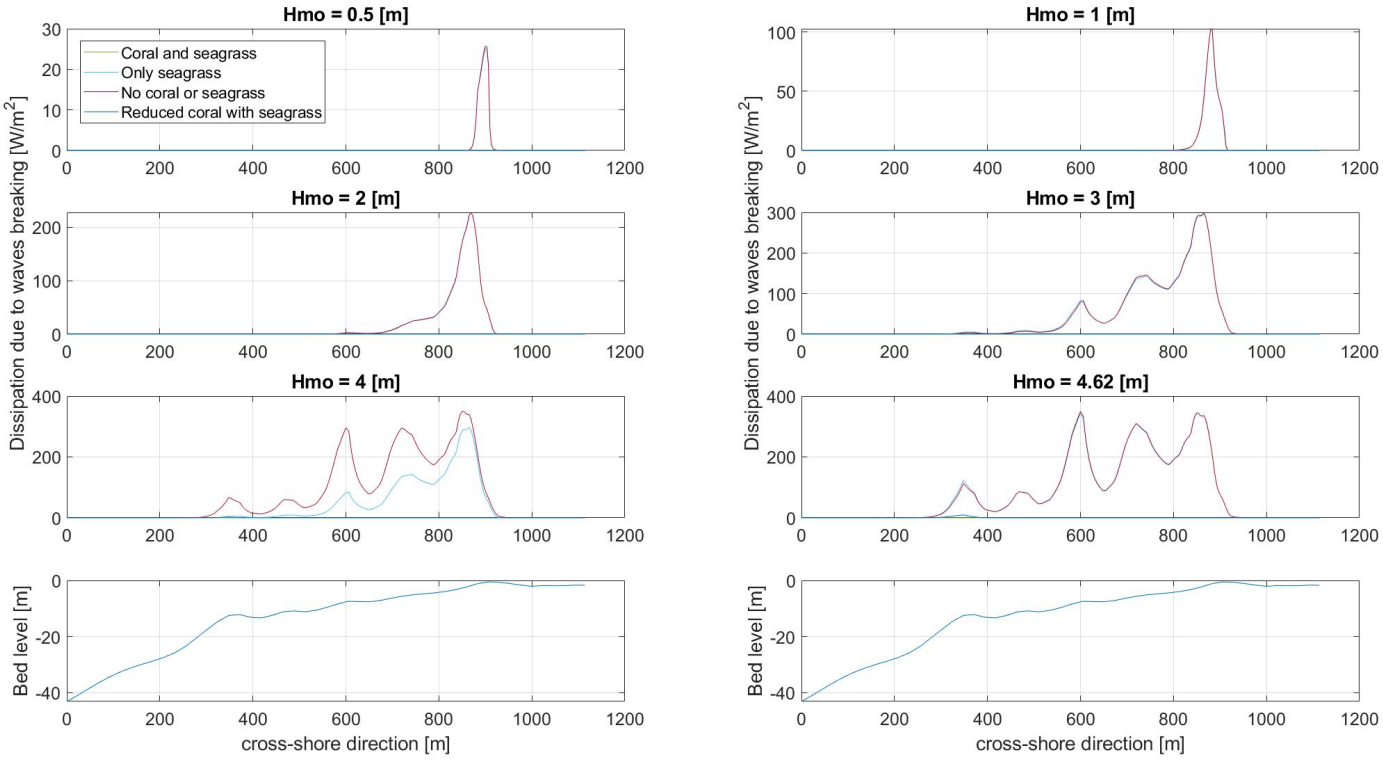

Figure 67: Dissipation due to waves breaking [W/m^2] for scenario S, S2, S3 and S4. Transect 3

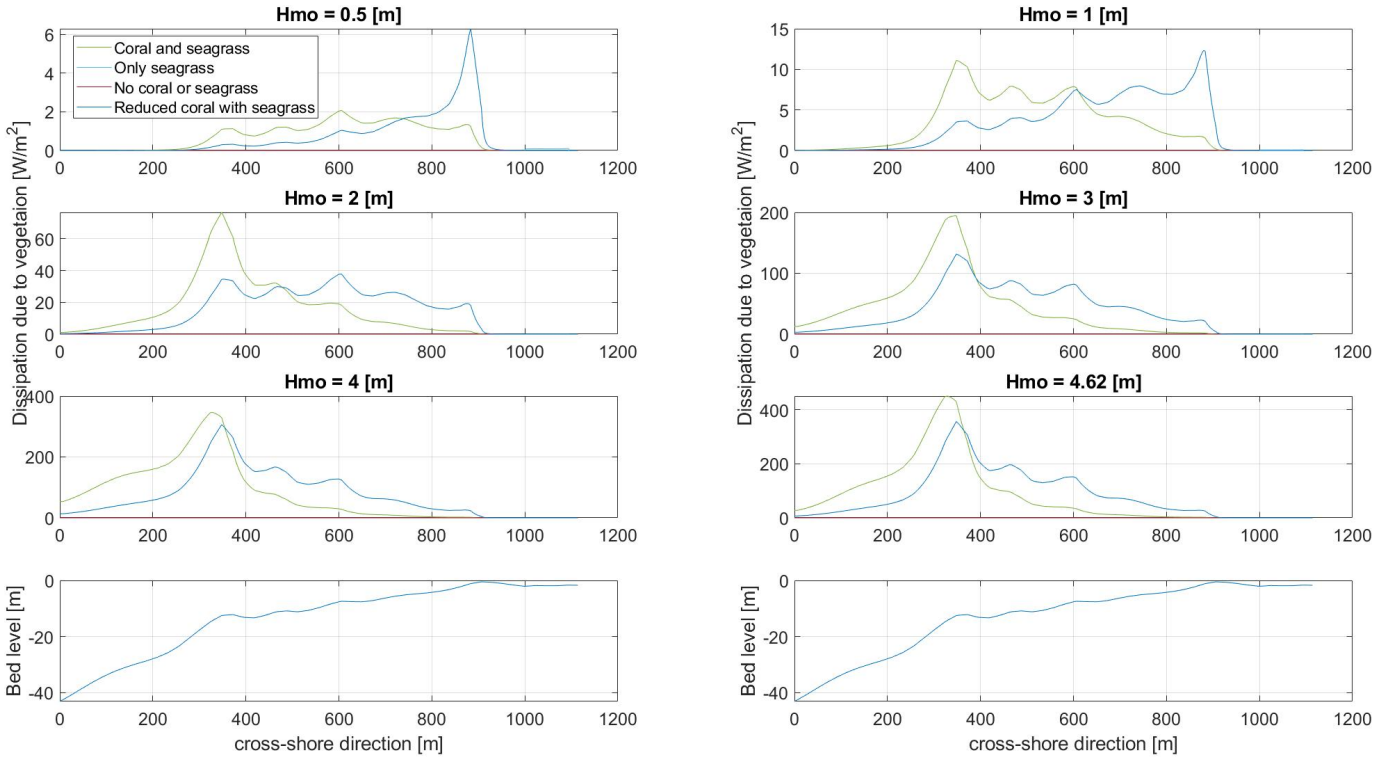

Figure 68: Dissipation due to vegetation [W/m^2] for scenario S, S2, S3 and S4. Transect 3

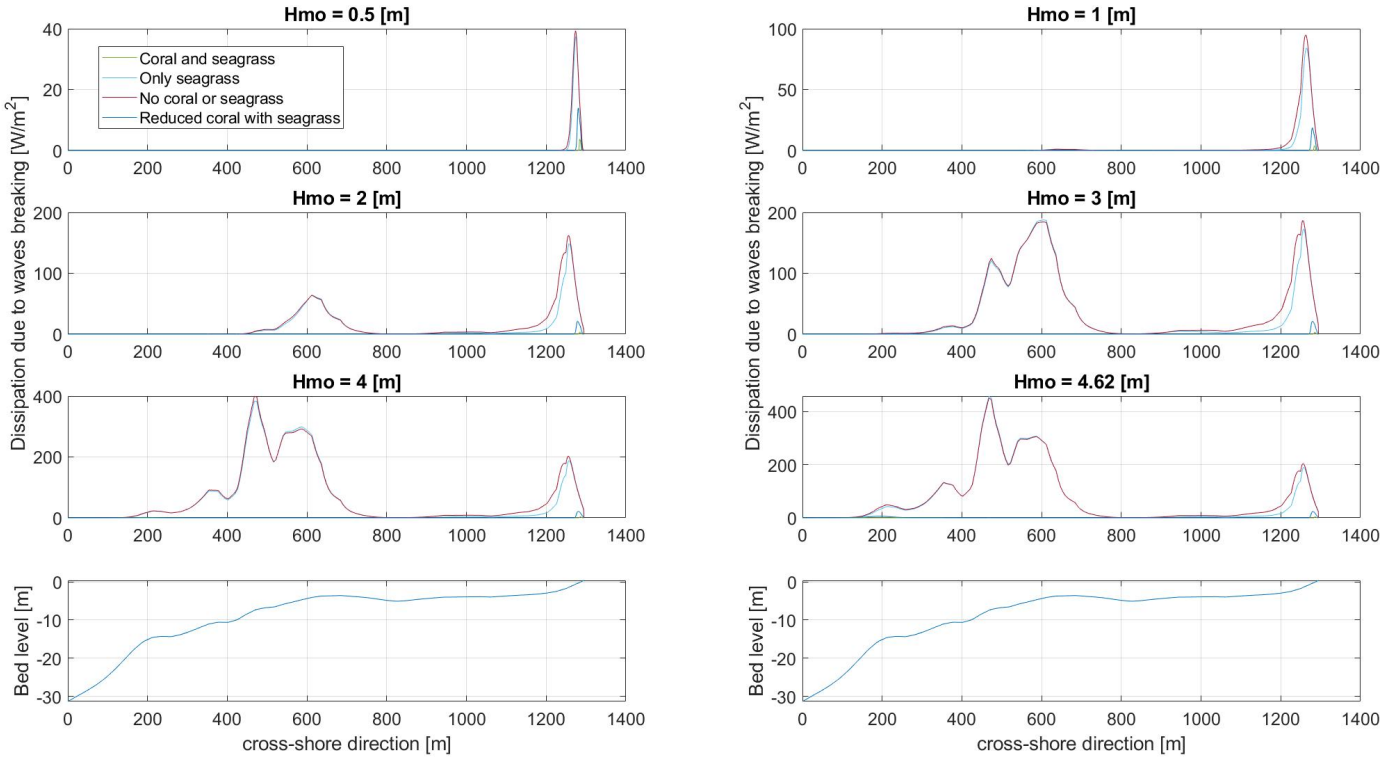

Figure 69: Dissipation due to waves breaking [W/m^2] for scenario S, S2, S3 and S4. Transect 4

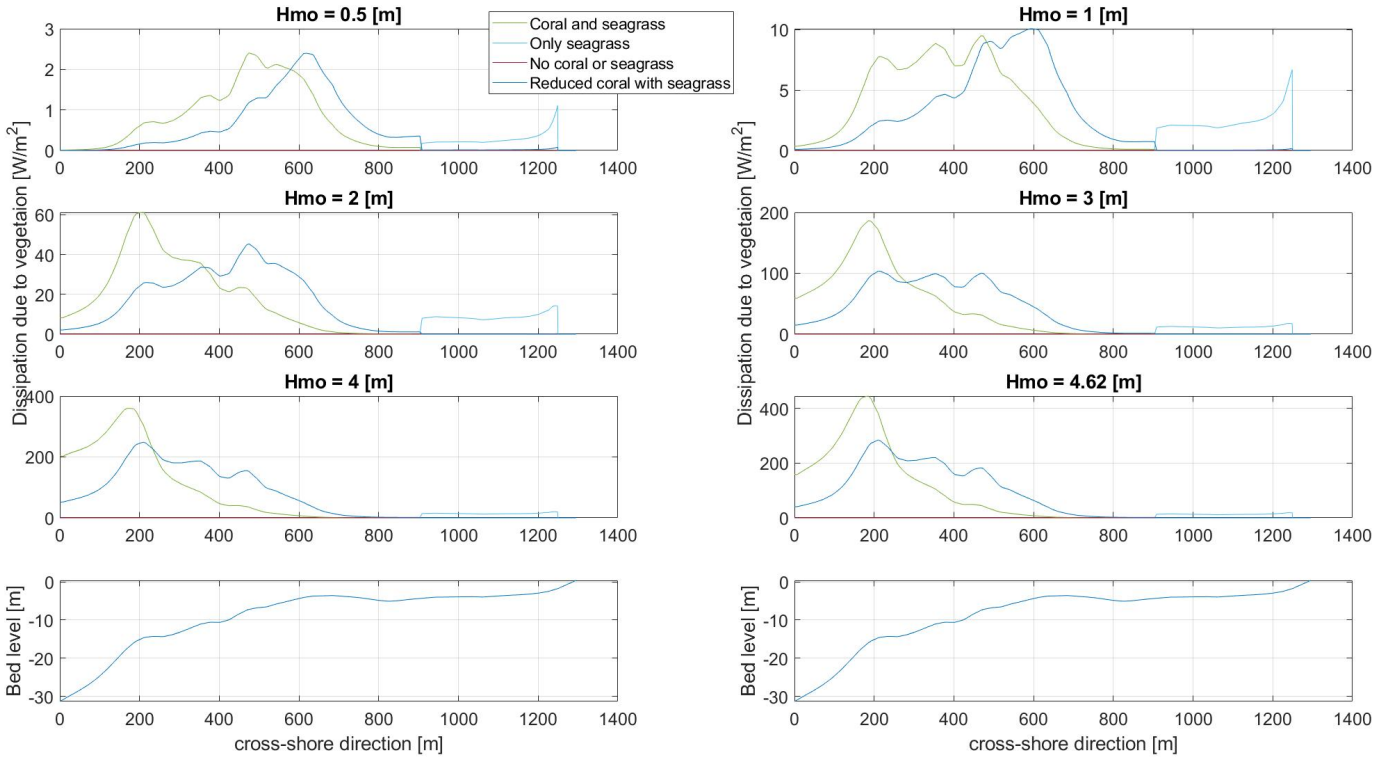

Figure 70: Dissipation due to vegetation [W/m^2] for scenario S, S2, S3 and S4. Transect 4

15.3 IG runup timeseries

Figure 71, 72, 73 and 74 show the time-series of the IG runup for transect 1, 2, 3 and 4 respectively.

Transect 1, 2 and 3 show a small increase in runup with an increase in offshore wave height for scenarios S1 and S2. These results also show a lower average runup value for scenario S1 and S2 compared to S3 and S4. Transect 4 shows different results. Here it can be seen that the runup for all four scenarios increase significantly with an increasing offshore wave height.

The transects with a profound reef crest (transect 2 and 3) show an increase in maximum and minimum runup values, but the runup average remains similar. These results also show a similar average runup for all four scenarios. Transect 1 and 4 show different results. Here it can be seen that both the maximum, minimum and the average values of the runup increases with an increasing offshore wave height. These results also show a lower average runup value for scenario S1 and S2 compared to S3 and S4.

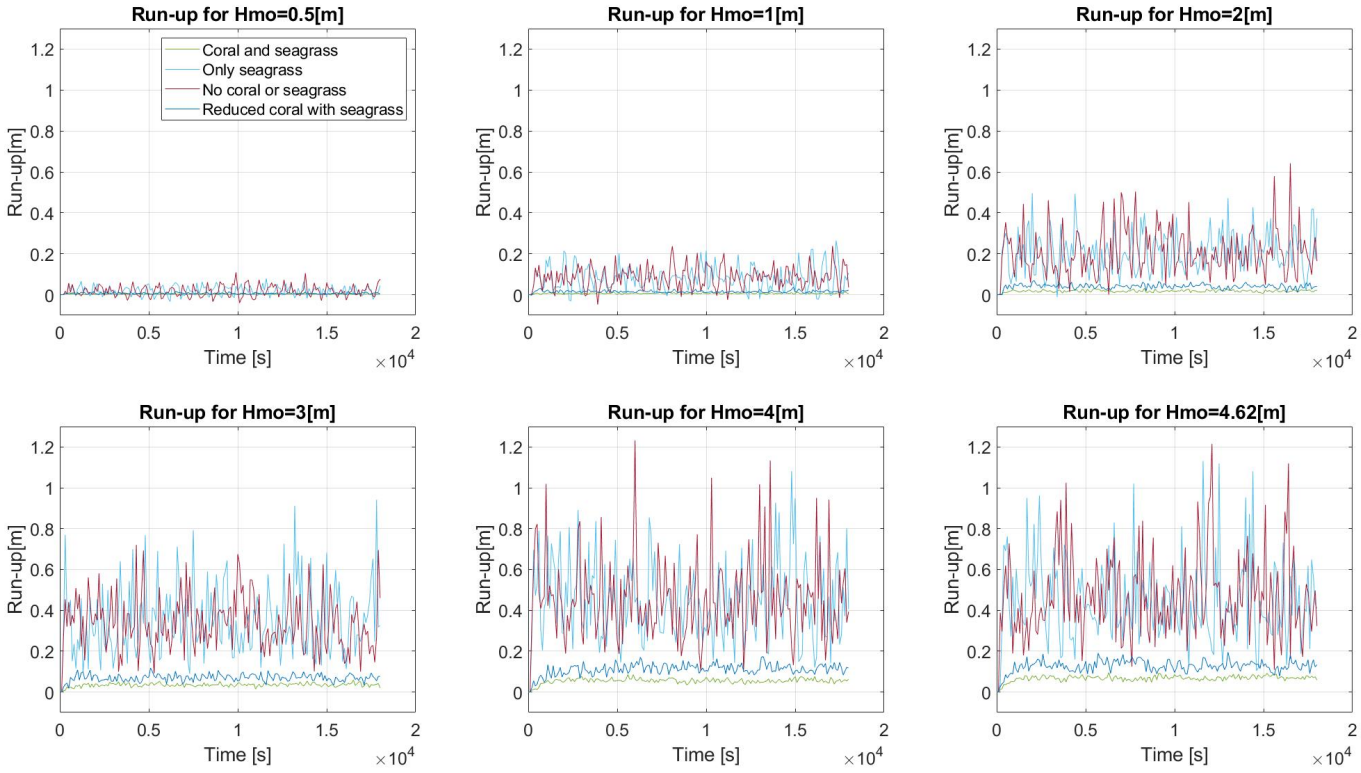

Figure 71: IG runup for scenario S, S2, S3 and S4. Transect 1

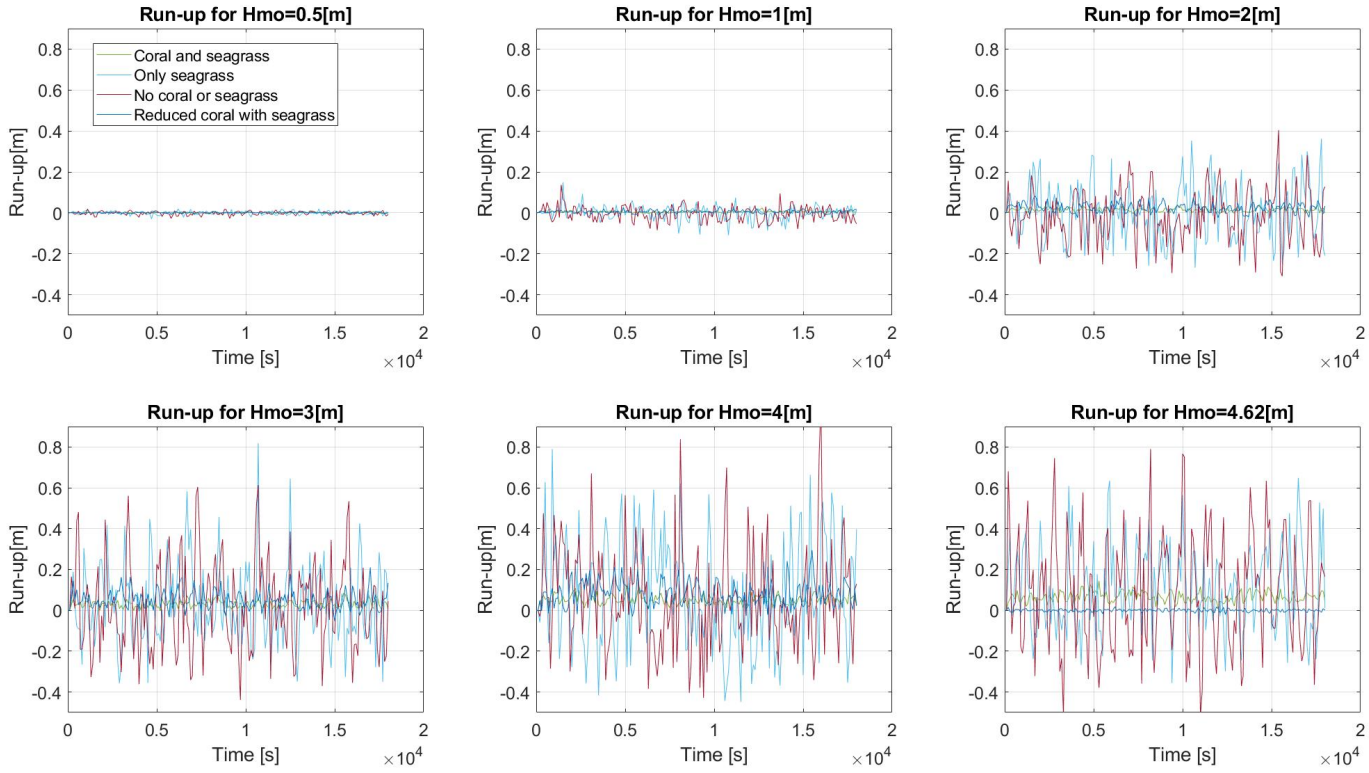

Figure 72: IG runup for scenario S, S2, S3 and S4. Transect 2

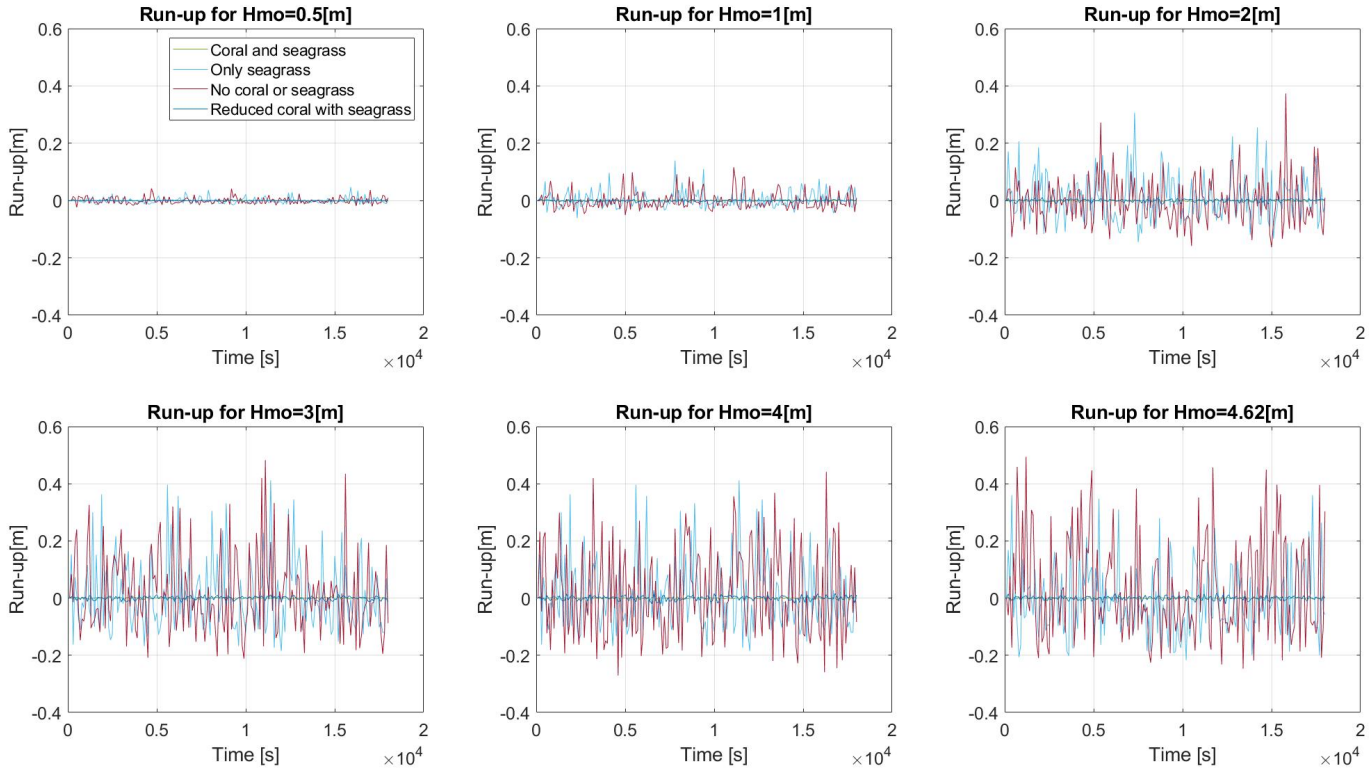

Figure 73: IG runup for scenario S, S2, S3 and S4. Transect 3

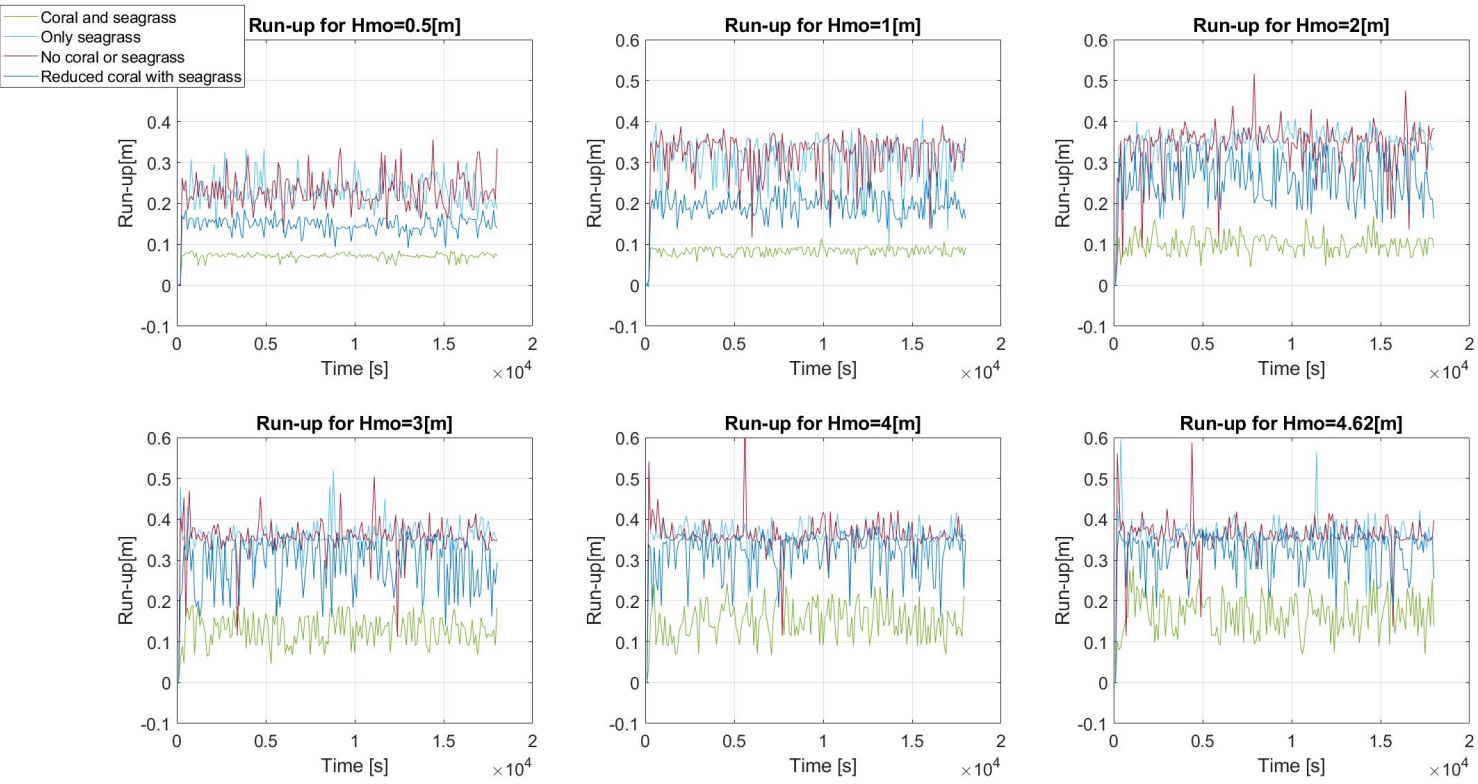

Figure 74: IG runup for scenario S, S2, S3 and S4. Transect 4